UNIVERSIDAD DE SEVILLA

ESCUELA TÉCNICA SUPERIOR
DE INGENIERÍA AGRONÓMICA

NEW STRATEGIES FOR ROW-CROP MANAGEMENT BASED ON COST-EFFECTIVE REMOTE SENSORS

International Ph. D

JORGE MARTÍNEZ GUANTER

2017

Thesis Directors

Dr. MANUEL PÉREZ RUIZ
Dr. JUAN AGÜERA VEGA

Universidad de Sevilla

Escuela Técnica Superior
de Ingeniería Agronómica

DOCTORAL THESIS

New Strategies for Row-Crop Management Based on Cost-Effective Remote Sensors

Authored by

JORGE MARTÍNEZ GUANTER

Thesis Directors

Dr. MANUEL PÉREZ RUIZ

Dr. JUAN AGÜERA VEGA

Sevilla, June 2017

Informe del Director de Tesis sobre Presentación de Tesis Doctoral

El **Dr. D. MANUEL PÉREZ RUIZ** como Tutor de la Tesis Doctoral titulada "*New Strategies for Row-Crop Management Based on Cost-Effective Remote Sensors*" realizada por **D. JORGE MARTÍNEZ GUANTER** en el programa de doctorado DOCTORADO INTERUNIVERSITARIO EN INGENIERÍA AGRARIA, ALIMENTARIA, FORESTAL Y DEL DESARROLLO RURAL SOSTENIBLE, regulado por el R.D. 99/2011 de 28 de enero, **INFORMA FAVORABLEMENTE EL DEPÓSITO DE LA MISMA Y LA IDONEIDAD DE SU REALIZACIÓN EN LA MODALIDAD DE COMPENDIO DE ARTÍCULOS**, dado que reúne las condiciones necesarias para su defensa.

Y para que así conste, firmo la presente.

En Sevilla a 20 de Junio de 2017.

El Director de la Tesis

Manuel Pérez Ruiz

Agradecimientos

Muchas son las personas que han contribuido directa o indirectamente a la realización de esta tesis doctoral, durante la cual he tenido la suerte de contar con un excepcional grupo de trabajo, sin cuyo apoyo y ayuda esto no hubiera sido posible.

En primer lugar, mi más sincero agradecimiento a mis directores de tesis, Manuel Pérez Ruiz y Juan Agüera Vega. Ha sido un camino largo, y a Manuel le agradezco su dedicación continua, su amistad y capacidad de trabajo, todo lo que me ha enseñado y su confianza en mí y mi trabajo desde el primer día. A Juan le debo el haberme iniciado en este mundillo, haber despertado mi interés y curiosidad hace algunos años, y haber compartido su amplio conocimiento para avanzar durante la tesis. Hay personas que *hacen* y personas que *hacen hacer*. Vosotros "hacéis hacer haciendo", un ejemplo muy valioso para quienes queremos seguir vuestros pasos. Gracias.

También agradecer a Gregorio Egea su colaboración y ayuda en los trabajos de la tesis, y su apoyo en el día a día. Su iniciativa y valiosas aportaciones han permitido desarrollar muchos de los aspectos de este trabajo, y sus consejos me han ayudado a avanzar en el camino de la investigación. Espero seguir aprendiendo y trabajando contigo.

Agradecer también a todos los colegas colaboradores e investigadores con quienes he disfrutado y aprendido a lo largo de la tesis. A los coautores de los papers: a Miguel Garrido (ha sido un placer conocerte y trabajar contigo), a Jose Enrique y Carmen del IRNAS, a Constantino Valero y David Slaughter, todos ellos se han ofrecido a ayudarme en todo momento y sus aportaciones han sido determinantes para este trabajo. Los trabajos que se presentan son colaborativos, y el mérito es de todos. Ojalá que podamos seguir colaborando en futuras investigaciones.

Un sincero agradecimiento a mis compañeros de la empresa Soluciones Agrícolas de Precisión. En ella he encontrado además de un grupo de trabajo, un gran grupo humano y unos amigos excepcionales. Sin vosotros esto no hubiera sido posible.

A mis amigos. Tengo la suerte de contar con muchos, de muchas partes y siempre estáis presentes allá donde esté. Os debo mucho de mi forma de ser y de la forma en la que valoro las cosas. Gracias por vuestro apoyo.

A mi abuela, agradecerle el inmenso amor que me tiene y que comparto, y porque sé la ilusión y alegría que le hace esto. Gràcies Yaya.

Sobre todo, a mis padres y hermano. A ellos les debo todo: mi educación, mis valores, mi afán por esforzarme y por hacer bien las cosas. El apoyo que me han dado siempre y su inmenso cariño hacen que esté donde estoy hoy, y harán que siga creciendo como persona. Qué orgullo de padres y hermano tengo.

A Marta, por todo lo que compartimos en la vida y por el cariño y apoyo, que es enorme y mutuo. Gracias.

Thesis Index

Figure List

Chapter 3

Table List

Abbreviation Index

CDI	Controlled deficit irrigation
CWSI	Crop water stress index
DI	Deficit irrigation
DIY	Do it Yourself
DOY	Day of the Year
DSS	Decision Support System
E_m	Leaf Transpiration Rate
ET	Evapotranspiration
ET_0	Reference Evapotranspiration
FI	Full irrigation
FMIS	Farm Management Information System
FOV	Field Of View
GNSS	Global Navigation Satellite System
GPS	Global Positioning System
g_s	Stomatal conductance
GSD	Ground Sampling Distance
IC	Intelligent cultivator
ICT	Information and Communication Technologies
I_g	Stomatal conductance index
IR	Infrared
IRTS	Infrared Thermometers
K	Emissivity
LAI	Leaf Area Index
LiDAR	Light Detection and Ranging
NWSB	Non water stressed baseline
OBIA	Object Based Image Analysis
ºC	Celsius degree
PA	Precision Agriculture
PWM	Pulse Width Modulation
RDI	Regulated Deficit Irrigation
RET	Relative Evapotranspiration
RGB	Red-green-blue images
RGB-D Camera	Red-Green-Blue-Depth cameras
RH	Relative Humidity
RPAS	Remotely Piloted Aircraft System
RTK	Real-Time Kinematic
SHD	Super-high-density
T_a	Air temperature
T_c	Canopy temperature
T_{dry}	Non-transpiring leaves temperature
TIR	Thermal Infrared
T_o	Targeted object temperature
T_{wet}	Wet leaves/canopy temperature
UAV	Unmanned Aerial Vehicle
VPD	Vapour pressure deficit
VRI	Variable Rate Irrigation
WARS	Wet artificial reference surfaces
θ	Volumetric Soil Water Content
ψ_L	Leaf water potential
ψ_{st}	Stem water potential

Abstract

Agricultural technology can be an excellent antidote to resource scarcity. Its growth has led to the extensive study of spatial and temporal in-field variability. The challenge of accurate management has been addressed in recent years through the use of accurate high-cost measurement instruments by researchers. However, low rates of technological adoption by farmers motivate the development of alternative technologies based on affordable sensors, in order to improve the sustainability of agricultural biosystems.

This doctoral thesis has as main objective the development and evaluation of systems based on affordable sensors, in order to address two of the main aspects affecting the producers: the need of an accurate plant water status characterization to perform a proper irrigation management and the precise weed control.

To address the first objective, two data acquisition methodologies based on aerial platforms have been developed, seeking to compare the use of infrared thermometry and thermal imaging to determine the water status of two most relevant row-crops in the region, sugar beet and super high-density olive orchards. From the data obtained, the use of an airborne low-cost infrared sensor to determine the canopy temperature has been validated. Also the reliability of sugar beet canopy temperature as an indicator its of water status has been confirmed. The empirical development of the Crop Water Stress Index (CWSI) has also been carried out from aerial thermal imaging combined with infrared temperature sensors and ground measurements of factors such as water potential or stomatal conductance, validating its usefulness as an indicator of water status in super high-density olive orchards.

To contribute to the development of precise weed control systems, a system for detecting tomato plants and measuring the space between them has been developed, aiming to perform intra-row treatments in a localized and precise way. To this end, low cost optical sensors have been used and compared with a commercial LiDAR laser scanner. Correct detection results close to 95% show that the implementation of these sensors can lead to promising advances in the automation of weed control.

The micro-level field data collected from the evaluated affordable sensors can help farmers to target operations precisely before plant stress sets in or weeds infestation occurs, paving the path to increase the adoption of Precision Agriculture techniques.

Research contribution

This thesis by compendium of articles includes three works in which the author has been involved. All three papers have been able to satisfactorily fulfil their initial hypotheses and have been published in scientific journals.

Because they are articles in collaboration with other co-authors, the contributions of the PhD candidate in each one of them are summarized below.

Publication 1. A cost-effective canopy temperature measurement system for precision agriculture: a case study on sugar beet

Contributions of the PhD candidate:

- Analysis of the problem and bibliographical study of the state of the art.
- Development of the temperature measurement system based on low cost sensors.
- Conducting laboratory and field experiments and analysis of results.
- Preparation, drafting and review of the article.

Publication 2. Assessing a crop water stress index derived from aerial thermal imaging and infrared thermometry in super-high-density olive orchards.

Contributions of the PhD candidate:

- Analysis of the problem and set-up of the thermal camera and infrared sensors.
- Conducting field experiments (flights) and contribution to image analysis.
- Review of the article.

Publication 3. Optical Sensing to Determine Tomato Plant Spacing for Precise Agrochemical Application: Two Scenarios

Contributions of the PhD candidate:

- Analysis of the problem and bibliographical study of the state of the art.
- Development of laboratory platform, sensing system and field platform.
- Design and conduction of field experiments.
- Development of image analysis algorithm and data analysis.
- Preparation, drafting and review of the article.

From these scientific publications, the following selected communications to relevant national and international congresses have been derived:

- **Jorge Martínez Guanter**, Manuel Pérez Ruiz, Gregorio Egea Cegarra, Juan Agüera Vega."*A cost effective canopy temperature measurement system for precision agriculture decision support: first year status update*" 10th European Conference on Precision Agriculture. July 2015 Bet Dagan, Israel.
- **Jorge Martínez Guanter,** Manuel Pérez Ruiz, Juan Agüera Vega, Miguel Garrido Izard, David C. Slaughter. ***"****Developing new tools to determine plant spacing for precise agricultural application"* Conference on Agricultural Engineering CIGR-AgEng Jun. 26–29, 2016, Aarhus, Denmark.
- Gregorio Egea Cegarra, Carmen M. Padilla Díaz, **Jorge Martínez Guanter**, José E. Fernandez, Manuel Pérez Ruiz. "*Use of aerial thermal imaging to assess water status variability in hedgerow olive orchards*" International Conference on Agricultural Engineering CIGR-AgEng Jun. 26–29, 2016, Aarhus, Denmark.
- **Jorge Martínez Guanter**, Manuel Pérez Ruiz, Miguel Garrido Izard, Juan Agüera Vega, David C. Slaughter. "*Determinación mediante sistemas ópticos de la distancia real entre plantas de cultivo para un control preciso de la mala hierba*". XV Congreso de la Sociedad Española de Malherbología, Octubre 2015, Sevilla, España.

I. Introduction

1.1 Background

Agriculture has undergone yield-enhancing shifts in the past, including mechanisation before the second world war and the introduction of new crop varieties and agricultural chemicals in the 1950s and 1960s (Grassini et al.,2013). Currently, achieving the transformation to digital and sustainable agriculture is a major challenge that will need to be overcome without jeopardising the capacity of the agriculture sectors to meet the world's food needs (FAO, 2016). In the coming decades, population increases will be concentrated in regions with the highest prevalence of undernourishment and high vulnerability to the impacts of climate change, while global food demand in 2050 is projected to increase by at least 60 per cent above today's levels (FAO, 2016). Therefore, food production must be increased and enhanced by adopting different methods such as expanding arable areas where possible or intensifying yields and cropping intensity. Whatever the alternative, its necessary to achieve this goal with the least disturbance to environmental parameters while meeting food safety requirements and with the highest efficiency possible with regard to the use of natural and human resources.

This context of food insecurity, similar to that proposed in Malthusian predictions, has been largely restrained by the advent of the so-called the "new green revolution". This new paradigm seeks an information-guided plant production, relying on precision agriculture (PA) techniques that allow the study of fields at a much finer resolution. Farmers have always known that crop in certain areas of their fields grow and produce differently than others (Mulla, 2017), but until the arrival of these site-specific handling techniques, farmers lacked the technology to enhance their ability to make spatially-precise management decisions. Accurate crop management helps farmers tailor inputs such as agrochemicals, water or energy based on diverse information sources. Advances in data collection, mechatronics, yield monitoring, remote and proximal sensing, and controlled agricultural traffic using improved GPS-guided farm machinery or variable rate application directly affect the quantity and quality of the crop, the efficiency of the operations and their environmental impact (Zude-Sasse et al., 2016).

The economic benefits of these site-specific management techniques are well documented (Heege, 2015; Smith et al., 2013; Zhang et al., 2012; Whipker et al., 2009)

and can lead to dramatically reduced environmental impacts while increasing profitability; however, a low adoption rate is still reported by experts and researchers (Lambert et al., 2015; Ellis et al., 2010; Tey et al., 2012). Among other factors, such as a lack of information and education on ICT or the access to bank credit (Aubert et al., 2012), wider adoption is also limited because of the high costs associated with the technology and because the development of new technology is designed for large-scale production, in which within-field variations are great enough to justify the cost of the technological equipment (Cassman, 1999).

The adoption of PA by small-scale producers can be accomplished progressively by focusing on incorporating technologies that are less expensive, adapted to the conditions of their fields or machinery, easy to use and with standardised components and programming languages. This adoption through cost reduction is essential if smallholders in high-potential areas are to intensify their production and contribute to economic growth. It is also essential in semi-arid or remote areas to manage and augment the natural resource base to promote development (Poulton et al., 2010).

Under this scenario, it is in horticultural or industrial crops (with higher added value) in which efforts must be made to incorporate more affordable systems, which allow data collection, field monitoring or variable applications to achieve the same yields but at a lower cost.

Horticultural crops are typically grown in row patterns, forming a semi-structured environment in which there are different canopy structures for different growth stages (Yao et al., 2009). This configuration allows greater individual plant control than arable crops at initial stages and the automation of certain tasks such as inter-row weeding, automatic plant scouting or autonomous navigation between crop lines.

Although drip or sprinkler irrigation systems are commonly used in the aforementioned row crops and intelligent weed control systems are already commercially viable (e.g. Weedseeker®) the heavy reliance of data for precision management still remains a barrier. Data is becoming ever more valuable, as agricultural business development and food policy decisions are being made based upon data (Ferris et al., 2016).

Traditional data collection through sampling or hand measurements in these environments can be a daunting task, which contributes to the fact that manual labour is an important cost component (Bechar et al., 2016). One of the important requirements of agricultural automation systems is that sensors must obtain accurate data in a robust and field-deployable manner. Thus, automated sensor-data gathering fulfils the need to

measure a biosystem's behaviour and allows the possibility of correction if measurements are not compliant with the proposed objectives.

Methods for this data collection can be roughly divided into proximal measurements taken from ground-based platforms or vehicles and remote measurements taken from airborne sensors on unmanned aerial vehicles (UAVs), planes or satellites (Slaughter, 2014).

On the one hand, sensing devices such as conductivity, optoelectronic, image or distance sensors mounted on terrestrial platforms have been widely applied in precision agricultural studies for mapping environmental and crop factors. In recent years, several studies on ground-based sensing have been conducted, including studies on soil characterisation from texture, salinity or ground-water content using electromagnetic induction sensors (Doolittle et al., 2014; Quebrajo et al., 2016; Niu et al., 2015; Gumiere et al., 2014), as well as on-the-go soil cutting resistance sensors (Agüera et al., 2013), which have also been designed and tested to generate soil strength profile maps. Ground-sensing vehicles or platforms have been developed for phenotyping and diagnosing crop conditions based on reflectance data through close visible, multispectral or hyperspectral sensing (Andrade-Sanchez et al., 2014; Busemeyer et al., 2013; Bu et al., 2017; Kitchen et al., 2010; Caturegli et al., 2015). Advanced ground image techniques have been employed for measuring structural crop parameters such as leaf area index (LAI) or seasonal canopy development (Yang et al., 2017). Weed detection and control have also been conducted using terrestrial optoelectronic sensors (Andújar et al., 2011) and using crop-plant precise spatial position (Sun et al., 2010), colour, shape or spectral signature features to discriminate between weeds and crops (Wendel et al., 2016; Zhang et al., 2012; Romeo et al., 2013; Peteinatos et al., 2014). Distance sensors such as ultrasonic and light detection and ranging (LiDAR) have been used mounted on terrestrial agricultural platforms not only as navigation and mapping elements but also for crop height and biomass measurements (Andújar et al., 2016), harvesting damage evaluation (Martinez-Guanter et al., 2017), characterisation of crop structures (Underwood et al., 2015; Escolá et al., 2015), and variable application of agrochemicals based on canopy dimensions (Llorens et al., 2010).

On the other hand, aerial data collection has undergone a considerable change with the growth of UAVs, which have given birth to new, powerful sensor-bearing platforms for various agricultural applications. The ability of UAVs to fly at low altitudes carrying airborne sensors, allows data acquisition with both ultra-high spatial and spectral resolutions (Pajares, 2015), while UAVs also provide easy and fast mission design,

reusability, and cost-effectiveness, and open-source frameworks are specifically designed for UAVs (Urbahs et al., 2013).

UAVs are a technology capable of obtaining and conveying agronomically relevant data: multispectral or hyperspectral airborne sensors allow tasks such as mapping vegetation cover (Torres-Sánchez et al., 2014), deriving vegetation index data (Agüera et al., 2015; Berni et al., 2009), field phenotyping and estimating nitrogen (Zaman-Allah et al., 2015), reconstructing 3D orchards (Nevalainen et al., 2017; Díaz-Varela et al. 2015), estimating topsoil moisture (Hassan-Esfahani et al., 2014) or early detection of diseases using chlorophyll fluorescence (Zarco-Tejada et al., 2012; West et al., 2017). As detailed in the subsections 1.2 and 1.3, multispectral airborne sensors have also been used in weed detection and mapping (Peña et al., 2013), while infrared thermal cameras have been employed to determine plant-water status and plant physiological conditions (Gonzalez-Dugo et al., 2015) through sensing approaches that must be assessed with plant-truth data, e.g., stomatal conductance (g_s) and leaf water potential measurements (c) (Gago et al., 2015).

However, the use of drones in agriculture is not limited to imaging or scouting of crop diseases, pests, weeds or water deficits. Recently, drones have been used to perform tasks such as selective ultra-low-volume herbicide application (Zhang et al., 2016; Giles et al., 2015; Huang et al., 2009) or remotely aerial controlled seeding and reforesting (Wired, 2015).

In this thesis, the use of low-cost remote sensors mounted on aerial and terrestrial platforms for different crop management tasks in row crops is addressed. The suitability of implementing this type of sensors to carry out sustainable agricultural activities on relevant crops in the Andalusian region was tested in comparison to commercial sensors of higher cost. Thus, affordable systems that will aid the advancement of automated weed control in tomato crops (*Solanum lycopersicum* L.) were developed. In addition, the use of infrared sensors mounted on UAVs to monitor water stress in sugar beet (*Beta vulgaris* L.) and to assess the crop water stress index in super-high-density olive groves (*Olea europaea* L.) was explored. The following subsections present in detail the advances that have been made in weed control and in the use of thermography as a tool for efficient irrigation water management.

1.2 Advances in Automated Weed Control

Infestations of crop weeds are a ubiquitous annual threat to productivity and must be minimised to ensure global food supply and food security. In today's context, where

agricultural labour costs are rising, the use of a human workforce in heavy, repetitive and potentially health-damaging tasks such as manual weed control is bound to decline dramatically (Perez-Ruiz et al. 2014).

Therefore, the emergence and advantages of synthetic herbicides over other control methods have made them a "technology" on which there is almost exclusive reliance for weed control; these compounds are highly effective but are not a completely suitable solution to the complex challenge that weeds present (Harker et al., 2013). Their overuse, intended to be addressed through the implementation of agri-environmental measures at the policy level, has led to a rapid onset of herbicide-resistant weeds, motivating researchers to propose a multifaceted approach in order to mitigate the evolution of herbicide resistance (Norsworthy et al, 2012), including diversification of weed-control techniques.

Automatic weed control can contribute to a reduction in both hand weeding and herbicide use, allowing the field deployment of other implements that have lower development costs than new herbicide active ingredients (Kraehmer et al., 2014).

1.2.1 Automatic weed-control systems.

Recent advances in mechatronics regarding electronic controllers and actuators, and their progressive implementation in agricultural fields, have enabled the development of effective labour-saving technologies for automatic weed control. These automatic systems can be divided into two major types: those that act by physically removing the weed, and those that apply herbicide accurate and selectively (Fennimore et al., 2016). Among the physical removal systems, we can distinguish between those involving mechanical means or those that use methods such as thermal control, abrasion or other types.

On the one hand, traditional mechanical control systems such as cultivators have proven their effectiveness in eliminating weeds between rows of crop. However, intra-row mechanical weed removal without damaging the crop remains a challenge on which producers and researchers are still working. From these studies regarding intra-row weeding, the development of advanced intelligent cultivators (ICs) has emerged: Perez-Ruiz et al. (2012) designed a system based on two cutting blades travelling below the soil and between transplanted tomato plants along the row-centreline. An intra-row weeding roller mechanism was designed and developed by Saber et al. (2013). Other examples of ICs are the intra-row weeding hoe developed by Rasmussen et al. (2012), where rotating tines are moved within the crop row, or the rotating disks designed and tested by Dedousis et al. (2007).

At present, there are only a few commercially available ICs, such as the *Robocrop InRow* system (Garford Farm Machinery Ltd, England) that uses a variable-speed rotating, semicircle-shaped disc blade for hoeing, and has been tested in celery, lettuce, and radicchio crops in California (Fennimore et al., 2014). Other examples of commercial ICs are the *Robovator* System (F. Poulsen Engineering ApS, Denmark), which employs a set of electronically controlled tines and which has been tested in lettuce and broccoli cultivars (Lati et al. 2016), and the finger weeder system developed by *Steketee* and tested in lettuce (Hemming et al., 2011). Most of these commercial systems are actually being semi-experimentally used in horticultural row-grown crops, where their capabilities and benefits are still being tested.

Other methods for physical weed control are in their earlier developmental stages but on their way to becoming commercially robust systems (Fennimore et al., 2016). The experimental use of on-the-go automated flamers such as the cross-flaming implement in the RHEA project (Frasconi et al. 2014) and the flaming implement mounted on the commercial IC *Robovator* System (F. Poulsen Engineering ApS, Denmark) are examples of reliable field-deployable machines that burn weeds where detected.

Non-chemical weed control has also been tested using laser technology, where the laser beam must heats the growing point of the weed (apical meristem) to stop its development eliminating it (Blackmore, 2014). Kaierle et al. (2013) performed trials with lasers of different wavelengths, while other research groups have mounted weeding lasers in robotic systems (Shah et al., 2015) or on robotic arms (Zhenyang et al., 2013). The efficiency of this type of laser system depends to a large extent on the accuracy of locating the apical meristem and on the exposure time, which limits its use in mobile systems at normal working speeds (1-2 $km.h^{-1}$). Effective control using these systems also depends on laser power and wavelength and the weed species (Fennimore et al., 2016).

Another approach to physical weed control involves abrasion by the projection of sand or residues of agricultural products on the apical meristem using a stream of high-pressure air (Wortman, 2014; Forcella, 2013; Forcella, 2012; Forcella, 2009). Currently, our research group is working on the feasibility of an implement capable of performing this abrasive weeding automatically.

On the other hand, automatic precision spraying is a form of chemical control that seeks to apply herbicides accurately and selectively. In this type of spatially selective applications, targeted areas may be on the scale of square centimetres, many orders of magnitude smaller than conventional, traditional herbicide application. Since the early

2000s, several researchers have developed robotic implements or platforms for precision spraying, obtaining acceptable results closely linked to low travel speeds (Young and Giles, 2014; Fennimore et al., 2016). Precise application systems such as the LettuceBot (BlueRiver, California) use a series of sensors to detect unwanted plants (see section 1.2.2) and can achieve a success rate up to 90% in detection and application using an intelligent nozzle control system. The steps in assembling this type of equipment in a conventional tractor were provided as part of the framework of the European project RHEA, in which an intelligent implement was designed and constructed that is capable of performing herbicide micro-applications in previously detected weed patches (Pérez-Ruiz et al., 2015). In addition, one of the systems that are experiencing a major boom in recent years regarding the automatic application of herbicides is that based on aerial platforms performing ultra-low-volume treatments on selected weed patches (Krishna, 2016; Zhang et al., 2016).

1.2.2 Automatic weed-detection systems.

Automatic weed-control systems such as those proposed in the previous subsection rely on an accurate detection of weeds, and the reliable discrimination between weeds and crop plants. Spatial distribution and plant spacing are considered key parameters for characterising a crop. Thus, the detection system is intended to collect information on target areas and make weed-control decisions. To this end, Sun et al. (2010) and Pérez-Ruiz (2012) proposed an approach using real-time kinematic (RTK) global navigation satellite systems (GNSS) to identify the exact position of each transplanted tomato plant in a field in a way that any subsequent task (including weed control) should avoid these coordinates. This approach has the advantages of requiring less computing resources or certain lighting conditions. However, the field tests carried out have shown differences between RTK-GNSS-based expected seed location versus actual plant position with an uncertainly of approximately 3 cm for seeds and tomato plants.

Today, the predominant technology for plant detection is computer vision, which it represents a robust and powerful method to discriminate between crops and weeds. Differentiation under field conditions becomes difficult because highly variable natural objects must be discriminated from a background with its own highly random characteristics. A variety of visual characteristics can be used for plant species identification such as morphology, spectral reflectance and visual texture (Slaughter et al., 2008). Several steps are involved in the process of a computer vision-based sensing system, beginning with image acquisition and subsequent image segmentation, features extraction (shape, colour, texture…) and final decision making (Peteinatos et al., 2014).

Multispectral and hyperspectral cameras on land platforms have been widely used to detect and locate weeds in lettuce and tomato crops (Zhang and Slaughter, 2011; Piron et al., 2009), even on commercial platforms such as the aforementioned IC Robovator System (F. Poulsen Engineering ApS, Denmark), and have achieved 90% effective discrimination rates.

As noted above, the use of these multispectral and hyperspectral sensors has also generated increasing interest in the growth of aerial platforms for remote sensing. Weed detection and location from UAV images have been extensively documented (Lopez-Granados et al., 2016; Torres-Sánchez et al., 2013) and demonstrate a greater spectral differentiation between crops and weeds. In addition to the use of 2D images, the price reduction of the 3D image sensors has motivated researchers to use them for the location and discrimination of weeds or crop plants (Gai et al., 2015).

Considering the structure of weeds, in most computer vision-based systems developed in recent years, an approach based on the combined use of images and machine learning is used to extract the morphological characteristics of weeds and classify and discriminate them from the crop. In this application, Bayesian classifiers have been employed (De Rainville et al., 2014), and classification algorithms based on Random Forest (Haug et al., 2014) and pattern-matching algorithms have been developed (Priyadharsini et al., 2015). This is a promising field, and more accurate classifiers capable of working under field conditions will be developed in next years.

Despite their advantages, computer vision systems still have some drawbacks: the use of delicate cameras in ground environments where there are external elements such as dust, mud, etc., may present difficulties for the acquisition of high-quality images. These systems also require complex hardware systems and environments with adequate lighting, which increases the costs of such systems. In addition, in agricultural environments, it is necessary to define suitable ground truth data, as machine learning systems have to be fed datasets that allow them to differentiate between different plant types.

Other sensors used in proximal sensing for the location of the plants and their classification are LiDAR (Light Detection and Ranging) sensors. These devices measure the distance between the sensor and the target by the emission and reception of an infrared light pulse, also capturing the intensity of the reflected signal, allowing one to distinguish between different elements of vegetation and to differentiate vegetation from the soil. LiDAR sensors provide the morphological structure of the plant/weed, allowing them to be characterised (Llop et al., 2016), defining the geometrical structure of the crop

lines (Andújar et al., 2013) and performing tailored treatments on crops based on their structure (Miranda-Fuentes et al., 2016). In addition to the present work, other authors have explored the use of inexpensive sensors to perform scanning tasks similar to those of LiDAR for the purpose of using them in phenotyping systems of sugar beet varieties (Paulus et al., 2014).

There are other sensors for weed detection that are not evaluated in the present work but have been studied in a relevant way by other authors, including fluorescence, X-ray or gamma sensors and ultrasonic sensors.

Chapter 3 of this thesis explores the use of optical sensors such as inexpensive infrared light-beam sensors and affordable vision systems compared to the use of LiDAR sensors for the measurement of space between plants as a preliminary step to perform tasks such as intra-row physical weed removal among tomato crop plants.

1.3 Crop Water Stress, Aerial Thermography and Smart Water Management.

Climate change has caused changes in seasonal patterns and triggered periods of more intense drought in recent years. Therefore, there is a special interest in drought prone areas in improving water management through new strategies, among which regulated deficit irrigation (RDI) has stood out in recent years. Through the use of new technologies based on remote sensing, it has been proposed to study the potential of thermal imaging and infrared thermometry to monitor the effects of this type of management in sugar beet crops and super high-density olive orchards.

Leaf or canopy temperature (T_C) has been defined as an indicator of the crop water status (Tanner, 1963; Jackson et al., 1977). A higher leaf temperature is a plant's physiological response to water stress. Plant moisture stress occurs when the demand for water exceeds available soil moisture. When this occurs, the stomata close to minimise water loss through evapotranspiration. This stomatal closure generates a decrease in the latent heat flux, and because the energy flow must be balanced, there is an increase in the sensible heat flux (increase in leaf temperature). Therefore, the difference between T_c and T_a (air temperature) is linearly related to evapotranspiration under stable conditions (Monteith, 1981) and has been frequently used to detect drought stress and to evaluate the response of a plant to variable irrigation regimes (García - Tejero et al., 2011).

In spite of this, T_c may not be completely adequate to evaluate plant-water relations accurately; temperature variations may be due to water stress, but they are also affected

by other changes such as daytime or seasonal temperature variation, meteorological phenomena or other morphological factors. Therefore, measured crop temperatures must be normalised. To this end, Idso et al. (1978) proposed the concept of stress degree day (SDD), which is calculated as the difference between the deck temperature and the measured ambient temperature at 14:00. This concept, which integrated a single measure per day, was modified by Jackson et al. (1981) and Idso et al. (1981), formulating the crop water stress index (CWSI), which has been widely accepted as a standard indicator, despite the need for additional climate information such as the vapour pressure deficit (Siegfried et al., 2017). This index provides a value between 0 (indicating no stress) and 1 (representing maximum stress), and there are three different methodologies for calculating the CWSI: the empirical method, the energy balance analytical method and a method that employs reference surfaces (Maes and Steppe, 2012).

The empirical method relates the measured air temperature T_a, canopy temperature T_c and vapour pressure deficit for plants (Idso et al., 1981). This method is based on the fact that the temperature variation value decreases linearly with the vapour pressure deficit. This relation results in a formulation of a minimum (lower) baseline or non-water stressed baseline (NWSB) for plants transpiring at a potential rate and an upper limit baseline for non-transpiring, completely stressed plants. (see figure 0.1).

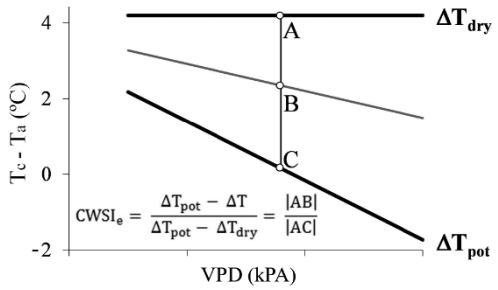

Figure 0.1: The canopy–air temperature difference (Tc -Ta) versus air vapour pressure deficit (VPD) for non-water stressed (ΔTpot) and maximally stressed (ΔTdry). Baseline approach of the crop water stress index calculation (Idso et al., 1981). Adapted from Maes and Steppe (2012).

The CWSI is obtained from the equation (1) as follows;

$$CWSI = \frac{(T_c - T_a) - (T_c - T_A)_{LL}}{(T_c - T_A)_{UL} - (T_c - T_A)_{LL}} \qquad (1)$$

where $T_c - T_a$ denotes the difference between air and canopy temperatures, $(T_c - T_A)_{LL}$ is the lower stress limit and $(T_c - T_A)_{UL}$ is the upper stress limit described above.

Because of low data collection requirements and the immediacy of the calculation (Maes and Steppe, 2012), the empirical method has been used by many authors for scheduling irrigations and mapping the variability of water status in different crops. Non-water stressed baselines (NWSB) should be defined for this empirical index calculation. Empirical $CWSI_e$ has been widely studied in different crops such as potatoes (Rud et al., 2014), citrus orchards (Gonzalez-Dugo et al., 2014), fruit trees such as nectarine or peaches (Bellvert et al., 2016), grapevines (Bellvert et al., 2014; Moller et al., 2007) and olives (Berni et al., 2009; Ben-Gal et al.,2009). $CWSI_e$ has also been used as a tool for irrigation scheduling in a variety of crops such as soybean (Nielsen, 1990), pistachio (Testi et al., 2008) and commercial palm trees (Cohen et al., 2012) or to estimate the yield of a corn crop (Irmak et al., 2000) and broccoli (Erdem et al., 2010).

However, the empirical method has a disadvantage in that it is a more reliable indicator in crops that homogeneously cover the soil (Maes and Steppe 2012). Furthermore, as it depends on the atmospheric factors: under conditions of low VPD, there is practically no difference between the T_c-T_a of well-watered and stressed plants. The energy balance method, in addition to the vapour pressure deficit, takes into account net radiation differences and crop aerodynamics (Jackson et al., 1982). The weakness of this method is that the variables used are very sensitive to change, increasing the complexity of the measurements. Wang et al. (2005) used this method to estimate $CWSI_a$ in an extensive crop such as wheat, and it has also been used in cotton (Alchanatis et al., 2010; González-Dugo et al., 2006) and in peach trees (Wang et al., 2010).

The third method for calculating the CWSI may also be the simplest; it is based on the use of wet and dry references (Jones 1999; Jones 2009; Cohen et al., 2005), which is particularly helpful since these references can readily be used for the derivation of indices that do not require detailed environmental information. The most common way to generate these references is to wet the leaves or canopy (T_{wet}) and to cover the leaves with glycerine to prevent the leaves from transpiring (T_{dry}), although it has also been proposed by different authors to the use of wet artificial reference surfaces (WARS).

Plant evapotranspiration (ET) is an alternative parameter used to determine crop water needs (Davis and Dukes, 2010), and its defined as the evaporation from the soil surface and the transpiration from the plant/tree. As its affected by environmental parameters such as air temperature, relative humidity, wind speed or solar radiation among others, a reference evapotranspiration ET_0 must be defined. ET_0 represents the theoretical ET of a well-watered, non-stressed lowland meadow crop as it was defined by Doorenbos and Pruitt (1977) and can be calculated by means of the Penman-Monteith equation

(FAO-PM, equation not presented here). As showed later, crop ET has been used for a widely number of studies to determine crop irrigation needs and scheduling irrigation.

To map the variability of the water content and needs of the crop or better understand the stomatal regulation of leaf gas exchange, conventional methods such as the use of gas exchange chambers (Turner et al., 1984; Ahmed et al., 2009; Moriana et al., 2002) or the pressure chamber for measuring leaf water potential (ψ_L) (Scholander et al., 1965) involve discrete sampling and can be time consuming and limited by the number of samples that must be obtained to be significant. Therefore, there is a need to analyze the water status of the crop in a quick, remote and non-invasive way, and thus in recent years, the use of infrared thermometry and thermal sensors has gained popularity, also motivated by the reduction of the costs and the improvement in its technology (Costa et al., 2013).

Infrared thermometry has proven its utility for measuring canopy and leaf temperatures, but like the CWSI, measures should be standardized based on the environmental and specific factors of each zone. Jones (1999) developed a stomatal conductance index I_g (see equation 2 below) specific for infrared thermometry, calculated by wet and dry reference, and taking into account the air temperature (Maes et al., 2011).

$$I_g = \frac{T_{dry} - T_1}{T_1 - T_{wet}} = \frac{g_s}{G} \qquad (2)$$

Where g_s is the stomatal conductance and G is the parameter dependent on the air temperature. In contrast to the CWSI, higher I_g values indicate lower plant stress (Costa et al., 2013).

In addition to developing water status indexes such as CWSI or I_g, infrared thermometry has been used for prediction of crop yields (Ajayi et al., 2004; Sepaskhah et al.,1994), crop canopy monitoring (Wang et al, 2010), water use estimations (e.g. for peaches, Glenn et al., 1989) or irrigation scheduling (Zhang et al., 2017; O'Shaughnessy et al., 2014; Davis and Dukes, 2010). The sensors used for infrared thermometry have evolved from the first thermocouple devices to a variety of both hand-held and stationary infrared thermometers, even been mounted on centre pivots (Colaizzi et al., 2017), where having a narrow field-of-view is valuated to properly separate between soil and plant measurements in cases where crops do not completely cover the soil. This type of sensor is generally interfaced with a datalogger for continuous data recording, although wireless infrared thermometer networks have been developed in recent years, which have great potential in outdoor applications (O'Shaughnessy et al., 2011).

The other method for plant stress sensing of scope for this thesis is the use of remote sensing techniques based on infrared thermal imaging (thermography), which has undergone a great boom since the 2000s due to commercial availability of (relatively) inexpensive thermal cameras (Maes and Steppe, 2012). Thermal cameras capture the energy of electromagnetic radiation that a body emits according to Plank's law. This amount of energy was defined by Stefan-Boltzmann's law, according to equation 3 below, as a function of the product of the emissivity, the Stefan-Boltzmann constant and the surface temperature.

$$W = \varepsilon \sigma T_s^4 \qquad (3)$$

Based on this, thermographic sensors are able to capture the region of the electromagnetic spectrum with infrared wavelengths of between 7 and 13 μm, and to obtain the crop temperatures. This type of remote sensing technologies have increased in several orders of magnitude the capacity to make a large and continuous spatial coverage in a short time, in a more economical way and allowing the obtaining of data in zones in which the manual temperature measurement could be complicated (Li et al. 2009). The radiometric surface temperature obtained in the thermal images allows to show differences between zones under different irrigation regimes (Zarco-Tejada et al., 2012). The use of thermal cameras for the stress quantification is particularly useful in the species or varieties that exhibit isohydric behaviour (Jones et al., 2009), in which the information provided by the pressure chamber is not significant. In this type of behaviour there is a strong stomatal regulation that prevents significant decreases in the water potential of the leaf (Fernandez et al, 2014).

As reviewed by Khanal et al. (2017), the thermal cameras have been evaluated at both ground and aerial levels. Ground-based measurements has been conducted with the cameras being mounted on masts or cranes for the determination of CWSI in crops such as vine, pistachio or peaches (Rud et al., 2014; Alchanatis et al., 2006, Testi et al. 2008, Wang and Gartung, 2010), while airborne thermal sensors have been used on manned aircraft overlying different crops such as olive trees and fruit trees (Bellvert et al., 2016; Sepulcre-Cantó et al., 2006; González-Dugo et al., 2013) or mapping water stress being mounted on UAVs and flown over vineyard (Bellvert et al., 2014) as a tool for precision irrigation on pistachio (González-Dugo et al., 2015) or for measuring canopy temperature and identification of different irrigation regimes in olive orchards (Berni et al., 2009) among other examples. Thermal cameras have also been used successfully in other aspects such as the detection of diseases such as fusarium or downy mildew (Calderón

et al., 2014; Oerke and Steiner, 2010; Oerke et al, 2006), or field phenotyping (Tattaris et al., 2016).

It is exactly due to the popularization of these unmanned aerial platforms that has caused the rise of the studies of thermography applied to agriculture, since they allow image capturing in sub-metric resolutions, with the sampling frequency needed for each case, allowing flight planning to be tailored to the needs of each crop and at different heights, and even perform static flights for aspects such as the detection of irrigation accidents.

However, it is necessary to emphasize that thermal cameras need a previous radiometric calibration (Berni et al., 2009) in order to provide accurate temperature measurements, which generally must be realized using a laboratory black body (with emissivity 1), that are usually expensive. In addition, the acquisition of thermal datasets frequently implies its later processing to obtain orthomosaics with embedded thermal information. Unfortunately, processing of thermal data with current commercial mapping software does not always work flawlessly, since the alignment and analysis of subsequent radiometric information still remains a challenge, due to limited information contained by thermal images compared to RGB images (Maes et al., 2017).

All of the data generated through the aforementioned remote sensors, and the information extracted from them, should revert to a practical utility for water management. Traditional irrigation systems undergo both social and political pressure to increase their irrigation efficiency, achieve higher water productivity and use less water (Pereira et al., 2012). These traditional irrigation systems have generally been aimed at preventing crop water stress throughout the growth cycle, and have been based mainly on qualitative data, previous experiences or shallow estimates, causing overirrigation in some areas of the field while others remain underirrigated. A new approach based on the use of quantitative data is necessary to be able to perform a specific water management.

In areas of water scarcity or drought-prone areas, controlled deficit irrigation (CDI) has become one of the most common strategies for maintaining production and reducing water consumption. CDI strategies are based on reducing irrigation during certain periods of the growth cycle where the crops have a low sensitivity to water stress (Egea et al., 2009). Information about plant, soil, weather, water supply systems must be considered on this scheduling to tailor irrigation operations to specific demands.

Smart water management must take into account the inherent variability of cropping systems, adapting management to different field areas to conduct a variable rate irrigation (VRI). VRI involves deciding when, where and how much water to apply on an

accurate way with techniques based on sensors that can assess soil, water and atmospheric parameters (Hedley et al., 2014).

Applying the concept of management units as zones in which the soil has similar characteristics in terms of texture or water retention capacity (Martínez-Casanovas et al., 2009), individual elements (plants or trees) that are representative of these management units can be monitored. This monitoring should be seen as the application of several sensing technologies to determine soil moisture dynamics and water use (Adeyemi et al., 2017).

In order to carry out on-site monitoring at field scale, sensors are installed to measure and characterize soil and plant properties, as well as small meteorological stations to record micro-climatic variables. Proximal soil sensing allows to know the moisture content of the bulb, based on measurements of electrical conductivity and temperature, while sensors can be placed at different depths to obtain various moisture profiles. Meanwhile, sensors can be used in the plant to monitor variables such as temperature using infrared thermometers, changes in trunk and sap flow using dendrometers or leaf turgor pressure. Climate sensors usually obtain data on relative humidity, wind speed, ambient temperature, etc. With the development of wireless technologies, in recent years there has been a boom in the development of networks of sensing devices known as sensor nodes or motes (Call ICT-Agri-Project VAROS, 2016; Yu et al., 2013; Shah et al., 2012), in which data is automatically collected continuously and sent to a cloud server, able to process them and display them in a graphical interface.

As reviewed by Hedley et al., (2014), modern VRI systems also can incorporate adaptive electronic control systems to automatically and continuously readjust the irrigation application system (i.e. by controlling electrovalves) and to apply the necessary dose, taking into account the spatial and temporal variability in the requirements and water intake of the crops.

A key component of any VRI system is the Decision Support System (Adeyemi et al., 2017), capable of managing in real time the information coming from sensors, generating irrigation alerts and giving recommendations. These DSS represent the core of any automated agricultural management based on variability, so that support decisions and control actions through the use of extensive databases obtained in real time. This type of management support system still presents some challenges, since algorithms that take into account the singularities of the crops and varieties of each region must be generated.

Information-to-action decision processes for field operations will be largely conditioned by the accuracy of the initial data taken in situ (Kitchen 2008), as well as the ability of the DSS to transform this data into knowledge and include it in farm management information systems (FMIS) (Fountas et al., 2015). In the near future, FMIS will play an important role in the adoption of precision technologies, in order to establish the interrelationships between farm machinery or irrigation systems and their surroundings, through proximal or remote sensing.

II. Overall Summary of the Objectives

This doctoral research focuses on the use of proximal sensors in row crops with the purpose of contributing to physical weed-control techniques and managing water resources for optimum crop development.

The **general objective** of the thesis is the analysis, design, implementation and validation of the use of affordable sensors, mounted on aerial and terrestrial platforms, for **i)** for the study of the response to water stress in sugar beet and super-intensive olive orchards and **ii) to** accurately measure plant spacing in transplanted tomato row crops. To validate of these types of sensors, the systems developed and tested must meet following requirements; i) achieving acceptable accuracy (compared to commonly used higher cost sensors), ii) requiring less computing power, and iii) being generic enough to be adapted to work under different conditions.

A series of **specific objectives** are proposed to achieve this global objective, which are:

1. To develop an affordable, robust system for infrared temperature measurement based on open-source software/hardware.
2. To determine, under the same field conditions, the effectiveness of the methodology by comparing sugar beet canopy temperature measurements taken by the developed system and those from a conventional thermal camera.
3. To evaluate the suitability of the crop water stress index (CWSI) derived from aerial thermal images as an indicator of seasonal dynamics on water status in super-high density olive orchards.
4. To design and evaluate a sensor platform with affordable components, for the accurate detection of tomato row plants and measurement of automated plant spacing.

   To compare, under the same conditions, the performance of the inexpensive optical sensors (light-beam and Kinect camera) on the platform to LiDAR sensor efficiency.

III. Publications: Chapter 1

A cost-effective canopy temperature measurement system for precision agriculture: a case study on sugar beet

Martínez-Guanter, J.[1]; Egea Cegarra, G.[1]; Agüera Vega, J.[2]; Pérez-Ruiz, M.[1]

[1]Area of Agroforestry Engineering, Aerospace Engineering and Fluids Mechanic Department, School of Agricultural Engineering, Universidad de Sevilla, Ctra. Utrera km.1, 41013 Seville, Spain

[2] Department of Rural Engineering University of Córdoba Córdoba Spain

Published on:

Precision Agriculture
February 2017, Volume 18, Issue 1, pp 95–110
DOI: 10.1007/s11119-016-9470-9

Abstract

Increasing agricultural efficiency in a sustainable manner will contribute to feed a growing population under limited land, nutrient and water resources. Water scarcity and the increasing social concern for this resource are already requiring more sophisticated irrigation and decision-support systems. To address the heterogeneity in crop water status in a commercial field, precision irrigation requires accurate information about crops (e.g., crop water status), soil (e.g., moisture content) and weather (e.g., wind speed and vapor pressure deficit). Numerous studies have shown that plant canopy temperature can be used to derive reliable plant water stress indicators, thus making it a promising tool for irrigation water management. However, efficient and cost-effective measurement techniques are still lacking. This paper assesses the potential of infrared thermometry and thermal imaging for monitoring plant water stress in a commercial sugar beet field by comparing canopy temperature data acquired from a conventional thermal camera with an inexpensive infrared sensor, both mounted on a rotary-wing unmanned aerial vehicle (UAV). Measurements were taken at various phenological stages of the sugar beet growing season. Laboratory tests were performed to determine the key features for accurate temperature measurements and flight altitude. Experiments were conducted in 2014 and 2015 in experimental and commercial sugar beet fields in Southwestern Spain to (i) develop an affordable infrared temperature system suitable for mounting on a UAV to obtain thermal information, (ii) compare sugar beet canopy temperature measurements collected with the low-cost platform with those obtained from a conventional thermal camera, both mounted on a rotary-wing UAV, (iii) identify the factors that will limit the use of the low-cost system to derive temperature-based water stress indices. To accomplish these objectives, well-watered and deficit irrigated plots were established. Results indicated that the lightweight canopy temperature system was robust and reliable, although there were some constraints related to weather conditions and delimitation of the area covered by the infrared sensor.

3.1 Introduction

Agricultural production must double by 2050 in order to meet the predicted food demands of the world population (Tilman et al. 2011). However, accomplishing this target will be a significant challenge for researchers and farmers because crop production would have to increase at a rate of 2.4 % per year; the average rate of increase is only 1.3 % (Ray et al. 2013). In the last five years, plant phenotyping techniques based on remote sensing have emerged and may be deployed for in situ screening with a wide range of breeding objectives, including yield potential, adaptation to abiotic (water stress, temperature, salinity) and biotic (susceptibility to pests and diseases) stresses, and even quality traits (Li et al. 2014). Thus, there is growing interest in adapting agricultural machinery and electronic sensors for field-based high-throughput phenotyping (White and Conley, 2013). Potential applications are mainly envisaged for genetic research (e.g., in the detection of quantitative trait loci, QTL) and crop improvement but also include monitoring of the crop response to soil and management variability (i.e. precision agriculture) (Andrade-Sanchez et al. 2014). While the tremendous potential for using agricultural and environmental unmanned aerial vehicles (UAV: fixed-wing and rotary-wing platforms capable of carrying different measurement devices) has become evident through multiple applications during the last few years, the challenging requirement profile for both UAVs and imaging sensor units has emerged as more and more farmers are beginning to demand service (e.g., variable-rate N application, finding faults in irrigation systems), and private firms that offer this service for a fee are emerging (Zhang and Kovacs 2012). In contrast to satellite (largely fixed with rigid coverage areas and observation times) or ground-based measurements, the use of a UAV allows coverage of specific areas and obtaining spatially distributed and geometrically high-resolution information on the canopy/ground temperature. Satellites compensate their rigid flight schedule with extremely large coverage areas, while UAVs are capable of flying at any time and much lower altitude, hence collecting imagery at a much higher spatial and temporal resolution (Hunt et al. 2010; Berni et al. 2009a). Many researchers agree that the main disadvantage of many UAVs is the very limited payload. However, light-weight sensor systems are currently being investigated (Crawford et al. 2014; Colomina and Molina 2014). The use of appropriate sensor platforms can support site-specific management strategies by providing information with a very high spatial (centimetre level), temporal or even radiometric resolution (Zhang and Kovacs 2012). These platforms are excellent tools for crop monitoring and they could significantly reduce the

crop scouting costs for growers (Ehmke 2013). Most importantly, early detection of plant diseases could prevent their spread and minimize crop losses. Xu et al. (2014) and (Li et al. 2014) developed and used a rotary-wing aircraft sensing system that included a spectral imager to automate disease detection and an analysis process for strawberries (Botrytis fruit rot) and citrus (citrus greening disease-*Huanglongbing*), respectively. Calderón et al. (2013) used a fixed-wing aircraft UAV to acquire hyperspectral and thermal imagery as an indicator of Verticillium Wilt infection and severity in olive orchards. Another recent and growing use of this new technology is to generate suitable weed maps early in the growing season, a task that has not been possible with conventional aerial or satellite imagery due to the lack of sufficient image spatial resolution (Lopez-Granados 2011; Peña et al. 2014). In addition, UAVs can work on demand with great flexibility at critical times according to agronomic goals, which is crucial for detecting small weed seedlings in the majority of crops. The UAV industry has identified precision agricultural applications, including weed control and resource management, as the single largest market opportunity through the year 2015 (Jenkins and Vasigh 2013).

Today, the increasing demand for water resources and increasing environmental concern render plant-sensing devices valuable for irrigation decision-making, such as the use of thermal sensors to generate accurate crop water stress index (CWSI) information (Jackson et al. 1981). This index has been widely used as a crop water status indicator and provides the crop stress level based on canopy-air temperature differences. Many authors have reported morpho-physiological responses of sugar beet to water stress conditions (Hoffmann 2014; Romano et al. 2013; Tsialtas and Maslaris 2012), which is widely considered to be the major limiting factor for yield (Pidgeon et al. 2006). The leaf temperature of sugar beet is considered to be a relevant indicator of drought stress (Shaw et al. 2002). Testi et al. (2008) concluded that more repeatable and effective CWSI values for evaluating tree water status for irrigation purposes were obtained from 1200 to 1500 h (local time), when the CWSI of stressed pistachio canopies reached their maximum diurnal value. To evaluate spatial variations in canopy temperature and relate them to the plant transpiration rate and drought stress, passive sensors (i.e., sensors that measure the characteristic radiation of an object) that provide detailed and highly refined information can be used (Mahlein et al. 2012). Thermography techniques can be applied to proximal or remote sensing. One major advantage of infrared thermal imaging is its non-invasive nature (Lenthe et al. 2007), which enables the use of airborne sensors, as was performed in this work. Thermal imagery used for this objective might provide a suitable tool for model evaluation under variable atmospheric conditions (Ahrens et al. 2014) and have been used for several crops, such

as cotton, soybean, wheat, citrus and grapes (O'Shaughnessy et al. 2011; Ballester et al. 2013; González-Dugo et al. 2013). However, the main concern with these thermal imagery techniques is their cost, especially when compared to the accuracy obtained, and the resolution is frequently insufficient for precision applications. For example, the system employed by (González-Dugo et al. 2013) is advertised to have a thermal image resolution of approximately 1 ºC, which may not be sufficient for measurements taken at times when there is a small range in canopy temperature differences (e.g., mornings). This hurdle can be overcome by using infrared point sensors, as in this work, which can provide an accuracy of 0.5 ºC at more affordable prices than conventional lightweight thermal cameras. The cost of an aerial thermal platform based on infrared point sensors of the type described in this work may represent 3–5 %, or even lower, of the cost of a conventional lightweight thermal camera, making this technology better suited for small to medium-sized farms that cannot afford costly equipment. The objective of this research was to design and validate a LIghtweight canopy TemperAture measurement System (LITAS) that can be mounted on a rotary-wing UAV with a limited payload of 2 kg maximum. The specific objectives were:

(i) to develop an inexpensive infrared temperature system suitable for mounting on a UAV platform to obtain thermal information.

(ii) to compare sugar beet canopy temperature measurements collected using LITAS with those obtained from a conventional thermal camera, both mounted on a rotary-wing UAV.

(iii) to identify the factors that will limit the use of LITAS to derive temperature-based water stress indices.

3.2 Materials and methods

Canopy temperature measurement platform

Canopy temperature measurements were collected by means of two remote sensing devices. These devices consisted of an inexpensive infrared sensor (Melexis, Ypres, Belgium) and a thermal camera (FLIR, Oregon, USA). The thermal camera was used as benchmark to determine whether the proposed low-cost sensing system may provide sufficiently accurate estimates of canopy temperature for sugar beet irrigation management. The inexpensive infrared sensor used an Arduino-based data logger. The infrared sensor, camera and data logger were mounted on a UAV and are described in detail below.

The microcontroller board

The microcontroller (model ATmega32u4, Aduino, Duemilanove, Italy) is an open source board, which has 20 digital input/output pins (of which 7 can be used as pulse width modulation (PWM) outputs and 12 as analog inputs). This microcontroller has built-in USB communication, eliminating the need for a secondary processor and allowing the microcontroller to take control of the USB ports (using libraries). The small dimensions and weight of this microcontroller facilitated mounting on the UAV platform without affecting the navigation performance (Table 3.1).

Table 3.1 Microcontroller specific features

Arduino board features	
Microcontroller:	ATmega32u4
Operating Voltage:	5 V
Input Voltage (recommended):	7-12 V
Input Voltage (limits)	6-20 V
Analog input channels	12
DC current per I/O Pin:	40 mA
Flash memory:	32 KB (ATmega 32a4) of which 4KB used by bootloader
EEPROM:	1 KB
Clock Speed:	16 MHz
Length, width, weigth:	68.6 mm. 53.3 mm, 20 g

Infrared sensor specifications

An infrared thermometer, model MLX90614, was tested over a reference surface at constant temperature in the laboratory, before taking temperatures of the sugar beet canopy. Table 3.2 shows the specifications of the sensor. The sensor was selected because of its small size and its high accuracy-to-cost ratio. The sensor kit consists of a long-wave filter that allows infrared radiation (with wavelengths of 5.5–14 µm) to pass through, a thermopile detector chip and a unique proprietary signal-conditioning chip. The two voltages, V*s* and V*o*, correspond to the respective sensor body temperature (T*a*) and the object or target temperature (T*o*), which is internally compensated for by T*a*. The voltage outputs were converted to temperatures using the following expression (Melexis Data Sheet 2009):

$$T_i(K) = V_j \; x \; 0.02 \qquad (1)$$

where T*i* represents either T*o* or T*a* in Kelvin, being later converted to Celsius degrees and V*j* (measured in Volts) is either V*o* or V*s*.

The advantages of this measurement method included the simple automation of data collection and the low-cost of the system components. The infrared sensor provides

spatial awareness to the infrared temperature measurements, which would otherwise require an expensive thermal imager. The sensor's parameters, such as the emissivity constant K, can be adjusted through an evaluation board (model EVB90614), which acts as the interface between the MLX90614 infrared thermometer and a personal computer (PC). The software enables temperature measurements using a PC as well as reconfiguration of the sensor by modification of the interface type, output ratings and temperature ranges, among other parameters. The emissivity of the sensor was set to 0.98 because this value has been reported to induce errors of less than 1º C (López et al. 2012). To properly calculate the emissivity of a leaf, the actual temperature must be known at each moment; thus, a noncontact hand-held pyrometer, model FLUKE 62 mini (FLUKE Europe, Eindhoven, Netherlands), was used to compare measurements from the infrared sensor and a thermometer in laboratory tests. The temperature measurements were taken such that 100 % of the temperature signal came from leaves. A similar hand-held pyrometer was used by Bellvert et al. (2014).

Table 3.2 MLX90614 temperature sensor technical data.

Sensor features	
Temperature ranges:	-40 … +125 ºC for ambient temperature
	-70 … + 380 ºC for object temperature
Measure resolution	0.02 ºC
Emissivity:	K = 0.85
Accuracy:	± 0.5ºC
Supply voltage:	5 V
Output:	10-bit PWM output
	SMBus compatible digital interface
Output high level: PWMHI	Isource = 2 mA
Field of View:	90º

The sensor was mounted vertically in the middle of the bottom side of the UAV in a nadir-view position. This position helps avoid the influence of air streams generated by the blades of the vehicle, which can artificially lower the registered temperature. The data acquired by the sensor were collected using an Arduino Leonardo board because of the broad possibilities of environmental adaptation provided by this method. An ethernet/ MicroSD shield was used as a data logger. This device allowed temperature readings to be stored on an SD card in a text format for analysis on a computer at a later time.

Thermal camera

Thermal images of sugar beet fields were acquired during daytime hours, when the foliage exhibited the highest temperature of the day. The uncooled thermal camera used was the Tau 2 324 model (FLIR Systems, Inc., Wilsonville, OR, USA), which was used for receiving thermal imagery from the crop canopy and comparing the temperature data with the data captured by the infrared sensor. Its main characteristics are summarized in Table 3.3. The camera was installed vertically on the middle of the bottom side of the UAV, positioned next to the IR sensor, and allowed to record video images and adjust the isotherm thresholds to colorize the temperatures of interest on a grey scale.

Table 3.3 Thermal camera technical data

Thermal Camera features	
Scene range	-25 … +135 ºC for ambient temperature
	-70 … + 380 ºC for object temperature
Measure resolution	0.02 ºC
Emissivity:	K = 0.85
Accuracy:	± 0.5ºC
Supply voltage:	5 V
Output:	10-bit PWM output
	SMBus compatible digital interface
Output high level: PWMHI	Isource = 2 mA
Field of View:	90º

Unmanned aerial vehicle

A small multi-rotor copter equipped with a GNSS receiver was used as an aerial platform to mount the body of the remote sensing system. The multi-rotor copter was powered by a 5200-mA lithium ion rechargeable battery pack allowing for a maximum flight time of 45 min without payload and 1000 m of operating communication distance in open areas. As mentioned before, the infrared sensor, red–green–blue (RGB) and thermal camera assembly were mounted on the bottom side of the UAV to determine the key features of accurate temperature measurements, flight altitude and image stabilization. The RGB camera mount incorporated an autonomous mechanical stabilizer.

Laboratory tests

Two preliminary laboratory tests were performed to (i) validate the infrared sensor and its configuration parameters and (ii) assess the feasibility of using the canopy temperature as a water stress indicator for sugar beets. The first test consisted of comparing measurements of leaf temperature performed in potted and field-grown sugar beets with the inexpensive infrared sensor and the hand-held infrared pyrometer Fluke

62 (Fig. 3.1). Both potted and field-grown sugar beet plants were grown outdoors at the University of Seville experimental facilities. The test was performed when plants were at the post-emergence stage with 4–5 true leaves. Measurements were taken at midday over the period November 20th to December 12th 2014. Clear-sky and overcast days prevailed during this period, characterized by midday air temperatures within the range 13.3–23.6 ºC and solar radiation within the range 4.5–11.1 MJ m^{-2} day^{-1}. These records were collected from a standard weather station located near the University facilities, belonging to the Agro-climatic Information Network of the Andalusia Government. The suitability of using canopy temperature as a decision-making tool in irrigation management of sugar beets was assessed for potted sugar beets grown in a greenhouse through trials conducted over the same period described earlier. Two irrigation treatments were established: FI (full irrigation), which met the full crop water requirements, and DI (deficit irrigation), in which irrigation was withheld over the course of experiment. Six potted plants (pot volume of 0.3 l) of similar size were used in each treatment. The pot weight of each of the potted plants was measured at midday. The daily evapotranspiration (ET) was estimated during the experimental period as the difference in the pot weights between two consecutive days. After pot weighing, the FI pots were watered, left to drain and weighed again to reliably determine the ET estimates under non-limiting soil water conditions. The relative ET (RET), used as reference crop water stress indicator to be compared with canopy temperature, was calculated as follows:

$$RET = \frac{ET_{DI}}{ET_{FI}} \qquad (2)$$

where ET_{DI} and ET_{FI} denote ET for DI and FI treatments, respectively.

The canopy temperature (T_c) was measured in both FI and DI plants with the low-cost infrared sensor (MLX90614) at the same time that the pot weight was measured. T_c measurements were performed before watering the FI plants by placing the infrared sensor approximately 20–30 mm from the leaf surfaces to ensure that the T_c readings were actual leaf surface measurements. At least two T_c measurements were collected per potted plant. The air temperature (T_a) and relative humidity (RH) were continuously recorded using a HOBO Pro Temp-HR U23-001 data logger (Onset Computer Corp., Bourne, Massachusetts, USA). The difference between the T_c and T_a values ($\Delta T = T_c - T_a$) was determined daily for the FI and DI plants.

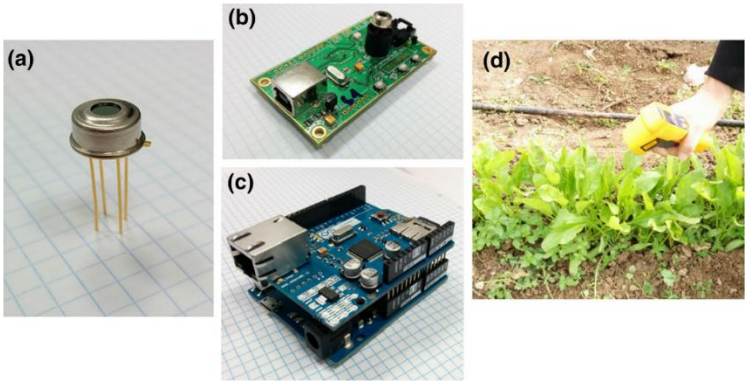

Figure III.1 Components of the temperature data acquisition system: a) infrared sensor MLX90614 b) evaluation board EVB90614, c) Arduino Leonardo board with Ethernet/SD shield mounted above, and d) hand-held infrared thermometer Fluke 62.

Field site and experimental design

Field tests were conducted during the spring of 2015 in a commercial sugar beet field in southern Spain with a fraction of ground covered by the canopy of nearly 100 %. A total of approximately 12 ha were planted in November 2014, 20–25 mm deep, 120 mm between plants and 500 mm between rows of plants, with a 12-row pneumatic drill seeder. Two sugar beet plots of 73 m^2 grown on clay soil were selected for the study (Latitude: 36.69560328º N, Longitude: 6.31925158º W). The sprinkler irrigation system was retrofitted to have two distinct areas: irrigated (according to the criterion of the farmer) plots and deficit irrigated plots that were subjected to a drying period that lasted 21 days. This consisted of withholding three irrigation events (one per week) that took place in the irrigated plot. Different flight altitudes (5, 10, 20, 30 and 40 m) were used over these areas to survey the surface temperature of the plots; here, some experience in manual flight control was essential in order to adjust the multi-rotor altitude. The assessment of the LITAS system to measure crop temperature at these flight altitudes was performed because variations in flight altitude are expected depending on the spatial variability of commercial fields. In fields with high spatial variability, lower flight altitudes to attain higher spatial resolution with the LITAS system may be required, whereas in more uniform fields the need for high spatial resolution is lower and higher flight altitudes will reduce the cost of the operation. A single-layer atmosphere with uniform conditions was considered because the atmospheric variation for a typical UAV flight altitude (150–200 m) can be neglected. However, the assumption that atmospheric corrections can be neglected for flight altitudes up to 40 m needs to be evaluated. The measurements were taken at the same time (between 12:00 and 1:00 pm) 2 days after irrigation. Before the measurements were taken, an internal calibration of the thermal camera was carried out in the laboratory using a blackbody. The total energy a blackbody radiates and the wavelength of maximum emittance depend on the temperature of the blackbody and can

be described by Stefan- Boltzmann's and Wien's laws, respectively (Walker 2008; Tipler 2000). After each flight, the data were transferred from the thermal sensors to the computer and the data quality was checked. Individual data and thermal image files were processed to obtain the sugar beet canopy temperature for the whole survey. A simplified workflow for the multi-rotor mission planning, survey and processing is provided in Fig. 3.2.

Statistical analysis

The normal distribution of the data set was tested using Shapiro–Wilk's test. This test specifies the distribution using a *W* statistic parameter. Small values of *W* values indicate deviation from a normal distribution. For each test, a p level >0.05 (5 % probability of error) was used as an acceptable error level.

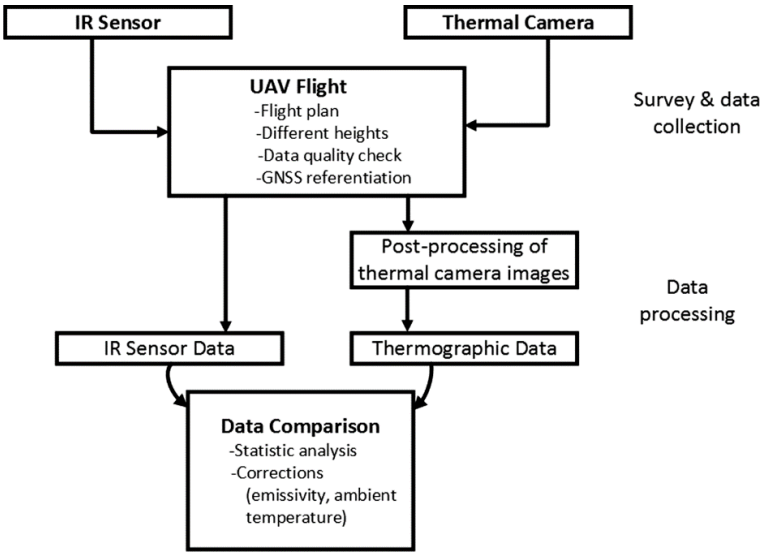

Figure III.2 Workflow scheme for the UAV mission planning, survey and processing

3.3 Results and discussion

The results of the inexpensive infrared sensor validation for the leaves of potted and field-grown sugar beet plants are shown in Fig. 3.3a, b, respectively. The experiment, which consisted of measuring leaf temperature in 26 sugar beet leaves (n = 13 in potted sugar beet plants, n = 13 in 2-row field plots of sugar beet plants), aimed to validate (i.e. prior to being mounted on the UAV) the usefulness of the inexpensive sensing platform envisaged in this study to accurately measure variations in leaf temperature.

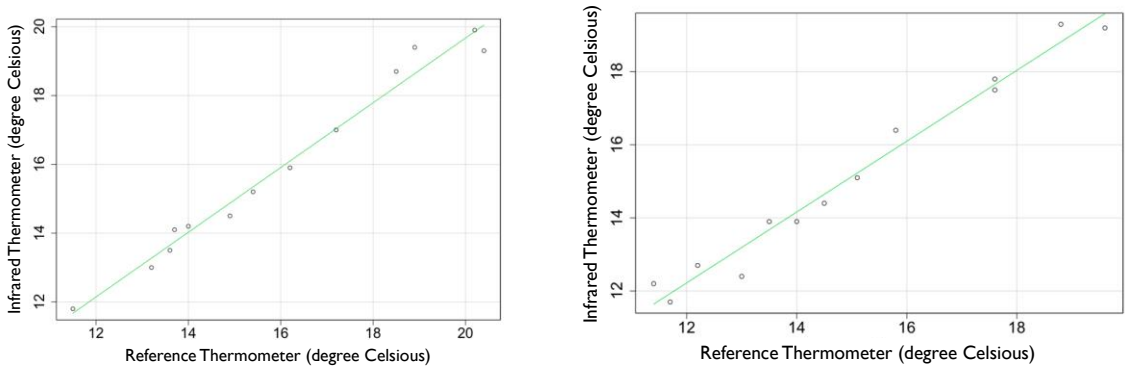

(a) (b)

Figure III.3 a) Correlation between leaf temperature measured with the reference thermometer and temperature measured with the inexpensive IR sensor in a potted sugar beet plants and; **b)** field-grown sugar beet plants.

As depicted in Fig. 3.3, a good linear correlation was observed between the temperatures measured with the reference thermometer and the low-cost IR sensor, evidencing a similar degree of accuracy among both sensing systems. The correlation coefficients were as follows: rxy = 0.977, $p < 10^{-4}$ (potted plants) and rxy = 0.975, $p < 10^{-4}$ (2-row field plot).

Assessment of the responsiveness of sugar beet leaf temperature to soil water availability.

The canopy-to-air temperature difference ($\Delta T = T_c - T_a$) was significantly affected by the irrigation regime (Fig. 3.4). DI plants had higher ΔT than FI plants from day 5 after the onset of the experiment. The ΔT of the DI plants (ΔT_{DI} hereafter) was generally greater than 0 ºC, whereas the corresponding value for FI plants (ΔT_{FI}) was normally less than 0 ºC. During the first days of the experiment and in the absence of soil water restrictions in both treatments, the FI and DI plants exhibited a decreasing trend of ΔT from approximately 3 ºC to approximately -1 ºC. From day 5 onwards, the ΔT values were not constant; a variable trend was observed in both treatments, although it was more accentuated in ΔT_{DI}.

ΔT variability can be ascribed to variations in soil water content but also to variations in a number of climatic variables, such as vapor pressure deficit, solar radiation or wind speed (Maes and Steppe 2012). Since the experiment was performed over a period with changing climatic conditions (see Materials and Methods section), ΔT variability in FI and DI was likely driven by changes in vapour pressure deficit and solar radiation on different measurement days. In order to use ΔT as a water stress indicator, it needs to be normalized as, for example, using an upper and lower boundary ΔT for the prevailing

weather conditions of the day of measurement. This is the base for CWSI calculation (Jackson et al. 1981), but this water stress indicator was not calculated in this study because it was outside the scope of the work. As stated in the objectives, the focus of the work was instead to demonstrate that canopy temperature is sensitive enough to water stress in this species and that the envisaged low-cost IR sensing platform (LITAS) is accurate enough to capture these differences.

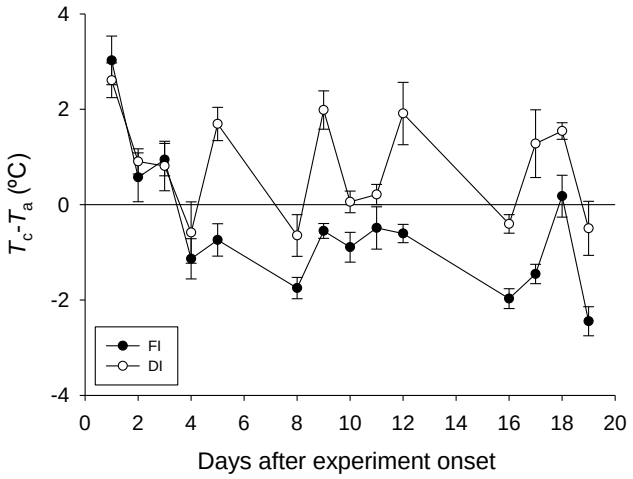

Figure III.4 Changes in canopy-to-air temperature differences ($\Delta T = T_c - T_a$) for FI and DI plants throughout the experimental period. Each point indicates the mean of six potted plants. The error bars denote the standard error.

The difference in ΔT between the DI and FI plants (which is equivalent to the differences in T_c between the treatments) was related to the RET, a surrogate of soil water deficit (Fig. 3.5). The results indicate that ΔT_{DI}-ΔT_{FI} increased with decreasing RET values, thereby confirming the sensitivity of this plant water status indicator to soil water deficit in sugar beets. Earlier work using infrared thermometry on sugar beets infected with *Phytium aphanidermatum* Edson (Fitz.) (Pinter et al. 1979), a root-rot disease of mature sugar beets, revealed that the midday leaf temperature of infected plants was 3–5 ºC warmer than that of adjacent plants with no sign of disease. Although their work was not focused on irrigation management, water stress is an early symptom of this disease and caused leaf temperature increments of a similar magnitude as those observed in this study for water-stressed plants (Fig. 3.5). The high scatter observed in the ΔT_{DI}-ΔT_{FI} Vs RET relationship (Fig. 3.5) can be explained by the influence that other factors (e.g., atmospheric demand represented by air vapor pressure deficit), besides soil water availability, have on T_c (Maes and Steppe 2012).

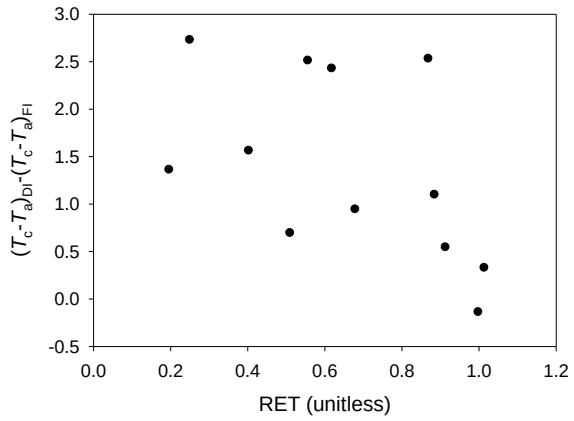

Figure III.5 Relationship between the difference among ΔT of FI and DI plants and the relative evapotranspiration (RET).

LITAS vs. a conventional thermal camera on a UAV

The mean and standard deviation values of the surface temperature of the irrigated and deficit-irrigated plots measured with the conventional thermal camera and LITAS during 7 UAV flights performed in the field site are shown in Table 4. The boxplot diagrams of these measurements are shown in Figs. 3.6 and 3.7. The mean canopy temperature (T_c) obtained with the thermal camera for the various flight altitudes varied between 25.60 ºC and 27.11 ºC in the DI plots and between 24.56 ºC and 26.86 ºC in the irrigated plots. The standard deviation (SD) values of the thermal camera measurements were between 1.26 ºC and 2.28 ºC for deficit irrigated plants and between 2.20 ºC and 3.54 ºC for those under normal irrigation regime, both being quite consistent for all flight levels (Table 3.4). The mean LITAS T_c for the various flight altitudes ranged within 26.34 and 27.3 ºC for the DI plots and between 26.30 ºC and 26.62 ºC for the irrigated plots. The LITAS SD values were between 0.47 ºC and 1.31 ºC for plots under deficit irrigation conditions, and between 1.06 ºC and 1.32 ºC for those under normal irrigation regime, both also consistent for all flight levels but lower than those obtained with the thermal camera (Table 4). The similarity in the mean T_c for both the irrigated and DI plots between the thermal camera and the inexpensive IR sensor confirms that LITAS is a promising low-cost alternative to conventional thermal cameras for remote estimations of surface temperature of crops covering the full ground surface. Moreover, the infrared sensor may be mounted on the aerial platform together with an RGB camera that both focus on the same target and record data simultaneously. This allows obtaining canopy temperature measurements from areas of clearly defined observation.

Table III.4. Mean IR canopy temperature (Tc) and standard deviation (SD) of the measurements taken with the conventional thermal camera and LITAS.

Flight Level, m	Conventional Thermal Camera				LITAS			
	Deficit irrigated		Irrigated		Deficit irrigated		Irrigated	
	T_c (ºC)	SD (ºC)	T_c (ºC)	SD (ºC)	T_c (ºC)	SD (ºC)	T_c (ºC)	SD (ºC)
h1, 5	26.21	2.05	25.96	2.24	27.30	0.63	26.53	1.25
h2, 10	27.11	1.26	26.86	2.64	27.01	0.65	26.56	1.25
h3, 20	26.07	1.93	26.73	3.54	26.62	0.70	26.62	1.32
h4, 30	25.81	2.28	25.06	2.28	26.34	0.47	26.55	1.08
h5, 40	25.60	1.83	24.56	2.20	27.21	1.31	26.30	1.06

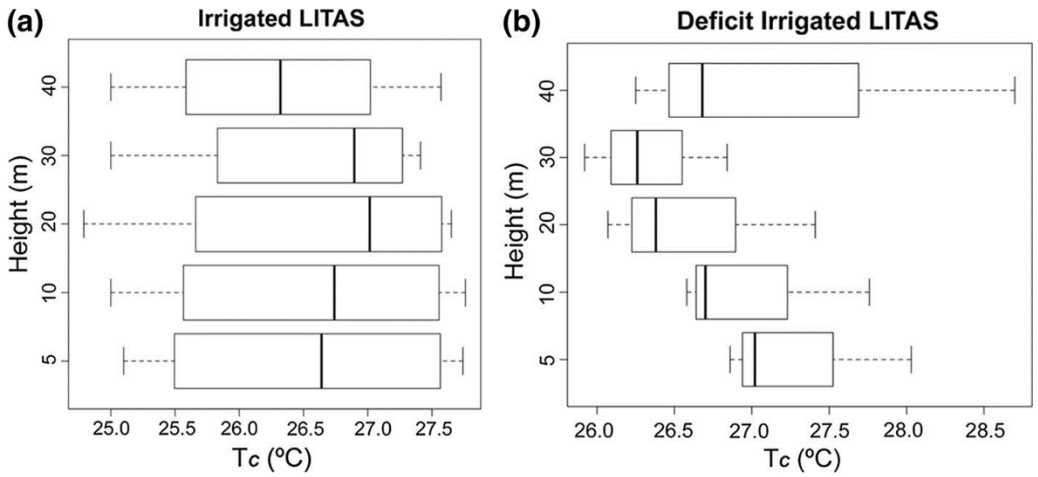

Figure III.6 Boxplot diagrams of mean canopy temperature (T_c) measured at various flight levels with LITAS. Measurements were taken throughout the irrigation season on both **a)** irrigated and **b)** deficit-irrigated plots.

The differences in T_c between the irrigated and DI plots were small ($T_c \approx 0.5$ ºC higher in DI plots) and consistent between the two sensing systems employed. These relatively small differences in T_c, compared with the values obtained in the laboratory tests (Fig. 3.5), indicate that the water shortage under DI was not sufficiently severe to trigger more intensive T_c-based crop water stress signals.

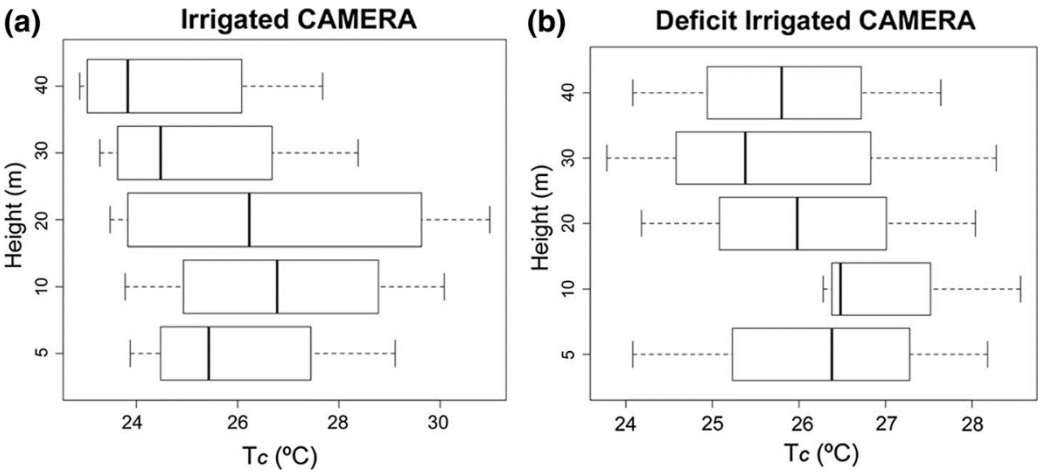

Figure III.7 Boxplot diagrams of mean canopy temperature (T_c) measured at various flight levels with the thermal camera. Measurements were taken throughout the irrigation season on both **a)** irrigated and **b)** deficit-irrigated plots.

Measurements of T_c with the conventional thermal camera decreased with flight altitude. The maximum mean T_c values were registered at a flight altitude of 10 m (26.86 and 27.11 ºC for the irrigated and DI plots, respectively), while minimum T_c values were obtained at a flight altitude of 40 m (24.56 and 25.60 ºC for the irrigated and DI plots, respectively). The fact that the sensor-target distance can influence remote estimations of surface temperatures is well documented (Jimenez-Munoz and Sobrino 2006; Meier et al. 2011). When remotely sensed from airborne or spaceborne sensors, an atmospheric correction of the thermal infrared imagery has to be performed for accurate determinations of surface temperatures. However, most studies that have focused on atmospheric corrections of remotely-sensed surface temperatures have been conducted for much larger sensor-target distances than those employed in this study (maximum flight altitude of 40 m). In fact, atmospheric effects for flight altitudes with less than ±50 m variation have normally been neglected (Berni et al. 2009b). The results confirm that thermal cameras using uncooled microbolometer sensors require atmospheric corrections to be performed even at flight altitudes as low as those used in this work.

These findings agree with the simulated effects of flight altitude and atmospheric conditions on the estimated surface temperature obtained by (Berni et al. 2009b) using the MOTRAN radiative transfer code (Berk et al. 1999). Their simulation outputs showed that for a flight altitude of 40 m, a relative humidity of 60 % and an air temperature within 20/30 ºC, the target to sensor temperature difference may increase to approximately 1.5 ºC, which is in agreement with the T_c reductions of approx. 1.5 - 2 ºC observed in this study.

Unlike the conventional thermal camera, the surface temperatures estimated with LITAS remained relatively constant with flight altitude (Table 4). The fact that LITAS does not seem to require atmospheric corrections at low altitude of flight may be regarded as an advantage of this system versus thermal cameras, as long as the estimated surface temperatures are sufficiently accurate to derive crop water status indices and that the percentage of ground covered by the crop is almost 100 %.

3.4 Conclusions

This work tested a low-cost sensing platform mounted on a small UAV for monitoring canopy temperature. The low-cost platform, called LITAS system, has been tested in a sugar beet field for irrigation management purposes. Laboratory tests showed that canopy temperature (T_c) measurements performed with the low-cost infrared sensor used in LITAS were correlated with Tc measurements obtained with a reference hand-held infrared thermometer. Under controlled laboratory conditions, sugar beet plants registered significantly higher leaf-to-air temperature differences in deficit irrigated potted plants than in well-watered plants. Under field conditions, the LITAS system mounted on a small aerial platform captured smaller T_c differences among well-watered and deficit irrigated sugar beet plots, suggesting that the level of water stress developed by the crop was not severe enough to trigger more intense T_c signals. LITAS measurements were compared to T_c derived from thermal images that were recorded simultaneously during the flights. When compared, both systems reported similar T_c differences between well-watered and deficit irrigated plots, indicating that the LITAS system is stable and a promising low-cost alternative to costlier thermal technologies.

A properly timed RGB camera accurately aligned with the infrared sensor can be used to indicate the area where the sensor is monitoring the temperature. Unlike the thermal camera, surface temperature measured with the low-cost infrared sensor was not affected by flight altitude, at least for the atmospheric conditions prevailing within the 0–40 m atmospheric layer of the experimental site.

An important challenge for the inexpensive IR sensing platform is to validate its utility in crops with reduced percentages of ground cover, e.g. fruit tree orchards. Although further research is needed, the combination of low flight altitudes with narrower sensor field-of-views (e.g. there are sensor models with 10º view angle rather than the 90º view angle, as used in this study) could overcome this constraint.

3.5 References

Ahrens, B., Hansson, K., Solly, E. F., & Schrumpf, M. (2014). Reconcilable differences: A joint calibration of fine-root turnover times with radiocarbon and minirhizotrons. *New Phytologist*, 204, 932–942.

Andrade-Sanchez, P., Gore, M.A., Heun, J.T., Thorp, K.R., Carmo-Silva, A.E., French, A.N., Salvucci, M.E., White, J.W. (2014). Development and evaluation of a field-based high-throughput phenotyping platform. *Functional Plant Biology* 41(1) 68-79.

Ballester, C., Jimenez-Bello, M., Castel, J., & Intrigliolo, D. (2013). Usefulness of thermography for plant water stress detection in citrus and persimmon trees. *Agricultural and Forest Meteorology*, 168, 120–129.

Bellvert, J., Zarco-Tejada, P. J., Girona, J., & Fereres, E. (2014). Mapping crop water stress index in a 'Pinot-noir' vineyard: Comparing ground measurements with thermal remote sensing imagery from an unmanned aerial vehicle. *Precision Agriculture*, 15(4), 361–376.

Berk, A., Anderson, G., Acharya, P., Chetwynd, J., Bernstein, L., Shettle, E., Matthew, M., Adler-Golden, S. (1999). *MODTRAN4 User's Manual*. Hanscom AFB, MA: Air Force Res. Lab.

Berni, J., Zarco-Tejada, P.J., Suárez, L., Fereres, E. (2009) Thermal and Narrowband Multispectral Remote Sensing for Vegetation Monitoring from an Unmanned Aerial Vehicle. *IEEE transactions on geoscience and remote sensing*, 47(3): 722-738.

Berni, J., Zarco-Tejada, P.J. Suarez, L., González-Dugo, V., Fereres, E., (2009) Remote sensing of vegetation from UAV platforms using lightweight multispectral and thermal imaging sensors. *ISPRS High Resolution Earth Imaging for Geospatial Information*, Hannover. Leibniz Universität. June 2-5.

Calderón, R., Navas-Cortés, J., Lucena, C., & Zarco-Tejada, P. (2013). High-resolution airborne hyperspectral and thermal imagery for early detection of verticillium wilt of olive using fluorescence, temperature and narrow-band spectral indices. *Remote Sensing of Environment*, 139, 231–245.

Colomina, I., Molina, P. (2014) Unmanned aerial systems for photogrammetry and remote sensing: a review. *ISPRS Journal of Photogrammetry and Remote Sensing*. 92: 79-97.

Crawford, K., Roach, J., Dhillon, R., Rojo, F., Upadhyaya, S. (2014). An inexpensive aerial platform for precise remote sensing of almond and walnut canopy temperature. *12th international conference on precision agriculture ISPA*: Monticello, IL, USA *https://www.ispag.org/media/ConferenceAbstracts2014_ FINAL.pdf.*

Ehmke, T. (2013). Unmanned aerial systems for field scouting and spraying. *Crops and Soils*, 46(6), 4-9.

González-Dugo, V., Zarco-Tejada, P. J., Nicolás, E., Nortes, P. A., Alarcón, J. J., Intrigliolo, D. S., et al. (2013). Using high resolution UAV thermal imagery to assess the variability in the water status of five fruit tree species within a commercial orchard. *Precision Agriculture*, 14, 660–678.

Hoffmann, C. M. (2014). Adaptive responses of *Beta Vulgaris* L. and *Cichorium Intybus* L. root and leaf forms to drought stress. *Journal of Agronomy and Crop Science*, 200, 108–118.

Hunt, J. E. R., W. D. Hively, S. Fujikawa, D. Linden, C. S. Daughtry and G. McCarty (2010). "Acquisition of NIRGreen-Blue Digital Photographs from Unmanned Aircraft for Crop Monitoring." *Remote Sensing* 2(1): 290-305.

Jackson, R. D., Idso, S. B., Reginato, R. J., & Pinter, P. J. (1981). Canopy temperature as a crop water stress indicator. *Water Resources Research*, 17(4), 1133–1138.

Jenkins, D., Vasigh, B. (2013). The economic impact of unmanned aircraft systems integration in the United States. *Association for Unmanned Vehicle Systems International.* Arlington, 38pp.

Jimenez-Munoz, J.C., Sobrino, J.A. (2006) Error sources on the land surface temperature retrieved from thermal infrared single channel remote sensing data. *International Journal of Remote Sensing*, 27(5-6): 999-1014.

Lenthe, J. H., Oerke, E. C., & Dehne, H. W. (2007). Digital infrared thermography for monitoring canopy health of wheat. *Precision Agriculture*, 8(1–2), 15–26

Li, H., Lee, W. S., Wang, K., Ehsani, R., & Yang, C. (2014a). Extended spectral angle mapping (ESAM) for citrus greening disease detection using airborne hyperspectral imaging. *Precision Agriculture*, 15, 162–183.

Li, L., Zhang, Q., & Huang, D. (2014b). A review of imaging techniques for plant phenotyping. *Sensors*, 14(11), 20078–20111.

López, A., Molina-Aiz, F. D., Valera, D. L., & Peña, A. (2012). Determining the emissivity of the leaves of nine horticultural crops by means of infrared thermography. *Scientia Horticulturae*, 137, 49–58.

Lopez-Granados, F. (2011) Weed detection for site-specific weed management: mapping and real-time approaches. *Weed Research*. 51(1):1-11.

Maes, W. H., Steppe, K. (2012) Estimating evapotranspiration and drought stress with ground-based thermal remote sensing in agriculture: a review. *Journal of Experimental Botany*, 63 (13): 4671-4712.

Mahlein, A. K., Steiner, U., Hillnhütter, C., Dehne, H. W., & Oerke, E. C. (2012). Hyperspectral imaging for small-scale analysis of symptoms caused by different sugar beet diseases. *Plant Methods*, 8, 3.

Meier, F., Scherer, D., Richters, J., Christen, A. (2011). Atmospheric correction of thermal-infrared imagery of the 3-D urban environment acquired in oblique viewing geometry. *Atmos. Meas. Tech*., 4, 909–922,

Melexis Data Sheet. (2009). MLX90614 family, single and dual zone infrared thermometer inTO-39. Revised. 5, March 30. Melexis NV, Ieper.

O'Shaughnessy, S. A., Evett, S. R., Colaizzi, P. D., & Howell, T. A. (2011). Using radiation thermometry to evaluate crop water stress in soybean and cotton. *Agricultural Water Management*, 98, 1523–1535.

Peña, J. M., Torres-Sánchez, J., de Castro, A. I., López-Granados, F., & Dorado, J. (2014) The TOAS project: UAV technology for optimizing herbicide applications in weed-crop systems. *12th International Conference on Precision Agriculture, Sacramento, California, USA. July 20-23, 2014.*

Pidgeon, J. D., Ober, E. S., Qi, A., Clark, C. J. A., Royal, A., & Jagard, K. W. (2006). Using multienvironment sugar beet variety trials to screen for drought tolerance. *Field Crop Research*, 95, 268–279.

Pinter, P. J., Stanghellini, M. E., Reginato, R. J., Idso, S. B., Jenkins, A. D., & Jackson, R. D. (1979). Remote detection of biological stresses in plants with infrared thermometry. *Science*, 205, 585–587.

Ray, D.K., Mueller, N.D., West, P.C., Foley, J.A. (2013) Yields trends are insufficient to double global crop production by 2050. *PLoS ONE* 8,

Romano, A., Sogona´, A., Lupini, A., Araniti, F., Stevanato, P., Cacco, G., et al. (2013). Morpho-physiological response of sugar beet (Beta vulgaris L.) genotypes to drought stress. *Acta Physiologiae Plantarum*, 35(3), 853–869.

Shaw, B., Thomas, T. H., & Cooke, D. T. (2002). Responses of sugar beet (Beta Vulgaris L.) to drought and nutrient deficiency stress. *Plant Growth Regulation*, 37, 77–83.

Testi, L., Goldhamer, D. A., Iniesta, F., & Salinas, M. (2008). Crop water stress index is a sensitive water stress indicator in pistachio trees. *Irrigation Science*, 26, 395–405.

Tilman, D., Balzer, C., Hill, J., Beford, B.L. (2011) Global food demand and the sustainable intensification of agriculture. *Proceedings of the National Academy of Sciences.* USA. 108, 20260-20264

Tipler, PA. (2000). *Physik*, 3rd edn. Spektrum Akademischer Verlag, Heidelberg, 1520 pp.

Tsialtas, J. T., & Maslaris, N. (2012). Leaf physiological traits and their relation with sugar beet cultivar success in two contrasting environments. *International Journal of Plant Production*, 6(1), 15–36.

Walker, J. (2008) *Fundamentals of physics*, 8th edn. Wiley, New York, 891pp. ISBN:9780471758013

White, J.W., Conley, M.M. (2013) A flexible, low-cost cart for proximal sensing. *Crop Science* 53, 1646-1649

Xu, Y., Ehsani, R., Kaplan, J., Ahmed, I., Kuzma, W., Orlandi, J., et al. (2014). An octo-rotor ground network for autonomous strawberry disease detection Year 1 Status Update. In: *Proceedings of 2nd international conference on robotics and associated high-technologies and equipment for agriculture and forestry*, Madrid. pp. 457-466.

Zhang, C., Kovacs, J.M. (2012) The application of small unmanned aerial systems for precision agriculture: a review. *Precision Agriculture* 13(6) 693-712

III. Publications: Chapter 2

Assessing a crop water stress index derived from aerial thermal imaging and infrared thermometry in super-high density olive orchards

Egea Cegarra, G.[1]; Padilla-Díaz, C.M. [2]; Martínez-Guanter, J.[1]; Fernández, J.E.[2]; Pérez-Ruiz, M.[1]

[1]Area of Agroforestry Engineering, Aerospace Engineering and Fluids Mechanic Department, School of Agricultural Engineering, Universidad de Sevilla, Ctra. Utrera km.1, 41013 Seville, Spain

[2] Irrigation and Crop Ecophysiology Group, Instituto de Recursos Naturales y Agrobiología de Sevilla (IRNAS, CSIC), Avenida Reina Mercedes 10, 41012, Seville, Spain

Published on:

Agricultural Water Management
June 2017, Volume 187, Pages 210–221
DOI: 10.1016/j.agwat.2017.03.030

Abstract

Characterization of the spatio-temporal variability of tree water status is a prerequisite to conducting precise irrigation management in fruit tree orchards. This study assessed the suitability of a crop water stress index (CWSI) derived from high-resolution aerial thermal imagery for estimating tree water status variability in super high density (SHD) olive orchards. The experiment was conducted at a commercial SHD olive orchard near Seville (southwestern Spain), with drip irrigated trees under three irrigation treatments (four plots per treatment in a randomized block design): a full irrigation treatment to replace the crop water needs (ETc) and two regulated deficit irrigation treatments to replace around the 45% of ETc. Meteorological variables, soil moisture content, leaf water potential, stem water potential and leaf gas exchange measurements were performed along the irrigation season. Infrared temperature sensors (IRTs) installed approximately 1 m above the canopies were used to derive the required Non-Water-Stressed Baselines (NWSBs) for CWSI calculation. NWSBs were not common during the growing season, although the seasonal effect could be partly explained with solar angle variations. A thermal camera installed on a mini Remotely Piloted Aircraft System (RPAS) allowed for the recording of high-resolution thermal images on 5 representative dates during the irrigation season. The CWSI values derived from aerial thermal imagery were sensitive to the imposed variations in tree water status within the SHD olive orchard. Among the recorded variables, maximum stomatal conductance showed the tightest correlation with CWSI. We concluded that high-resolution thermal imagery captured from a mini RPAS is a suitable tool for defining tree water status variability within SHD olive orchards.

4.1 Introduction

Hedgerow olive orchards with high plant densities (>1500 trees ha^{-1}), or super high density (SHD) olive orchards, have expanded dramatically since the early 1990s. Over 100,000 ha are currently under this management system, half of them in Spain (Rius and Lacarte, 2010). Most SHD olive orchards are underirrigation, requiring ca. 5000 m3ha−1to replace maximum crop evapotranspiration in semi-arid areas such as SW Spain (Fernández et al., 2013). This explains the increasing interest in developing precision irrigation techniques to increase water productivity (Cuevas et al., 2013; Egea et al., 2016; Fernández et al., 2013; Gómez Del Campo and García, 2013; Padilla-Díaz et al., 2016). The spatial variability in crop water needs caused by soil heterogeneity and differences in canopy cover may be an important limitation for efficient irrigation when water is applied uniformly across the orchard (Couvreur et al., 2016). Characterization of the spatial variability of crop water needs is therefore a prerequisite to apply precise irrigation management within SHD olive orchards. It will allow to supply different irrigation amounts to zones within the orchard with different water requirements. Mapping the spatio-temporal variability of tree water needs with conventional methods such as the pressure chamber (Scholander et al., 1965) is time and labour consuming (Jiménez-Bello et al., 2011). In addition, the reliability of the information provided by the pressure chamber decreases when the species shows an isohydric behaviour, characterized by a strong stomatal regulation that avoids marked decreases in leaf water potentials under conditions of low soil, water and high evaporative demand (Fernández, 2014). There are other conventional although reliable indicators of water stress, such as the stomatal conductance but, once again, measurements must be made manually (Jones, 2007).

Remote sensing techniques offer a promising alternative to traditional tree water status measurements, as they provide a snap-shot of the whole orchard over a reduced period of time. The advent of Remote Piloted Aerial Systems (RPAS) has offered an opportunity to develop remote sensing-based methodologies for precision irrigation more affordably than the costly airborne campaigns with manned aircrafts and with higher spatial and temporal resolutions than those normally offered by satellites. Various sources of remotely sensed imagery, with differences in spectral, spatial, radioactive and temporal characteristics, are known to be suitable for different purposes of vegetation mapping (Xie et al., 2008).

Among these sources, thermal imagery of vegetation is becoming popular for water stress detection and for irrigation management purposes (Bellvert et al., 2016b; Berni et

al.,2009). This is due to the existing relationship between crop transpiration rate and canopy temperature through a cooling effect that the former exerts on vegetation temperature (Maes and Steppe,2012). Since the refinement of the technique for measuring crop surface temperature with infrared thermometers in the 1960s(Fuchs and Tanner, 1966), thermal remote sensing has been extensively used to diagnose plant water stress in multiple crop species(Hatfield et al., 1985; Nielsen and Anderson, 1989; Sepulcre-Cantó et al., 2006; Testi et al., 2008). Variations in crop temperature are due to water stress, but are also affected by various meteorological land morphological factors (Maes and Steppe, 2012). Therefore, crop temperature must be normalized before being used as water stress indicator. In the early 1980s, Idso et al. (1981) and Jackson et al. (1981) developed the concept of CWSI, a normalized index that overcomes the influence that other environmental variables play on the relationship between crop temperature and water stress. Since then, CWSI has been successfully used in a variety of crops, in which temperature readings were often made with hand-held infrared thermometers (Alderfasi and Nielsen, 2001; Hatfield et al.,1985).

Currently, the combined used of modern high-resolution thermal infrared cameras and RPAS offer the possibility to map spatial variability in tree water status from thermal imaging and temperature-derived indicators (Bellvert et al., 2016a). As reviewed in Maes and Steppe (2012), CWSI can be determined by at least three different methodologies. Among them, the empirical CWSI has attained much more popularity and become more successful among scientists and non-scientists mainly due to the limited data requirements and straightforward calculation as compared to the analytical and direct methodologies (Agam et al., 2013; Maes and Steppe, 2012). Idso et al. (1981) calculated the empirical CWSI as follows:

$$CWSI = \frac{(T_c - T_a) - (T_c - T_A)_{LL}}{(T_c - T_A)_{UL} - (T_c - T_A)_{LL}} \quad (4.1)$$

where T_c-T_a denotes the measured canopy-air temperature difference; $(T_c\text{-}T_a)_{LL}$ is the lower limit of $(T_c\text{-}T_a)$ for a given vapor pressure deficit (VPD) which is equivalent to a canopy transpiring at the potential rate; and $(T_c\text{-}T_a)_{UL}$ is the maximum (Tc-Ta), which corresponds to a non-transpiring canopy. $(T_c\text{-}T_a)_{LL}$ is a linear function of VPD (non-water-stressed baseline, NWSB) that, once empirically obtained, $(T_c\text{-}T_a)_{LL}$ is calculated by solving the baseline equation for the actual VPD.

To our knowledge, there are two reports in the literature that provide empirical NWSBs for olive trees (Bellvert et al., 2016a; Berni et al., 2009). However, both equations are reasonably different as denoted by the very small (expressed as absolute value) slope (−0.35ºC kPa^{-1}) obtained by Berni et al. (2009) as compared to that (−2.05ºC kPa^{-1})

reported in Bellvert et al. (2016a). These differences in the sensitivity of T_c-T_a to VPD in olive are so important that more research is needed to reduce the degree of uncertainty in the appropriate NWSB to be used in SHD olive orchards. Moreover, these studies provided a single NWSB obtained with measurements collected at a certain daytime (e.g. 12:30 GMT in Berni et al. (2009)), but a comprehensive study on how NWSB varies both along the day and the season is lacking in olive trees. To reduce the lack of information mentioned above on the use of CWSI and NWSB in olive, we design this study according to the following objectives:

(i) to determine the NWSB for olive in a commercial SHD olive orchard as well as its diurnal and seasonal (throughout the irrigation season) time courses,
(ii) to compute CWSI throughout the irrigation season in trees under three irrigation treatments from the obtained NWSB and high-resolution aerial thermal imagery taken from a mini RPAS, and
(iii) to assess the suit-ability of the derived CWSI values to estimate the variation of tree water status within SHD olive orchards.

4.2 Materials and methods

4.2.1 Experimental site

The experiment was conducted in 2015 at a commercial SHD olive orchard near Seville, in southwestern Spain (37.248979, −5.796538). Nine-year-old olive trees (*Olea europaea* L., cv. Arbequina) were planted with 4 m x 1.5 m tree spacing (1667 trees ha^{-1}). The drip irrigation system consisted of one drip line per tree row and three 2 L h^{-1} pressure compensating drippers (0.5 m apart) per tree. One flow meter per irrigation treatment recorded the amount of water applied during each irrigation event. An irrigation controller (Agronic 2000, Sistemes Electrònics PROGRÉS, S.A., Lleida, Spain) was used for irrigation scheduling. Trees were fertilized to cover the crop needs and no weeds were allowed to grow in the inter-row spacing over the spring-summer seasons. The climate of the study area was Mediterranean, with rainfall occurring normally from late September to May. The average annual value of potential reference evapotranspiration (ET_0) and precipitation calculated for the 2002–2014 period from data recorded by a standard weather station belonging to the Andalusian government and located near the orchard, were 1528 mm and 540 mm, respectively. Table 4.1 below shows the weather data (monthly averages) recorded over the experimental year. The orchard soil has a

sandy loam top layer (0.0–0.4 m) and a sandy clay layer (0.4–1.0 m) underneath. The electrical conductivity of the saturated soil-paste (ECe), pH and organic matter content determined in the 0.0-0.4 m soil layer were 2.5 dS m^{-1}, 6.34% and 0.28%, respectively.

Table 4.1 Weather variables measured during 2015 at a nearby standard weather station belonging to the Agroclimatic Information Network of the Junta of Andalusia. P (mm): rainfall; T_a (ºC): air temperature; RH (%): relative humidity; u (m s^{-1}): wind speed; Rs (MJ m^{-2} d^{-1}): solar radiation; ET_0 (mm d^{-1}) is the calculated FAO-Penman Monteith reference crop evapotranspiration. The suffixes av, max and min indicate the average, maximum and minimum, respectively.

Month	P	T_{av}	T_{max}	T_{min}	RHav	RH_{max}	RH_{min}	u	R_s	ET_0
Jan	42.2	8.8	16.0	2.8	82	99	50	2.3	10.3	1.5
Feb	6.8	9.4	15.8	3.4	75	95	45	2.5	12.5	2.1
Mar	42.0	12.8	21.1	5.2	73	95	40	1.7	18.2	3.1
Apr	26.8	16.4	24.0	9.3	71	97	38	1.6	21.5	4.0
May	0.4	21.6	31.4	11.9	50	86	20	1.6	27.6	6.2
Jun	2.2	24.0	32.8	14.8	47	77	23	2.4	28.5	7.3
Jul	0.0	28.1	37.4	18.6	42	66	17	2.6	29.9	8.9
Aug	1.6	26.1	34.3	18.7	50	73	26	2.6	23.6	7.0
Sep	28.6	21.7	29.4	14.8	59	83	31	2.6	20.4	5.2
Oct	73.4	18.7	25.0	13.7	74	92	45	1.9	12.6	2.9
Nov	33.0	13.7	22.1	7.0	68	91	39	1.7	12.5	2.1
Dec	25.2	12.0	20.3	5.5	70	90	42	1.3	9.1	1.6
Year	282.2	17.8	25.8	10.5	63	87	35	2.1	18.9	4.3

4.2.2. Irrigation treatments

Three irrigation treatments were established in the orchard, as described in Padilla-Díaz et al. (2016): a full irrigation treatment (FI) in which the trees were irrigated daily for the whole irrigation season to supply 100% of the irrigation needs (IN), and two regulated deficit irrigation treatments (45RDI) for which the total water supplied during the season was aimed to replace 45% of IN. One of the 45RDI treatments was scheduled on the basis of the crop coefficient method ($45RDI_{CC}$), whereas the other 45RDI treatment was scheduled from leaf turgor related measurements ($45RDI_{TP}$) made with ZIM probes (Zimmermann et al., 2008). More details about the irrigation scheduling and the 45RDI strategies can be found in Padilla-Díaz et al. (2016). We used four 16 m x 12 m plots per treatment, in a randomized block design. Each plot contained 32 trees, of which measurements were made on the central 8 trees to avoid border effects.

4.2.3. Thermal imagery acquisition

A thermal infrared (TIR) camera (Tau 2 324, FLIR Systems, Inc., Oregon, USA) was mounted on a multirotor RPAS (Remote Piloted Aerial System) model Phantom 2 (SZ DJI Technology Co., Ltd., Shenzhen, China). The RPAS is equipped with a GNSS

receptor, has flight autonomy of 25 min and a remote-control range of 1,000 m in open spaces. The TIR camera was installed to aim vertically downward (nadir view) at the bottom of the RPAS. The camera spectral range is 7.5–13.5 µm with a resolution of 324 x 256 pixels, a focal length of 9 mm, and a field of view of 49° (H) x 39° (V). The RPAS was flown across the experimental orchard on five clear sky days, at 20 m above the ground level and at solar noon, delivering thermal images with a ground spatial resolution of 5 cm. The thermal images were stored on board in a raw format with 14-bit radiometric resolution. At the time of each flight, surface temperature measurements of ground targets were used for indirect calibration of the thermal imagery (Bellvert et al., 2014; Dupin et al., 2011). In particular, a cold (wet cotton sheet) and hot references (40 cm x 50 cm black plastic panels) located in the center of each experimental plot along with four monitored trees with infrared thermometers (IRTS) (Section 4.2.4) were used as ground targets. The cold and hot references were measured with a hand-held infrared thermometer model FLUKE 62 Max (FLUKE, Washington, DC, USA).

4.2.4. Measurements at ground level

Volumetric soil water content (θ) was measured in all plots (n=4) with a PR2-type Profile Probe (Delta-T Devices Ltd, Cambridge, UK). On each location, measurements were made at 0.1, 0.2, 0.3, 0.4, 0.6 and 1.0 m depth, once every 7-10 days throughout the irrigation season. The θ measurements were always performed after an irrigation event, between 10:00 and 12:00 Greenwich Mean Time (GMT), *i.e*. close to solar noon at the longitude of our experimental site. The probe was calibrated in situ by Fernández et al. (2011). The θ values were used to calculate changes in the relative extractable water (REW) for all treatments, as described elsewhere (Fernández et al., 2013). The midday stem water potential (ψ_{st}) was measured with a Scholander-type pressure chamber (PMS Instrument Company, Albany, Oregon, USA) on the same days that the RPAS was flown. One leaf per tree, from the inner part of the canopy, was wrapped in aluminum foil ca. 2 h before sampling, in two representative trees per plot (n=8). Measurements of ψ_{st} were made at 11:30 – 12:30 GMT when minimum daily values are usually recorded in olive. Stomatal conductance (g_{sm}) was measured on the same days and on the same trees where ψ_{st} was measured, but between 09:00–10:00 GMT, the time of maximum daily stomatal conductance in this species (Fernández et al., 1997). A Licor LI-6400 portable photosynthesis system (Li-cor, Lincoln Nebraska, USA) with a 2 cm × 3 cm standard chamber that was used to measure gsm and leaf transpiration rate (Em) in sunny leaves of current-year shoots from the outer part of the canopy facing SE and in ambient light (≈ 1,500 µmol m^{-2} s^{-1}) and CO2 (370 – 400 µmol mol^{-1}) conditions.

Four Infrared Remote Temperature Sensors (IRTs) (model IR120, Campbell Scientific Ltd., Shepshed, UK) were mounted over two representative trees of one out of four plots in FI and 45RDI$_{TP}$ treatments. The sensors had an angular field of view of 20º (half angle), and the accuracy over the calibrated range was ± 0.2 ºC. The IRTs were mounted on galvanized steel masts with a horizontal mounting arm (model IR1X0, Campbell Scientific Ltd., Shepshed, UK) ending with a white PVC solar shield (model IR-SS, Campbell Scientific Ltd., Shepshed, UK) to protect the sensor. The IRTs were mounted to aim vertically downward (nadir view), targeting the center of the canopy from a distance of approximately 1 m. The dense canopies typical of hedgerow olive orchards allowed the IRTs to view mostly foliage in a circular area of approximately 0.7 m diameter at the top of the canopy. The IRTs were connected to two dataloggers (model CR1000, Campbell Scientific Ltd., Shepshed, UK), which recorded the canopy temperatures (T_c) every minute and stored the 15-min averages. The canopy temperature measurements began on June 16th, 2015 (DOY 167) and continued with a sole interruption of 12 days due to power outage until November 5th (DOY 275).

Values of T_c measured with the IRTs above the FI trees were used to derive the Non-Water-Stressed Baselines (NWSB) for CWSI calculation. Only clear-sky days were used for NWSB determination. Clear-sky days following a rainfall event were also discarded to avoid errors associated with wet foliage. Air temperature (T_a) along with VPD data recorded in the orchard every 30 min with a Campbell weather station (Campbell Scientific Ltd., Shepshed, UK) at the same time that T_c were used to derive the NWSB of the SHD olive orchard.

4.2.5. Image processing and CWSI calculation

The thermal images taken with the RPAS (Fig. 4.1) were used to calculate the mean canopy temperature (T_c) of each experimental plot. Only the central 8 trees of each plot were used to calculate the mean T_c to avoid border effects. An image segmentation algorithm written in R (R Core Team, 2015) was used to extract pure vegetation pixels from the thermal image. At solar noon, the effects of tree shadow are minimized, and the thermal images are composed mainly of canopy, soil and mixed plant-soil pixels. Firstly, vegetation pixels from a bi-modal histogram (i.e. a histogram with two clearly differentiated peaks ascribed to soil and vegetation pixels in the point cloud) (Fig. 4.2) were selected with the mentioned algorithm. Then, the 'full width at one-eighth maximum (FWEM)' rule was used to distinguish the pixels with high probability of being pure vegetation from pixels that were likely to be mixed vegetation with soil and/or shadow effects. The FWEM rule is similar to the 'full width at half maximum' (FWHM) rule that

has been previously used to extract pure vegetation pixels from olive canopies (Rud et al., 2015), but differed in the amplitude of the selected histogram (one-eighth of the maximum in FWEM versus half the maximum in FWHM). FWHM demonstrated a lack of suitability for segmenting thermal images with multiple trees that differ greatly in their T_c, since vegetation pixels from trees with severe water stress can be erroneously discarded by the FWHM rule (Fig. 4.3). The selected segment resulting from the FWEM rule was then used to compute the mean T_c for each experimental plot.

Mean T_c was used to calculate the CWSI for each experimental plot using Eq. 4.1. For each day of flight, $(T_c\text{-}T_a)_{LL}$ was calculated from the NWSB that was determined with the IRTs, as described in Section 4.2.4 and with the actual air VPD. The value of $(T_c\text{-}T_a)_{UL}$ was determined as T_a + 5ºC based on previous studies conducted in different crop species (Irmak et al., 2000; Möller et al., 2007), including olive trees (Agam et al., 2014, 2013; Ben-Gal et al., 2009; Rud et al., 2015).

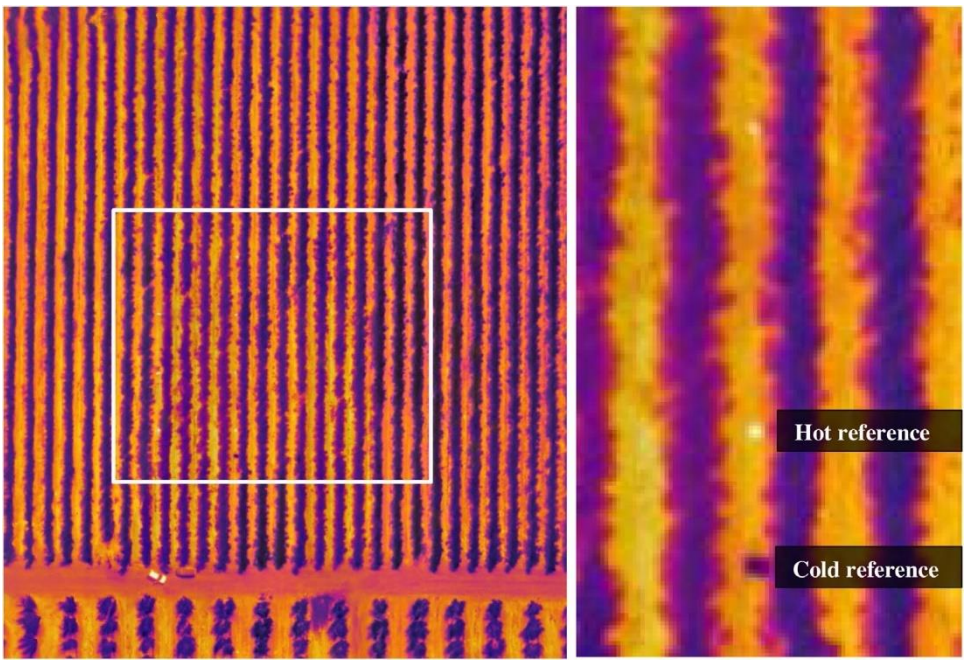

Figure 4.1 Thermal mosaic acquired with a FLIR Tau 2 324 thermal camera on board a RPAS model Phantom 2 observing (left) the experimental SHD olive orchard (white rectangle), and (right) details of the hot and cold reference surfaces.

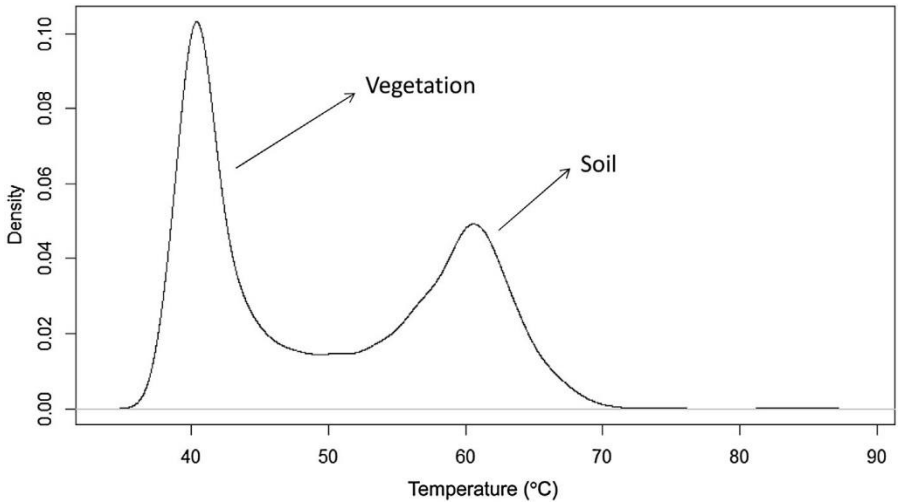

Figure 4.2 Example of bi-modal histogram of temperatures obtained from a thermal image of an experimental plot.

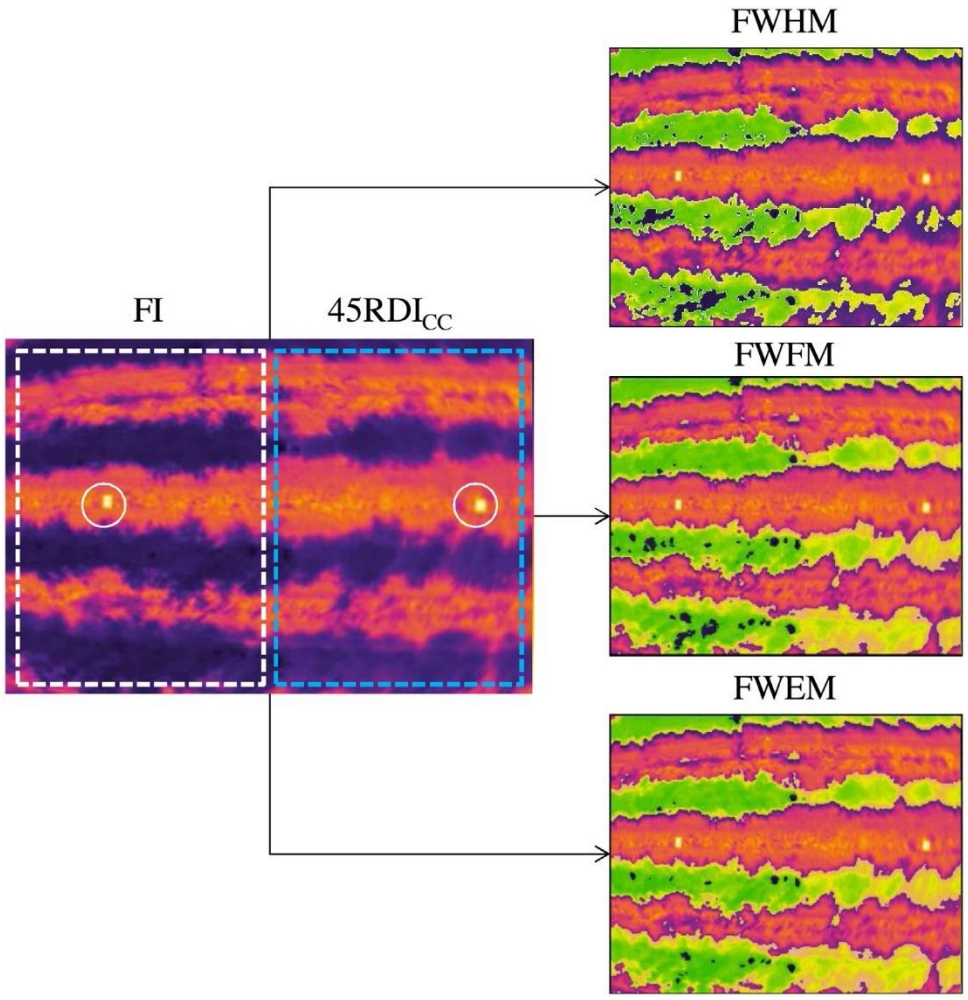

Figure 4.3 (**left**) Fraction of a thermal mosaic in which FI and 45RDI$_{CC}$ trees have been delimited with white and blue dashed rectangles, respectively. The white circles show the hot reference surfaces. Date of flight: DOY 218; (**upper right**) thermal image plotted in the left panel with a superimposed layer denoting the vegetation pixels selected by the segmentation algorithm based on the full width at half maximum rule (FWHM); (**middle right**) thermal image with a superimposed layer showing the vegetation pixels selected by the segmentation algorithm based on the full width at one fifth maximum rule (FWFM); (**lower right**) thermal image with a superimposed layer showing the vegetation pixels selected by the segmentation

algorithm based on the full width at one-eighth maximum rule (FWEM). (For interpretation of the references to colour in this figure legend, the reader is referred to the web version of this article.)

4.2.6. Statistical analyses

The relationships between T_c-T_a and VPD (NWSBs) as well as between CWSI and the physiological measurements were analyzed through linear regression analyses. The diurnal time-course of slopes and intercepts of the derived NWSBs was modeled through non-linear regression analysis. In all cases, the coefficient of determination (R^2) was used to assess the goodness of fit of the associations among variables. Significant differences between slopes and non-zero intercepts of the NWSBs obtained diurnally and seasonally were evaluated with the *Comparison of Regression Lines* tool included in the statistical package Statgraphics (Statgraphics Centurion XV).

4.3 Results

4.3.1. Non-Water-Stressed Baselines

The relationship between hourly ΔT ($T_c - T_a$) and VPD values derived for FI olive trees in clear-sky days throughout the study period, did not yield any significant relationship when all hours and days were pooled together (data not shown). The relationships became significant when ΔT and VPD were regressed for a given time of the day, as shown in Table 4.2. The coefficients of determination (R^2) were notably affected by the daytime. The highest R^2 were observed early in the morning (R^2 = 0.74 at 8.00 GMT). These values decreased progressively down to 0.28 (14:00 GMT), recovering partially afterwards (R^2 = 0.51 at 18.00 GMT). The intercepts and slopes of the fitted NWSBs also varied throughout the day. The intercepts were higher at midday (2.50 at 12:00 GMT) and lower in the morning and afternoon whereas the slopes showed an increasing trend throughout the day (from -0.77 ºC kPa^{-1} at 8.00 GMT to around -0.3 ºC kPa^{-1}in the evening).

Table 4.2 Fitted parameters for the non-water stressed baselines (T_c-T_a = a + b·VPD). Only clear-sky days from day of year 167–275 were used in the analyses. GMT: Greenwich Mean Time.

GMT	Intercept ºC	Slope ºC kPa^{-1}	R^2
8:00	0.94	-0.77	0.74
9:00	0.97	-0.67	0.64
10:00	1.44	-0.61	0.67

11:00	2.18	-0.55	0.7
12:00	2.5	-0.36	0.49
13:00	2.43	-0.3	0.32
14:00	2.05	-0.32	0.28
15:00	1.43	-0.3	0.35
16:00	0.83	-0.3	0.41
17:00	0.31	-0.31	0.42
18:00	-0.09	-0.32	0.51

In addition to the diurnal effect on the NWSBs, a marked seasonal effect in the ΔT vs VPD relationship was also observed (Fig. 4.4), as the NWSB shifted in August (Period B) and September (Period C), compared to the values derived in June-July (Period A). When ΔT and VPD of a given time of the day and for a given phenological period were regressed, the level of agreement of the NWSBs increased significantly, and the diurnal effect of R^2 observed using pooled data (Table 4.2) was not noticed (Table 4.3). Seasonal variations in the NWSBs were mainly due to significant variations in the NWSB-intercepts, as the NWSB-slopes remained almost invariant throughout the irrigation season (Table 4.3).

Table 4.3 Fitted parameters for the non-water-stressed baselines (T_c-T_a = a+b·VPD) determined for three representative periods: A (June-July, day of year –DOY- 167–212), B (August, DOY215–243), C (September, DOY 244–273). Only clear-sky days were used. GMT: Greenwich Mean Time.

GMT	Period	Intercept ºC	Slope ºC kPa^{-1}	R^2
8:00	A	1.02a	−0.79a	0.72
8:00	B	1.15a	−1.00a	0.68
8:00	C	1.32a	−1.40a	0.75
9:00	A	1.28a	−0.73a	0.74
9:00	B	0.97b	−0.83ab	0.56
9:00	C	1.79b	−1.50b	0.82
10:00	A	1.68a	−0.64a	0.77
10:00	B	1.67b	−0.89a	0.67
10:00	C	1.91b	−1.02a	0.7
11:00	A	2.60a	−0.62a	0.82
11:00	B	2.06b	−0.58a	0.52
11:00	C	2.84b	−0.98a	0.68
12:00	A	3.29a	−0.50a	0.82
12:00	B	2.85b	−0.54a	0.71
12:00	C	2.86c	−0.70a	0.56
13:00	A	3.53a	−0.47a	0.82
13:00	B	2.68b	−0.45a	0.67
13:00	C	2.98c	−0.71a	0.66
14:00	A	3.42a	−0.53a	0.81
14:00	B	2.76b	−0.59a	0.65
14:00	C	2.35c	−0.71a	0.63
15:00	A	2.60a	−0.48a	0.82
15:00	B	2.09b	−0.54a	0.76
15:00	C	1.67c	−0.62a	0.6
16:00	A	1.55a	−0.41a	0.8
16:00	B	1.40b	−0.49ab	0.65
16:00	C	1.33c	−0.67b	0.66
17:00	A	1.11a	−0.45a	0.69
17:00	B	0.88b	−0.50a	0.77
17:00	C	0.64c	−0.68a	0.79

18:00	A	0.56a	−0.45a	0.79
18:00	B	0.56a	−0.64b	0.88
18:00	C	0.01b	−0.64ab	0.9

As observed for the NWSBs obtained with pooled data (Table 4.2), the NWSBs derived during the three periods of study (A, B and C) also exhibited a strong diurnal variation (Fig. 4.5).

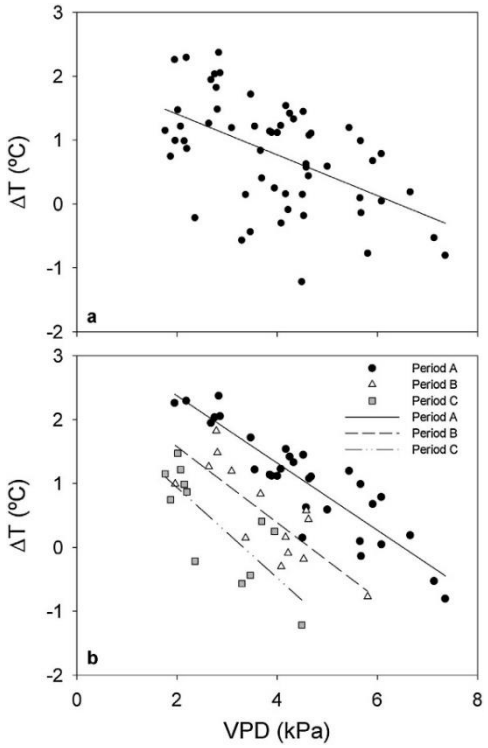

Figure 4.4 Example of seasonal effect on the NWSB ($\Delta T = a + b \cdot VPD$). The upper panel **(a)** shows the ΔT vs VPD relationship when data of the period DOY 167–275 are gathered together. The lower panel (**b**) shows the same relationship when data are split in three periods: A (June-July, DOY 167–212), B (August, DOY 215–243), C (September, DOY 244–273). Only clear-sky days were used in the calculations. In both panels, data for GMT = 14 h have been used. The straight lines represent the best fit to the data, whose fitted parameters and coefficients of determination are shown in Tables 2 (panel a) and 3 (panel b).

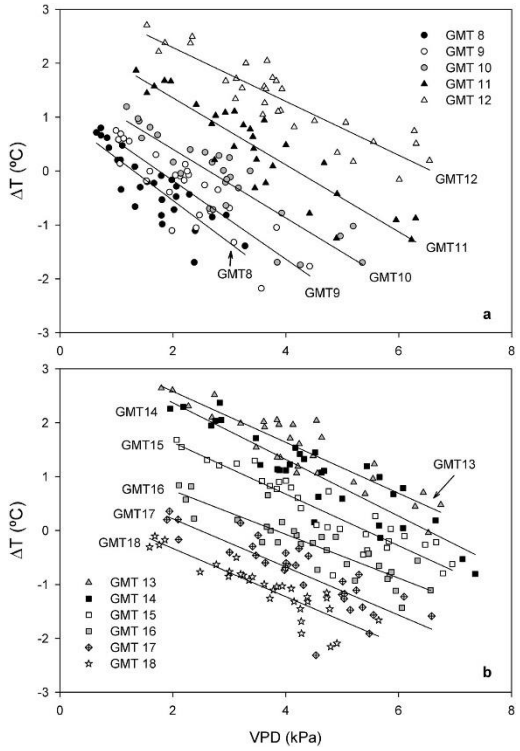

Figure 4.5 Diurnal variation of the NWSB ($\Delta T = a + b \cdot VPD$) for the period June–July (DOY 167–212). The upper panel (**a**) shows the ΔT vs VPD relationship for GMT 8 to GMT 12. The lower panel (**b**) shows the same relationship for GMT 13 to GMT 18. Only clear-sky days were used in the calculations. The straight lines represent the best fit to the data, whose fitted parameters and coefficients of determination are shown in Table 4.3.

The diurnal time-course of the NWSB-intercepts was successfully modeled with fourth-order polynomial equations during the three periods of study (A, B and C) (Fig. 4.6), whereas that of the NWSB-slopes was successfully modeled with second-order polynomial equations (Fig. 4.7). In order to reduce the empiricism and site specificity of these models, the parameters of the NWSBs obtained were regressed against the zenith solar angle (Testi et al., 2008).

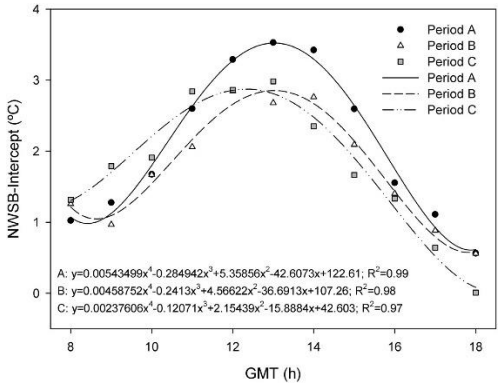

Figure 4.6 Diurnal evolution of the NWSB-intercept (◦C) for the three different periods of study: A (June–July, DOY 167–212), B (August, DOY 215–243), C (September, DOY 244–273). The lines represent the best-fit to the data.

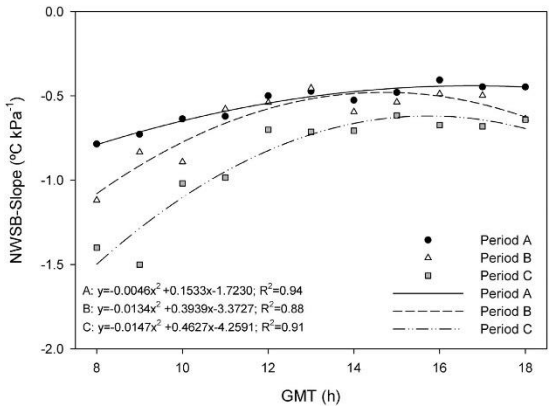

Figure 4.7 Diurnal evolution of the NWSB-slope (◦C kPa^{-1}) for the three different periods of study: A (June–July, DOY 167–212), B (August, DOY 215–243), C (September, DOY 244–273). The lines represent the best-fit to the data.

While the relation between the NWSB-slopes and zenith solar angle was not significant (data not shown), the NWSB-intercepts showed a tight relationship with solar angle (Fig. 4.8). As depicted in Fig. 4.8a, this relationship showed a marked hysteresis during periods A and B but not in period C. When the dataset was split into morning and afternoon data, it was observed that the relationship NWSB-intercept vs solar angle was season-dependent during the morning hours only (period C differed from A and B) (Fig. 4.8b), whereas no seasonal effect on NWSB-intercept was observed during the afternoon (Fig. 4.8c).

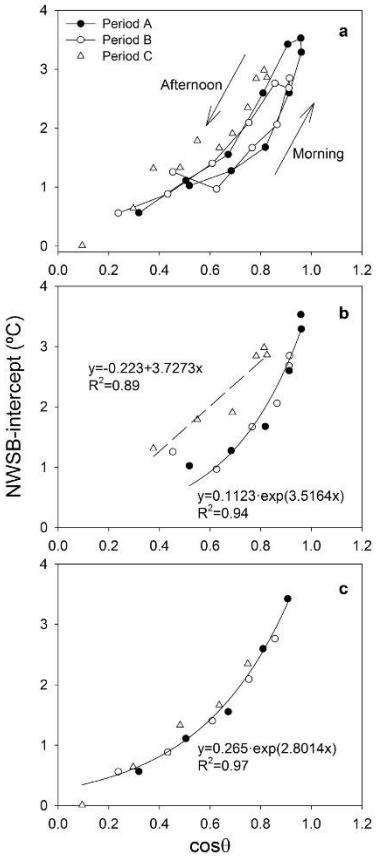

Figure 4.8. Relationship between NWSB-intercepts and zenith solar angle for the period **(a)** 08:00-18:00, **(b)** 08:00-13:00 and **(c)** 13:00-18:00.

4.3.2. Crop Water Stress Index derived from IRTs and RPAS

The canopy temperature measurements obtained with the IRTs and with the thermal camera mounted on the RPAS were used to derive the seasonal dynamics of CWSI in the irrigation treatments (Figs. 4.9a, b). The CWSI obtained from the IRT readings was markedly influenced by the irrigation regime (Fig. 4.9a). In FI, CWSI values ranged within the interval -0.17 to 0.15 throughout the irrigation season, with a mean value of 0.00. During the first water stress period depicted in Fig. 9 (DOY 174-236), the deficit irrigation treatment monitored with the IRTs ($45RDI_{TP}$) exhibited values of CWSI that were much higher than those found in FI trees, up to approximately 0.7 (Fig. 4.9a). During the last water stress period (DOY 258 onwards), the differences in CWSI between FI and $45RDI_{TP}$ were lower, with values close to 0 and 0.2, respectively.

The CWSI values determined from aerial thermal imaging in FI, $45RDI_{TP}$ and $45RDI_{CC}$ treatments are depicted in Fig. 4.9b. The FI trees exhibited values of CWSI that ranged from -0.07 to 0.17, with mean seasonal values of 0.04. The $45RDI_{TP}$ and $45RDI_{CC}$ treatments showed similar trends, with maximum values close to 0.8 observed during the first water stress period. The differences in CWSI between FI and 45RDI treatments for DOY 239 and 281 were much smaller and not statistically significant, with mean values close to 0.3-0.4 in $45RDI_{TP}$ and $45RDI_{CC}$ and close to 0 in FI. The seasonal trend of CWSI derived from aerial thermal imaging was similar to that of REW (Fig. 4.9c), which also revealed significant differences between FI and the 45RDI treatments during the first water stress period but not afterwards.

4.3.3. Relationship between CWSI and other plant-based water status indicators

The CWSI values derived from aerial thermal imaging for the five days of flight and the three irrigation treatments were plotted against stem water potential (Ψ_{st}), leaf water potential (Ψ_l), stomatal conductance (g_{sm}) and leaf transpiration rate (E_m) (Fig. 10). In all cases, significant (P <0.01) linear regressions were observed. The goodness of fit of the relationship between Ψ_{st} and Ψ_l with CWSI were similar, with coefficients of determination close to 0.7 (Figs. 4.9a, 4.9b). The relationship between leaf transpiration rate (E_m) and CWSI was somewhat weaker than that previously described for Ψ_{st} and Ψ_l, with a coefficient of determination of 0.6 (Fig. 4.10d). Stomatal conductance (g_{sm}) was the physiological variable that exhibited the tightest linear relationship with CWSI, with a coefficient of determination of 0.91 (Fig. 4.10c).

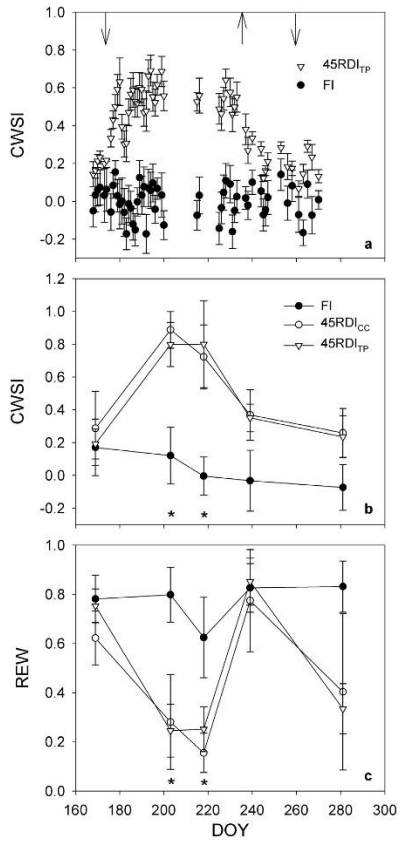

Figure 4.9 Seasonal time-course of (**a**) CWSI determined from canopy temperature measured with the infrared thermometers (IRTS) at 12.00 GMT, (**b**) CWSI derived from RPAS thermal imaging (12.00 GMT) and (**c**) REW. The NWSB shown in Table 4.3 for periods A, B & C were used in CWSI calculation. In (**a**), only clear-sky days were used for CWSI determination. Each point is the mean of two (**a**), four (**b**) and three (**c**) replicates per treatment. Down-facing arrows indicate the onset of water stress periods in RDI treatments; the up-facing arrow indicates the end of a water stress period. The error bars represent the standard error of the mean (SE). In (**b**) and (**c**), asterisks denote significant differences at $P < 0.05$.

4.4. Discussion

The diurnal variation observed in the non-water-stressed baselines (NWSBs) derived for olive trees (Fig. 5) has already been described in other woody species, such as pistachio (Testi et al., 2008) and grapevine (Bellvert et al., 2014). Both of these studies found that diurnal shifts in the NWSBs were mainly due to variations in the NWSB-intercept, as the slope of the baselines was rather stable. As explained theoretically by Jackson et al. (1981), the intercept of the NWSB is expected to increase with solar radiation and to decrease with wind speed. decrease with wind speed.

In our case study, diurnal variations of the NWSB-intercept due to wind speed are unlikely since the experimental area is not particularly windy (diurnal wind speed was below 2 m s^{-1} most of the days) and the effect of low to moderate wind speed on NWSB has been reported to be negligible (Testi et al., 2008), although it has to be noted that was in a different species with different aerodynamic conductance for sensible heat flux.

Therefore, the observed diurnal variation in the NWSB-intercept (Tables 4.2, 4.3) was likely driven by solar radiation, as evidenced by the tight relationship found with zenith solar angle (Fig. 4.8). As compared to previous findings in which NWSB-intercept and solar angle were linearly related (Testi et al., 2008), in olive trees the relationship showed a marked hysteresis during periods A and B (Fig. 4.8a).

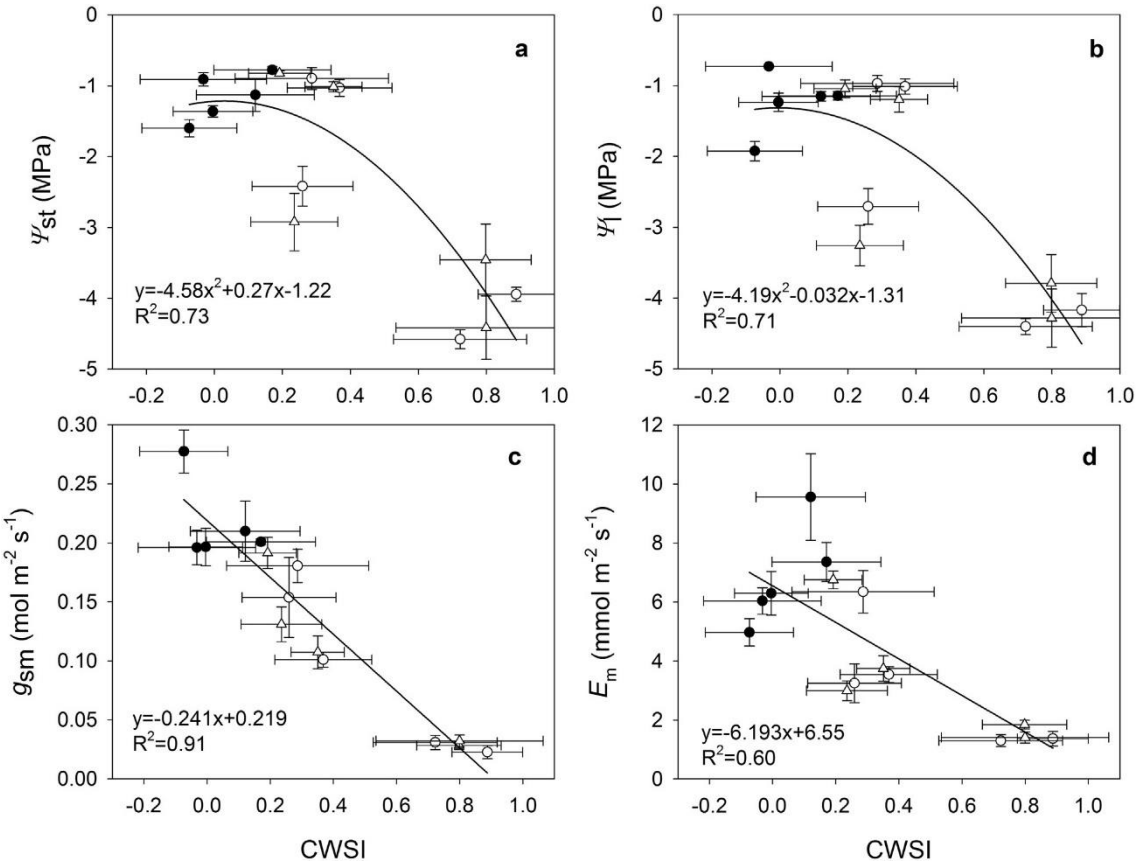

Figure 4.10 Relationship between CWSI determined from aerial thermal imaging and (a) midday stem water potential (ψ_{st}), (b) midday leaf water potential (ψ_l), (c) stomatal conductance (g_{sm}) and (d) leaf transpiration rate (E_m) for FI, 45RDI$_{CC}$ and 45RDI$_{TP}$ treatments. The straight lines represent the fitted regression lines to the data.

This behaviour indicates that, for similar radiation and VPD levels, the cooling effect of transpiration in the summer (periods A and B) is higher during the morning hours. This can be due to the fact that, in olive, stomata opening is greater in the morning than in the afternoon (Fernández et al., 1997). Therefore, transpiration and its cooling effect is also greater in morning than in afternoon hours. Unlike what has been observed in previous studies on woody crops (Bellvert et al., 2014; Testi et al., 2008), the diurnal evolution of the NWSB-slope in olives was stable only from 12:00 GMT onwards, whereas an increasing trend that was more pronounced as the season progressed was observed between 8:00 to 12:00 GMT.

Compared to other crop species, the NWSB-intercept derived for olives (the maximum was approximately 3.5 ºC for period A and close to 3 ºC in periods B and C; Fig. 4.6) was within the order of magnitude of those found in the literature for other herbaceous (Idso, 1982) and woody crop species (Bellvert et al., 2015; Testi et al., 2008). However, the NWSB-slope (maximum values around −0.5 ºC kPa^{-1} for periods A and B and close to −0.7 ºC kPa^{-1} in period C; Fig. 4.7) derived for olives was substantially lower (expressed as an absolute value) than the slopes derived for other crop species, with the sole exception of the values derived for citrus trees (Gonzalez-Dugo et al., 2014). In herbaceous crops, Idso (1982) found NWSB-slope values within the interval −3.25 ºC kPa^{-1} to −1.23 ºC kPa^{-1}, whereas in other fruit tree species the corresponding midday values were around −1.35 ºC kPa^{-1} (pistachio), −1.7 ºC kPa^{-1} (peach) and −1.9 ºC kPa^{-1} (vineyard) (Bellvert et al., 2016a, 2014; Testi et al., 2008). In olive trees, two previous studies provided controversial NWSB-slope values, as denoted by the very small slope (−0.35 ºC kPa^{-1}) obtained by Berni et al. (2009) compared to that (−2.05 ºC kPa^{-1}) reported by Bellvert et al. (2016a). Our findings are in agreement with the small slope value found by Berni et al. (2009), who argued that this value was a consequence of the small size of olive leaves, which makes them to be highly coupled to the atmosphere, causing a marked stomatal closure when the evaporative demand increases, even in trees under non-limiting soil water conditions (Fernández et al., 1997).

Seasonal differences in the NWSBs were already reported early in the 1980s for two herbaceous crops, wheat and barley (Idso, 1982), but little is known about the seasonal stability of the NWSBs derived for many others herbaceous and woody crop species. In peach trees, within season differences in the NWSB were small (Bellvert et al., 2016a); thus, a unique NWSB for the whole growing season was recommended by the authors. In olive trees, Berni et al. (2009) obtained their NWSB (Tc− Ta = −0.35·VPD + 2.08, R2 = 0.67) by computing the values from clear days (12:30 GMT) from April to September. They did not report any seasonal effect on such a relationship, but stressed the high scatter and the low slope as compared to those reported by other authors. By comparing their NWSB with the one obtained in this study ($T_c - T_a$ = −0.36·VPD + 2.50, R^2 = 0.49) for the period June-September at a similar time (12:00 GMT, Table 4.2), it can be observed that there are no differences in the slopes and the intercepts are very similar. Therefore, a plausible explanation for the high scatter reported by Berni et al. (2009) is a within-season shift in the NWSB, like the one shown by our results. Recently, Bellvert et al. (2015) found that some vineyard cultivars exhibited seasonal NWSB shifts, which were associated to variations in the energy balance of the canopy, zenith solar angle or leaf orientation. In our case study, the seasonal shift of the NWSBs (Figs. 4.6 and 4.7)

was partly explained by variations in zenith solar angle (Fig. 4.8). In fact, the seasonal variation of NWSB-intercept derived for afternoon hours could be explained by zenith solar angle variations (Fig. 4.8c). However, this could not be done for the morning NWSB-intercept values, since NWSB-intercept of period C was higher than that of periods A and B for similar solar angles (Fig. 4.8b). In any case, the robustness of the derived NWSB to be used for irrigation scheduling, as well as its daily and seasonal dynamics, should be assessed in different locations and cultivars similarly to what has been performed for other olive water status indicators (Corell et al., 2016).

Although the CWSI values calculated from IRTs and RPAS are not fully comparable, since the former was calculated from measurements collected at one out of the four plots used to compute CWSI from RPAS measurements, both indicators followed the same seasonal trend and depicted values within the same order of magnitude, both for the FI and 45RDI$_{TP}$ treatments (Fig. 4.9). Although CWSI is supposed to vary within 0 and 1, slightly negative values of CWSI may also be found in well-watered plants, as in our FI trees (Fig. 4.9a, b), due to the data scatter of the NWSBs (Bellvert et al., 2015; Testi et al., 2008). Values of CWSI derived from the FI trees with both sensing platforms throughout the irrigation season were close to zero. The deficit treatment that was monitored with IRTs and RPAS exhibited the highest values during the first water stress period depicted in Fig. 4.9 (end of June-end of August), reaching *ca.* 0.7 and 0.8 respectively for REW values *ca.* 0.2 (Fig. 4.9c). The close matching in CWSI trends among proximal (IRTs) and remote (RPAS) thermal sensing indicates that the T_c measurements derived from the mini RPAS using a segmentation method based on a bi-modal histogram analysis and the FWEM rule are suitable for monitoring the CWSI in SHD olive orchards.

The suitability of CWSI as a water stress index for SHD olive orchards was also demonstrated through the sound relationships found between CWSI and the reference plant water stress indicators, such as ψ_{st}, ψ_l, gsm and E_m (Fig. 4.10). Interestingly, the CWSI explained 91% of the variability observed in gsm across treatments and periods (Fig. 4.10c), whereas the variability of ψ_{st}, ψ_l and E_m that could be explained with CWSI was only 60%–73% (Fig. 4.10a, b and d). These results are in agreement with the theoretical basis of CWSI (Maes and Steppe, 2012) which denotes that, under water stress, variations in CWSI are driven by variations in T_c and g_{sm} is a main driving physiological variable. However, and due to the near-isohydric behaviour of the olive tree (Cuevas et al., 2010), decreases in leaf and stem water potential under conditions of water stress are minimized by stomatal regulation, thus explaining the poorer relationships found between CWSI and these variables. In a previous work conducted in

an olive orchard with less tree density than ours, Berni et al. (2009) also found that CWSI was linearly related to both g_{sm} and ψ_l and that CWSI was better correlated with gsm than with ψ_l. However, g_{sm} is not always better correlated with CWSI than ψ_l, as recently found in nectarines (Bellvert et al., 2016a). Despite that leaf transpiration (E_m) and gsm are strongly related (Jones, 1992), the relationship between CWSI and E_m was weaker than that with g_{sm} (Fig. 10), likely because E_m depends not only on g_{sm} but also on the boundary layer conductance (g_b) (Jones, 1992), whose value within the leaf cuvette of the gas analyzer set by the user may greatly differ from the prevailing g_b values in the orchard.

In the majority of studies performed to assess CWSI performance on fruit tree species, the variable used to validate the suitability of CWSI as a water status indicator was ψ_{st} (Gonzalez-Dugo et al., 2014, 2013; Testi et al., 2008) or ψ_l (Bellvert et al., 2016a, 2015, 2014). However, reported relationships between CWSI and these variables are not always linear, as it has also been observed in this study (Figs. 4.10a, b). For mandarin and orange trees, for instance, curvilinear relationships have been reported (Gonzalez-Dugo et al., 2014). In other species, such as grapevine (Bellvert et al., 2015, 2014) or peach (Bellvert et al., 2016a; Gonzalez-Dugo et al., 2013) both linear and curvilinear relationships have been reported.

4.5. Conclusions

The Non-Water-Stressed Baseline (NWSB) for CWSI calculation in SHD olive orchards was not constant throughout the growing season, but its seasonal shift could be partly explained by variations in zenith solar angle. Both NWSB-intercepts and NWSB-slopes exhibited diurnal variation, but these trends were successfully modelled with polynomial equations to ease CWSI calculation at any time of the day. In order to reduce the empiricism and site specificity of these models, a sound relationship between NWSB-intercept and solar angle was found. The CWSI values derived from high-resolution thermal imagery captured from a mini RPAS demonstrated to be a suitable indicator for both monitoring water stress and assessing water status variability in SHD olive orchards. Stomatal conductance had the tightest relationship with CWSI, over performing other widely used plant water status indicators such as leaf or stem water potential.

4.6 References

Agam, N., Cohen, Y., Berni, J.A.J., Alchanatis, V., Kool, D., Dag, A., Yermiyahu, U., Ben-Gal, A., 2013. An insight to the performance of crop water stress index for olive trees. *Agricultural Water Management*. 118, 79–86. doi:10.1016/j.agwat.2012.12.004

Agam, N., Segal, E., Peeters, A., Levi, A., Dag, A., Yermiyahu, U., Ben-Gal, A., 2014. Spatial distribution of water status in irrigated olive orchards by thermal imaging. *Precision Agriculture* 15, 346–359. doi:10.1007/s11119-013-9331-8

Alderfasi, A.A., Nielsen, D.C., 2001. Use of crop water stress index for monitoring water status and scheduling irrigation in wheat. *Agricultural Water Management*. 47, 69–75.

Bellvert, J., Zarco-Tejada, P.J., Girona, J., Fereres, E., 2014. Mapping crop water stress index in a “Pinot-noir” vineyard: Comparing ground measurements with thermal remote sensing imagery from an unmanned aerial vehicle*. Precis. Agric*. 15, 361–376. doi:10.1007/s11119-013-9334-5

Bellvert, J., Marsal, J., Girona, J., Zarco-Tejada, P.J., 2015a. Seasonal evolution of crop water stress index in grapevine varieties determined with high-resolution remote sensing thermal imagery. *Irrigation Science* doi:10.1007/s00271-014-0456-y

Bellvert, J., Zarco-Tejada, P.J., Marsal, J., Girona, J., González-Dugo, V., Fereres, E., 2015b. Vineyard irrigation scheduling based on airborne thermal imagery and water potential thresholds. *Aust. J. Grape Wine Res*. doi:10.1111/ajgw.12173

Bellvert, J., Marsal, J., Girona, J., Gonzalez-Dugo, V., Fereres, E., Ustin, S.L., Zarco-Tejada, P.J., 2016. Airborne thermal imagery to detect the seasonal evolution of crop water status in peach, nectarine and Saturn peach orchards. *Remote Sensing* 8, 1–17. doi:10.3390/rs8010039

Ben-Gal, A., Agam, N., Alchanatis, V., Cohen, Y., Yermiyahu, U., Zipori, I., Presnov, E., Sprintsin, M., Dag, A., 2009. Evaluating water stress in irrigated olives: Correlation of soil water status, tree water status, and thermal imagery. *Irrigation Scienc*e 27, 367–376. doi:10.1007/s00271-009-0150-7

Berni, J.A.J., Zarco-Tejada, P.J., Sepulcre-Cantó, G., Fereres, E., Villalobos, F., 2009. Mapping canopy conductance and CWSI in olive orchards using high resolution thermal remote sensing imagery. *Remote Sens. Environ*. 113, 2380–2388. doi:10.1016/j.rse.2009.06.018

Corell, M., Pérez-López, D., Martín-Palomo, M.J., Centeno, A., Girón, I., Galindo, A., Moreno, M.M., Moreno, C., Memmi, H., Torrecillas, A., Moreno, F., Moriana, A., 2016. Comparison of the water potential baseline in different locations. Usefulness for irrigation scheduling of olive orchards. *Agricultural Water Management*. 177, 308–316. doi:10.1016/j.agwat.2016.08.017

Couvreur, V., Kandelous, M.M., Sanden, B.L., Lampinen, B.D., Hopmans, J.W., 2016. Downscaling transpiration rate from field to tree scale. *Agric. For. Meteorol*. 221, 71–77. doi:10.1016/j.agrformet.2016.02.008

Cuevas, M. V., Martín-Palomo, M.J., Diaz-Espejo, A., Torres-Ruiz, J.M., Rodriguez-Dominguez, C.M., Perez-Martin, A., Pino-Mejías, R., Fernández, J.E., 2013. Assessing water stress in a hedgerow olive orchard from sap flow and trunk diameter measurements. *Irrigation Science* 31, 729–746. doi:10.1007/s00271-012-0357-x

Cuevas, M. V., Torres-Ruiz, J.M., Álvarez, R., Jiménez, M.D., Cuerva, J., Fernández, J.E., 2010. Assessment of trunk diameter variation derived indices as water stress indicators in mature olive trees. *Agricultural Water Management*. 97, 1293–1302. doi:10.1016/j.agwat.2010.03.011

Dupin, S., Gobrecht, A., B.Tisseyre, 2011. Airborne Thermography of Vines Canopy: Effect of the Atmosphere and Mixed Pixels on Observed Canopy Temperature. *8 ème Conférence Eur. sur l'Agriculture Précision* 1, 1–9.

Egea, G., Diaz-Espejo, A., Fernández, J.E., 2016. Soil moisture dynamics in a hedgerow olive orchard under well-watered and deficit irrigation regimes: Assessment, prediction and scenario analysis. *Agricultural Water Management*. 164, 197–211. doi:10.1016/j.agwat.2015.10.034

Fernández, J.E., 2014. Understanding olive adaptation to abiotic stresses as a tool to increase crop performance. *Environ. Exp. Bot*. 103, 158–179. doi:10.1016/j.envexpbot.2013.12.003

Fernández, J.E., Moreno, F., Girón, I.F., Blázquez, O.M., 1997. Stomatal control of water use in olive tree leaves. *Plant Soi*l 190, 179–192. doi:10.1023/A:1004293026973

Fernández, J.E., Moreno, F., Martín-Palomo, M.J., Cuevas, M.V., Torres-Ruiz, J.M., Moriana, A., 2011. Combining sap flow and trunk diameter measurements to assess water needs in mature olive orchards. *Environ. Exp. Bot*. 72, 330–338. doi:10.1016/j.envexpbot.2011.04.004

Fernández, J.E., Perez-Martin, A., Torres-Ruiz, J.M., Cuevas, M. V., Rodriguez-Dominguez, C.M., Elsayed-Farag, S., Morales-Sillero, A., García, J.M., Hernandez-Santana, V., Diaz-Espejo, A., 2013. A regulated deficit irrigation strategy for hedgerow olive orchards with high plant density. *Plant Soi*l 372, 279–295. doi:10.1007/s11104-013-1704-2

Fuchs, M., Tanner, C.B., 1966. Infrared Thermometry of Vegetation1. *Agron. J.* 58, 597. doi:10.2134/agronj1966.00021962005800060014x

Gómez Del Campo, M., García, J.M., 2013. Summer deficit-irrigation strategies in a hedgerow olive cv. arbequina orchard: Effect on oil quality. *J. Agric. Food Chem*. 61, 8899–8905. doi:10.1021/jf402107t

Gonzalez-Dugo, V., Zarco-Tejada, P., Nicolás, E., Nortes, P.A., Alarcón, J.J., Intrigliolo, D.S., Fereres, E., 2013. Using high resolution UAV thermal imagery to assess the variability in the water status of five fruit tree species within a commercial orchard. Precis. Agric. 14, 660–678. doi:10.1007/s11119-013-9322-9

Gonzalez-Dugo, V., Zarco-Tejada, P.J., Fereres, E., 2014. Applicability and limitations of using the crop water stress index as an indicator of water deficits in citrus orchards. Agric. For. Meteorol. 198–199, 94–104. doi:10.1016/j.agrformet.2014.08.003

Hatfield, J.L., Wanjura, D.F., Barker, G.L., 1985. Canopy temperature response to water stress under partial canopy. Trans. Am. Soc. Agric. Eng. 28, 1607–1611.

Idso, S.B., 1982. Non-water-stressed baselines: A key to measuring and interpreting plant water stress. Agric. Meteorol. 27, 59–70.

Idso, S.B., Jackson, R.D., Pinter, P.J., Reginato, R.J., Hatfield, J.L., 1981. Normalizing the stress-degree-day parameter for environmental variability. Agric. Meteorol. 24, 45–55. doi:10.1016/0002-1571(81)90032-7

Irmak, S., Haman, D.Z., Bastug, R., 2000. Determination of Crop Water Stress Index for Irrigation Timing and Yield Estimation of Corn. Agron. J. 92, 1221. doi:10.2134/agronj2000.9261221x

Jackson, R.D., Idso, S.B., Reginato, R.J., Pinter, P.J., 1981. Canopy temperature as a crop water stress indicator. Water Resour. Res. 17, 1133–1138. doi:10.1029/WR017i004p01133

Jiménez-Bello, M.A., Ballester, C., Castel, J.R., Intrigliolo, D.S., 2011. Development and validation of an automatic thermal imaging process for assessing plant water status. Agric. Water Manag. 98, 1497–1504. doi:10.1016/j.agwat.2011.05.002

Jones, H.G., 2007. Monitoring plant and soil water status: Established and novel methods revisited and their relevance to studies of drought tolerance. J. Exp. Bot. 58, 119–130. doi:10.1093/jxb/erl118

Jones, H.G., 1992. Plants and microclimate: a quantitative approach to environmental plant physiology. Cambridge University Press.

Maes, W.H., Steppe, K., 2012. Estimating evapotranspiration and drought stress with ground-based thermal remote sensing in agriculture: a review. Jorunal Exp. Bot. 63, 4671–4712. doi:10.1093/jxb/ers165

Möller, M., Alchanatis, V., Cohen, Y., Meron, M., Tsipris, J., Naor, A., Ostrovsky, V., Sprintsin, M., Cohen, S., 2007. Use of thermal and visible imagery for estimating crop water status of irrigated grapevine. J. Exp. Bot. 58, 827–838. doi:10.1093/jxb/erl115

Nielsen, D.C., Anderson, R.L., 1989. Infrared thermometry to measure single leaf temperatures for quantification of water-stress in sunflowe. Agron. J. 81, 840–842.

Padilla-Díaz, C.M., Rodriguez-Dominguez, C.M., Hernandez-Santana, V., Perez-Martin, A., Fernández, J.E., 2016. Scheduling regulated deficit irrigation in a hedgerow olive orchard from leaf turgor pressure related measurements. Agric. Water Manag. 164, 28–37. doi:10.1016/j.agwat.2015.08.002

R Core Team, 2015. R: A language and environment for statistical computing. R Foundation for Statistical Computing. Vienna, Austria.

Rius, X., Lacarte, J.M., 2010. La revolución del olivar. El cultivo en seto. Locator Maps PTY. LTD.

Rud, R., Cohen, Y., Alchanatis, V., Beiersdorf, I., Klose, R., Presnov, E., Levi, A., Brikman, R., Agam, N., Dag, A., Ben-Gal, A., 2015. Characterization of salinity-induced effects in olive trees based on thermal imagery. Precis. Agric. 2015 - Pap. Present. 10th Eur. Conf. Precis. Agric. ECPA 2015 511–517.

Scholander, P.F., Hammel, H.T., Bradstreet, E.D., Hemmingsen, E.A., 1965. Sap Pressure in Vascular Plants: Negative hydrostatic pressure can be measured in plants. Science (80-.). 148, 339–346. doi:10.1126/science.148.3668.339

Sepulcre-Cantó, G., Zarco-Tejada, P.J., Jiménez-Muñoz, J.C., Sobrino, J.A., Miguel, E. De, Villalobos, F.J., 2006. Detection of water stress in an olive orchard with thermal remote sensing imagery. Agric. For. Meteorol. 136, 31–44. doi:10.1016/j.agrformet.2006.01.008

Testi, L., Goldhamer, D.A., Iniesta, F., Salinas, M., 2008. Crop water stress index is a sensitive water stress indicator in pistachio trees. Irrig. Sci. 26, 395–405. doi:10.1007/s00271-008-0104-5

Xie, Y., Sha, Z., Yu, M., 2008. Remote sensing imagery in vegetation mapping: a review. J. Plant Ecol. 1, 9–23. doi:10.1093/jpe/rtm005

Zimmermann, D., Reuss, R., Westhoff, M., Gessner, P., Bauer, W., Bamberg, E., Bentrup, F.-W., Zimmermann, U., 2008. A novel, non-invasive, online-monitoring, versatile and easy plant-based probe for measuring leaf water status. J. Exp. Bot. 59, 3157–67. doi:10.1093/jxb/ern171

III. Publications: Chapter 3

Optical Sensing to Determine Tomato Plant Spacing for Precise Agrochemical Application: Two Scenarios

Martínez-Guanter, J.[1]; Garrido-Izard, M.[2]; Valero, C. [2]; Slaughter, D.C.[3] Pérez-Ruiz, M.[1]

[1]Area of Agroforestry Engineering, Aerospace Engineering and Fluids Mechanic Department, School of Agricultural Engineering, Universidad de Sevilla, Ctra. Utrera km.1, 41013 Seville, Spain

[2] Laboratorio de Propiedades Físicas (LPF_TAGRALIA), Universidad Politécnica de Madrid (UPM), 28040 Madrid, Spain

3 Department of Biological and Agricultural Engineering, University of California, Davis, CA 95616, USA;

Published on:

Sensors
May 2017, Sensors 2017, 17, 1096
DOI: 10.3390/s17051096

Abstract:

The feasibility of automated individual crop plant care in vegetable crop fields has increased, resulting in improved efficiency and economic benefits. A systems-based approach is a key feature in the engineering design of mechanization that incorporates precision sensing techniques. The objective of this study was to design new sensing capabilities to measure crop plant spacing under different test conditions (California, USA and Andalucía, Spain). For this study, three different types of optical sensors were used: an optical light-beam sensor (880 nm), a Light Detection and Ranging (LiDAR) sensor (905 nm), and an RGB camera. Field trials were conducted on newly transplanted tomato plants, using an encoder as a local reference system. Test results achieved a 98% accuracy in detection using light-beam sensors while a 96% accuracy on plant detections was achieved in the best of replications using LiDAR. These results can contribute to the decision-making regarding the use of these sensors by machinery manufacturers. This could lead to an advance in the physical or chemical weed control on row crops, allowing significant reductions or even elimination of hand-weeding tasks.

5.1. Introduction

Precision agriculture requires accurate plant or seed distribution across a field. This distribution is to be optimized according to the size and shape of the area in which nutrients and light are provided to plant to obtain the maximum possible yield. These factors are controlled by the spacing between crop rows and the spacing of plants/seeds in a row (Klenin et al., 1985). For many crops, row spacing is determined as much by the physical characteristics of agricultural machinery used to work in the field as by the specific biological spacing requirements of the crop (Blas et al., 2013). According to the crop and machinery used, the accuracy of planting by the precision transplanter/seeder to the desired square grid pattern must be adequate for the operation of agricultural machinery in both longitudinal and transverse crop directions.

The current designs of vegetable crop transplanters and seeders utilize several uncoordinated planting modules mounted to a common transport frame. These systems use sub-optimal open-loop methods that neglect the dynamic and kinematic effects of the mobile transport frame and of plant motion relative to the frame and the soil. The current designs also neglect to employ complete mechanical control of the transplant during the entire planting process, producing an error in the final planting position, due to the increased uncertainty of plant location as a result of natural variations in plant size, plant mass, soil traction and soil compaction (Prasanna Kumar et al., 2008).

Accurately locating the crop plant, in addition to allowing automatic control of weeds, allows individualized treatment of each plant (e.g., spraying, nutrients). Seeking to ensure minimum physical interaction with plants (i.e., non-contact), different remote sensing techniques have been used for the precise localization of plants in fields. For these localization methods, some authors have decided to address automatic weed control by localizing crop plants with centimeter accuracy during seed drilling (Ehsani et al., 2004) or transplanting (Sun et al., 2010; Pérez-Ruiz et al., 2012) using a global positioning system in real time (RTK-GNSS). These studies, conducted at UC Davis, have shown differences between RTK-GNSS-based expected seed location versus actual plant position. The position uncertainly ranged from 3.0 to 3.8 cm for seeds, and tomato transplants, the mean system RMS was 2.67 cm in the along-track direction. Nakarmi and Tang used an image acquisition platform after planting to estimate the inter-plant distance along the crop rows (Nakarmi and Tang, 2012). This system could measure inter-plant distance with a minimum error of ±30 cm and a maximum error of ±60 cm.

Today, one of the biggest challenges to agricultural row crop production in industrialized countries is non-chemical control of intra-row (within the crop row) weed plants. Systems such as those developed by Pérez-Ruiz et al. (2014) or the commercial platforms based on computer-controlled hoes developed by Dedousis et al. (2007) are relevant examples of innovative mechanical weeding systems. However, the current effectiveness of mechanical weed removal is constrained by plant spacing, the proximity of the weeds to the plant, the plant height and the operation timing. Other methods for non-chemical weed control, such as the robotic platform developed by Blasco et al. (2002) (capable of killing weeds using a 15-kV electrical discharge), the laser weeding system developed by Shah et al. (2015) or the cross-flaming weed control machine designed for the RHEA project by Frasconi et al. (2014), demonstrate that research to create a robust and efficient system is ongoing. A common feature of all these technological developments is the need for accurate measurement of the distance between plants. Spatial distribution and plant spacing are considered key parameters for characterizing a crop. The current trend is towards the use of optical sensors or image-based devices for measurements, despite the possible limitations of such systems under uncontrolled conditions such as those in agricultural fields. These image-based tools aim to determine and accurately correlate several quantitative aspects of crops to enable plant phenotypes to be estimated (Li et al., 2014; Fahlgren et al., 2015).

Dworak et al. (2011) categorized research studying inter-plant location measurements into two types: airborne and ground-based. Research on plant location and weed detection using airborne sensors has increased due to the increasing potential of unmanned aerial systems in agriculture, which have been used in multiple applications in recent years (López-Granados, 2011). For ground-based research, one of the most widely accepted techniques for plant location and classification is the use of Light Detection and Ranging (LiDAR) sensors (Garrido-Izard et al., 2015). These sensors provide distance measurements along a line scan at a very fast scanning rate and have been widely used for various applications in agriculture, including 3D tree representation for precise chemical applications (Rosell et al., 2009; Garrido-Izard et al., 2012) or in-field plant location (Shi et al., 2013). This research continues the approach developed by Garrido-Izard et al (2014), in which a combination of LiDAR + IR sensors mounted on a mobile platform was used for the detection and classification of tree stems in nurseries. Based on the premise that accurate localization of the plant is key for precision chemical or physical removal of weeds, we propose in this paper a new methodology to precisely estimate tomato plant spacing. In this work, non-invasive methods using optical sensors such as LiDAR, infrared (IR) light-beam sensors and RGB-D cameras have been employed. For this purpose, a platform was developed on which different sensor

configurations have been tested in two scenarios: North America (UC Davis, CA, USA) and Europe (University of Seville, Andalucia, Spain). The specific objectives, given this approach, were:

-To design and evaluate the performance of multi-sensor platforms attached to a tractor (a UC Davis platform mounted on the rear of the tractor and a University of Seville platform mounted on the front of the tractor).

-To refine the data-processing algorithm to select the most reliable sensor for the detection and localization of each tomato plant.

5.2. Materials and Methods

To develop a new sensor platform to measure the space between plants in the same crop row accurately, laboratory and field tests were conducted in Andalucia (Spain) and in California (USA). This allowed researchers to obtain more data under different field conditions and to implement the system improvements required, considering the plant spacing objective. These tests are described below, characterizing the sensors used and the parameters measured.

5.2.1. Plant Location Sensors

5.2.1.1. Light-Beam Sensor Specifications

IR light-beam sensors (Banner SM31 EL/RL, Banner Engineering Co., Minneapolis, MN, USA) were used in two configurations: first as a light curtain (with three pairs of sensors set vertically, Figure 5.1 central and Figure5. 4) and later a simpler setup, using only one pair of sensors (Figure 5.2), which simplifies the system while still allowing the objective (plant spacing measurement) to be attained. In the light curtain, light-beam sensors were placed transversely in the middle of the platform to detect and discriminate the plant stem in a cross configuration to prevent crossing signals between adjacent sensors. Due to the short range and focus required in laboratory tests, it was necessary to reduce the field of view and the strength of the light signal by masking the emitter and receiver lens with a 3D-printed conical element. In laboratory tests, the height of the first emitter and receiver pair above the platform was 4 cm, and the height of 3D plants (artificial plants were used in laboratory tests; see Section 5.2.2) was 13 cm. In the field tests, the sensor was placed 12 cm from the soil (the average height measured manually for real plants in outdoor tests was 19.5 cm) to avoid obstacles in the field (e.g., dirt clods, slight surface undulations). In both cases, the receiver was set to obtain a TTL output pulse each time

the IR light-beam was blocked by any part of the plant. The signals generated by the sensors were collected and time-stamped by a microcontroller in real time and stored for off-line analysis. Technical features of the IR light-beam sensors are presented in Table 5.1.

Table 5.1. IR light-beam sensor features.

Operational Voltage (V)	10–30 V
Detection range (m)	30 m
Response time (milliseconds)	1 ms
Sinking and sourcing outputs (mA)	150 mA

5.2.2.2 Laser Scanner

A LMS 111 LiDAR laser scanner (SICK AG, Waldkirch, Germany), was used in the laboratory and field testing platforms to generate a high-density point cloud on which to perform the localization measurements. Its main characteristics are summarized in Table 5.2. The basic operating principle of the LiDAR sensor is the projection of an optical signal onto the surface of an object at a certain angle and range. Processing the corresponding reflected signal allows the sensor to determine the distance to the plant. The LiDAR sensor was interfaced with a computer through an RJ 45 Ethernet port for data recording. Data resolution was greatly affected by the speed of the platform's movement; thus, maintenance of a constant speed was of key importance for accurate measurements. During data acquisition, two digital filters were activated for optimizing the measured distance values: a fog filter (becoming less sensitive in the near range (up to approximately 4 m)); and an N-pulse-to-1-pulse filter, which filters out the first reflected pulse in case that two pulses are reflected by two objects during a measurement (LMS100 Product Family Operating Instructions, Waldkirch SA). Different LiDAR scan orientations were evaluated: scanning vertically with the sensor looking downwards (Figure 5.1), scanning with a 45° inclination (push-broom) and a lateral-scanning orientation (side-view).

Figure 5.1. Details of the sensors on the laboratory platform (vertical LiDAR and Light-beam sensors) for the detection and structure of the modular 3D plant.

Table 5.2. LMS 111 technical data.

Operational Range	From 0.5 to 20 m
Scanning field of view	270°
Scanning Frequency	50 Hz
Angular resolution	0.5°
Light source	905 nm
Enclosure rating	IP 67

5.2.1.3. RGB-D Camera

A Kinect V2 commercial sensor (Microsoft, Redmond, WA, USA), originally designed for indoor video games, was mounted sideways on the research platform during field trials. This sensor captured RGB, NIR and depth images (based on time-of-flight) of tomato plants, although for further analysis, only RGB images were used for the validation of stick/tomato locations obtained from the LiDAR scans, as detailed in Section 5.2.4.3. Kinect RGB-captured images have a resolution of 1920 × 1080 pixels and a field of view (FOV) of 84.1 × 53.8°, resulting in an average of approximately 22 × 20 pixels per degree. NIR images and depth camera have a resolution of 512 × 424 pixels, with an FOV of 70 × 60° and a depth-sensing maximum distance of 4.5–5 m. Although systems such as the Kinect sensor were primarily designed for use under controlled light conditions, the second version of this sensor has higher RGB resolution (640 × 480 in v1) and its infrared sensing capabilities were also improved, enabling a more lighting-independent view and supporting its use outdoors under high-illumination conditions. Despite this improvement, we observed that the quality of the RGB images were somewhat affected by luminosity and direct incident light, and therefore, the image must be post-processed to obtain usable results. The images taken by the Kinect sensor were simultaneously acquired and synchronized with the LiDAR scans and the encoder pulses. Because the LabVIEW software (National Instruments, Austin, TX, USA) used for obtaining the scan data was developed to collect three items (the scans themselves, the encoder pulses and the timestamp), a specific Kinect recording software had to be developed to embed the timestamp value in the image data. With the same timestamp for the LiDAR and the image, the data could be matched and the images used to provide information about the forward movement of the platform.

5.2.2. Lab Platform Design and Tests

To maximize the accuracy of the distance measurements obtained by the sensors, an experimental platform was designed to avoid the seasonal limitations of testing outdoors. Instead of working in a laboratory with real plants, the team designed and created model plants (see Figure 5.1) using a 3D printer (Prusa I3, BQ, Madrid, Spain). These plants were mounted on a conveyor chain at a predetermined distance. This conveyor chain system, similar to that of a bicycle, was driven by a small electric motor able to move the belt at a constant speed of 1.35 $km \cdot h^{-1}$. For the odometry system, the shaft of an incremental optical encoder (63R256, Grayhill Inc., Chicago, IL, USA) was mounted so that it was attached directly to the gear shaft and used to measure the distance travelled, thus serving as a localization reference system. Each channel in this encoder generates 256 pulses per revolution, providing a 3-mm resolution in the direction of travel. The data generated by the light-beam sensors and the cumulative odometer pulse count were collected using a low-cost open-hardware Arduino Leonardo microcontroller (Arduino Project, Ivrea, Italy) programmed in a simple integrated development environment (IDE). This device enabled recording of data that were stored in a text file for further computer analysis. Several repetitions of the tests were made on the platform to optimize the functions of both light-beam and LiDAR sensors. From the three possible LiDAR orientations, lateral scanning was selected for the field trials because it provided the best information on the structure of the plant, as concluded in Garrido-Izard et al., (2015). In lab tests, two arrangements of light-beam sensors were assessed: one in a light curtain assembly with three sensor pairs at different heights and another using only one emitter-receiver pair.

5.2.3. Field Tests

The initial tests, performed in Davis, CA (USA), were used to assess the setup of the light-beam sensor system and detected only the stem of the plants rather than locating it within a local reference system. Once the tomato plants were placed in the field, tests were conducted at the Western Center for Agriculture Equipment (WCAE) at the University of California, Davis campus farm to evaluate the performance of the sensor platform for measuring row crop spacing. For this test, an implement was designed to house the sensors as follows. The same IR light-beam sensor and encoder, both described in Section 5.2.1, were used (Figure 5.2). The output signals of the sensors were connected to a bidirectional digital module (NI 9403, National Instruments Co.), while the signal encoder was connected to a digital input module (NI 9411, National Instruments Co.). Both modules were integrated into an NI cRIO-9004 (NI 9411, National Instruments Co.), and all data were recorded using LabVIEW (National Instruments Co.).

In these early field trials, the team worked on three lines of a small plot of land 20 m in length, where the methodology for detecting the plants within a crop line was tested.

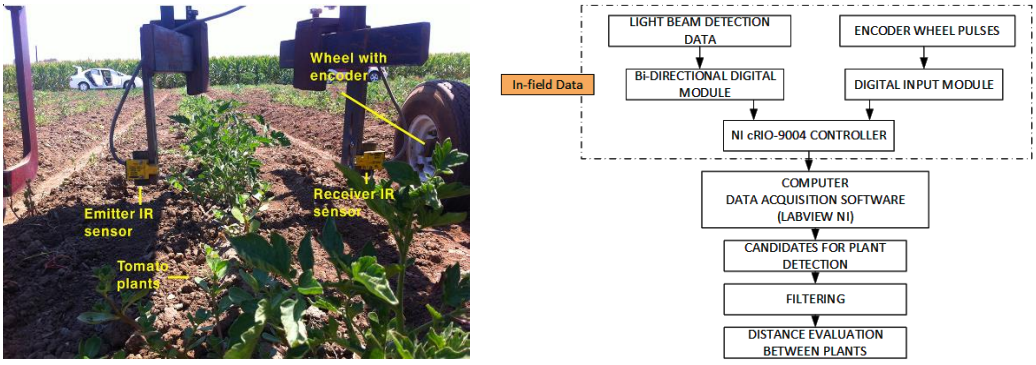

(**a**) (**b**)

Figure 2. (**a**) Light-beam sensors mounted on the experimental platform designed for field trials at UC Davis, California; (**b**) Progressive monitoring flowchart using light-beam sensors.

To continue the study of plant localization in a different scenario, additional experiments were designed at the University of Seville, in which a refinement of the LiDAR sensors and data processing were performed. These tests were conducted on several lines of tomato plants manually transplanted from trays, with the plants placed with an approximate, though intentionally non-uniform, spacing of 30 cm. Two of these lines were analyzed further, one with 55 tomato plants and the other with 51, and a line of 19 wooden sticks was also placed to provide an initial calibration of the instruments. Due to the initial test conditions, where tomato plants were recently transplanted and had a height of less than 20 cm, the team built an inverted U-shaped platform attached to the front of a small tractor (Boomer 35, New Holland, New Holland, PA, USA, Figure 5.3). The choice of the small tractor was motivated by the width of the track, as the wheels of the tractor needed to fit on the sides of the tomato bed, leaving the row of tomatoes clear for scanning and sensors.

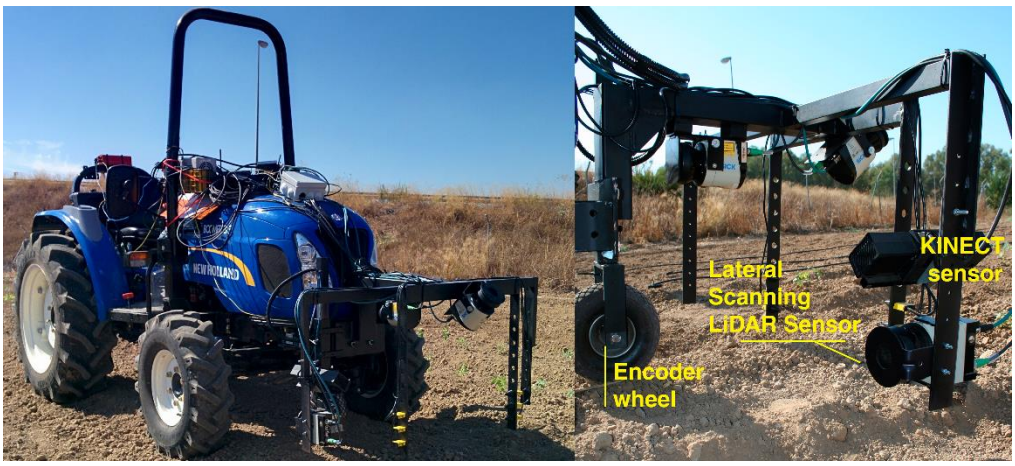

(**a**)

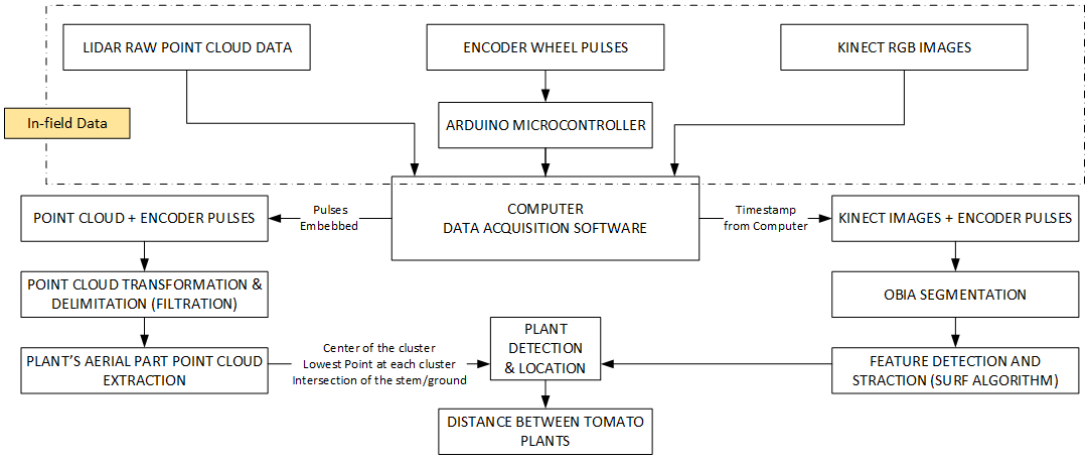

(**b**)

Figure 3. (**a**) Structure housing the sensors mounted on the tractor (left) and detail of the LiDAR and Kinect setup (right) for field trials at the University of Seville; (**b**) Progressive monitoring flowchart using LiDAR and Kinect sensors.

As was done in the laboratory platform, the encoder described in Section 5.2.1 was used as an odometric system, this time interfaced with an unpowered ground wheel, to determine the instantaneous location of the data along the row.

During the tests, the platform presented several key points that were addressed: (i) The encoder proved to be sensitive to vibrations and sudden movements, so it was integrated into the axis of rotation of an additional wheel, welded to the structure and dampened as much as possible from the vibrations generated by the tractor. In addition, the team had to reduce the slippage of the encoder wheel on the ground to avoid losing pulses; (ii) Correct orientation of the sensors was also key because the mounting angles of the LiDAR sensors would condition the subsequent analysis of the data obtained in the scans and the determination of which data contributed more valuable information; (iii) The speed of the tractor should be as low as possible remain uniform (during the test the average speed was 0.36 m/s) and maintain a steady course without steering wheel movements to follow a straight path.

5.2.4. Data-Processing Methodology

To detect precisely and determine properly the distances between plants in both laboratory and field tests, the data provided by the sensors were merged and analyzed.

5.2.4.1. Plant Characterization Using Light-Beam Sensors

The methodology followed to analyze data obtained from the light-beam curtain (which was formed by three light-beam sensors in line) was similar to that described in Garrido et al., (2014). The algorithm outputs the moment that the beam was interrupted and associates the beam with an encoder pulse. Because the 3D plants had a wider shape at the top (leaves) than the bottom (stem), and therefore more interruptions were received, the algorithm had to be adapted to each sensor pair and each height for plant detection. To discriminate correctly between plants for the light curtain case, the developed algorithm implemented a distance range, measured in pulses from the encoder, that allowed the verification of the presence or absence of a plant after the detection of the stem, inferring that interruptions received from the sensors placed at the middle and top heights before and after the stem corresponded to the leaves and the rest of the plant structure, respectively. For the analysis of data obtained from the single pair of IR light-beam sensors, a Matlab routine (MATLAB R2015b, MathWorks, Inc., Natick, MA, USA) was developed. System calibration was performed using 11 artificial plants in the laboratory test and 122 real tomato plants in the UC Davis field test. The methodology used for the detection of tomato plants was based on the following steps:

1. Selection of Values for the Variables Used by the Programme for Detection:

    a) Pulse_distance_relation: This variable allowed us to convert the pulses generated by the encoder into the distances travelled by the platforms. In laboratory trials, the encoder was coupled to the shaft that provided motion to the 3D plants, and in the field, it was coupled to a wheel installed inside the structure of the platform. The conversion factors used for the tests were 1.18 and 0.98 mm per pulse for the laboratory and the field, respectively.

    b) Detection_filter: To eliminate possible erroneous detections, especially during field trials due to the interaction of leaves, branches and even weeds, the detections were first filtered. We filtered every detection that corresponded to an along-track distance of less than 4 mm while the sensor was active (continuous detection).

    c) Theoretical_plant_distance: The value for the theoretical distance between plants in a crop *line*. The value set during testing was 100 mm and 380 mm for the laboratory and the field, respectively.

    d) Expected_plant_distance: Expected distance between plants in a crop line was defined as the theoretical plant distance plus an error of 20%.

2. Importing of raw data recorded by the sensors (encoder and existence “1” or absence “0” of detection by the IR sensors). The conversion factor (*pulse_distance_relation*) provided the distance in mm for each encoder value.

3. Data were filtered by removing all detections whose length or distance travelled, while the sensors were active, was less than the set value (*detection_filter*). Thus, potential candidates were selected by registering the following:

a) The distance at the start of the detection;
b) The distance at the end of the detection;
c) The distance travelled during detection and (iv) the mean distance during the detection, which was considered the location of the stem of the plant.

4. Distance evaluation between the current candidate and the previous potential plant:

a) If the evaluated distance was greater than the value set (*expected_plant_distance*), we considered this candidate as a potential new plant, registering in a new matrix: the number of the plant, the detections that defined it, the midpoint location and the distance from the previous potential plant.
b) If the evaluated distance was less than the set value (*expected_plant_distance*), plant candidate data was added to the previous potential plant, recalculating all components for this potential plant. The new midpoint was considered the detection closest to the theoretical midpoint.

5.2.4.2. Plant Characterization Using a Side-View LiDAR

For the analysis of the data obtained from the LiDAR, it is important to mention the high complexity of its data, in both volume and format, compared with those data obtained by the light-beam. This is reflected in the following section, which explains the proposed methodology for obtaining both the aerial point clouds of the tomato rows referenced to the encoder sensor and the tomato plant identification. This is a prerequisite for tomato plant localization. For this purpose, it was necessary to pre-process the data, followed by a transformation and translation from the LiDAR sensor to the scanned point.

5.2.4.2.1. Pre-Processing of Data

(i) Data pre-processing performed at the LiDAR sensor.

An off-line Matlab process was used with the actual field data collected during the field experiments. Data were filtered to eliminate false positives or those that did not contribute relevant information, considering only those detections with a distance greater than 0.05 m. Later, the resulting detections were transformed from polar to Cartesian coordinates using a horizontal orientation coordinate system as a reference.

(ii) From the LiDAR sensor to the scanned point: transformations and data delimitation.

To transform the horizontal LiDAR coordinates to the actual LiDAR orientation (lateral in our case), the following steps were followed:

a) The starting points were the Cartesian coordinates obtained using the horizontal orientation as a reference $(x'_{point}, y'_{point}, z'_{point})$.

b) To integrate the scan from LiDAR into the platform coordinate system, a different transformation $(x_\varphi, y_\theta, z_\psi)$ was applied (see Equation (5.1)), considering the actual orientation of the LiDAR (see Table 5.3). Each LiDAR scanned point in the platform coordinate system $(x_{point}, y_{point}, z_{point})$ was obtained:

$$\begin{bmatrix} x_{\text{point}} \\ y_{\text{point}} \\ z_{\text{point}} \\ 1 \end{bmatrix} = \begin{bmatrix} x'_{\text{point}} \\ y'_{\text{point}} \\ z'_{\text{point}} \\ 1 \end{bmatrix} \times \begin{bmatrix} 1 & 0 & 0 & 0 \\ 0 & \cos(x_\varphi) & \sin(x_\varphi) & 0 \\ 0 & -\sin(x_\varphi) & \cos(x_\varphi) & 0 \\ 0 & 0 & 0 & 1 \end{bmatrix} \times \begin{bmatrix} \cos(y_\theta) & 0 & -\sin(y_\theta) & 0 \\ 0 & 1 & 0 & 0 \\ \sin(y_\theta) & 0 & \cos(y_\theta) & 0 \\ 0 & 0 & 0 & 1 \end{bmatrix} \times \begin{bmatrix} \cos(z_\psi) & \sin(z_\psi) & 0 & 0 \\ -\sin(z_\psi) & \cos(z_\psi) & 0 & 0 \\ 0 & 0 & 1 & 0 \\ 0 & 0 & 0 & 1 \end{bmatrix} \times \begin{bmatrix} 1 & 0 & 0 & 0 \\ 0 & 1 & 0 & 0 \\ 0 & 0 & 1 & 0 \\ Enc_t & 0 & 0 & 1 \end{bmatrix} \quad (5.1)$$

Table 5.3. Transformation and translation values applied to LiDAR data with a lateral orientation.

Roll "φ" (°)	Pitch "θ" (°)	Yaw "ψ" (°)	x Translation (m)
0	−180	0	Enct

Once transformed, the x translation was applied to coordinates obtained for the actual LiDAR orientation. The encoder values recorded at each scan time were used to update the point cloud x coordinate related to the tractor advance. Additionally, the height values (*z* coordinate) were readjusted by subtracting the minimum obtained.

5.2.4.2.2. Plant Localization

The 3D point cloud processing was performed at each stick or tomato row. Thus, using manual distance delimitation, point clouds were limited to the data above the three seedbeds used during the tests.

(i) Aerial Point Cloud Extraction

The aerial point data cloud was extracted using a succession of pre-filters. First, all points that did not provide new information were removed using a gridding filter, reducing the size of the point cloud. A fit plane function was then applied to distinguish the aerial points from the ground points. In detail, the applied pre-filters were:

a) Gridding filter: Returns a downsampled point cloud using a box grid filter. GridStep specifies the size of a 3D box. Points within the same box are merged to a single point in the output (see Table 5.4).
b) pcfitplane (Thor et al., 2000): This Matlab function fits a plane to a point cloud using the M-estimator SAmple Consensus (MSAC) algorithm. The MSAC algorithm is a variant of the RANdom SAmple Consensus (RANSAC) algorithm. The function inputs were: the distance threshold value between a data point and a defined plane to determine whether a point is an inlier, the reference orientation constraint and the maximum absolute angular distance. To perform plane detection or soil detection and removal, the evaluations were conducted at every defined evaluation interval (see Table 5.4).

Table 5.4 shows the parameter values chosen during the aerial point cloud extraction. The chosen values were selected by trial and error, selecting those that yielded better results without losing much useful information.

Table 5.4. Aerial point cloud extraction parameters selected.

Test	Grid Step (m^3)	MSAC				
		Theoretical Distance Between Plants (m)	Evaluation Intervals (m)	Threshold (m)	Reference Vector	Maximum Absolute Angular Distance
Sticks	$(3 \times 3 \times 3) \times 10^{-9}$	0.240	0.08	0.04	[0,0,1]	5
Tomatoes 1		0.290	0.096			
Tomatoes 2						

(ii) Plant Identification and Localization (Plant Clustering)

A k-means clustering (Arthur et al., 2007) was performed on the resulting aerial points to partition the point cloud data into individual plant point cloud data. The parameters used to perform the k-means clustering were as follows:

- An initial number of clusters: Floor *((distance_travelled_mm/distance_between_plants_theoretical) + 1) × 2*
- The squared Euclidean distance for the centroid cluster. Each centroid is the mean of points in the cluster.

- The squared Euclidean distance measure and the k-means++ algorithm were used for cluster centre initialization.
- The clustering was repeated five times using the initial cluster centroid positions from the previous iteration.
- Method for choosing initial cluster centroid positions: Select k seeds by implementing the k-means++ algorithm for cluster centre initialization.

A reduction in the number of clusters was determined directly by evaluating the cluster centroids. If pair of centroids were closer than the *min_distance_between_plants*, the process was repeated by reducing the number of clusters by one (Table 5.5).
A clustering size evaluation was performed, excluding clusters smaller than *min_cluster_size*.

Table 5.5. Plant identification and stem identification parameters.

Minimum Distance between Plants	Minimum Cluster Size	Histogram Jumps (mm)
Distance_between_plants_theoretical×0.2	5	4

(iii) Plant Location

Three different plant locations were considered:

- Centre of the cluster
- Location of the lowest point at each plant cluster
- Intersection of the estimated stem line and ground line
    - By dividing the aerial plant data in slices defined by “histogram jumps”, the x limits on the maximal number of counts were obtained. For the z limits, data belonging to the bottom half of the aerial point cloud were considered.
    - The remaining data inside these limits were used to obtain a line of best fit, which was considered the stem line.
    - Plant location was defined as the intersection between the stem line and the corresponding ground line obtained previously from the MSAC function.

5.2.4.3. Validation of Plant Location Using RGB Kinect Images

To obtain the distance between the stems of two consecutive plants using the Kinect camera, it is necessary to characterize the plants correctly and then locate the stems with RGB images from the Kinect camera. This characterization and location of the stem was conducted as follows: a sequence of images of the entire path was obtained (~250

images in each repetition), where the camera's shooting frequency was established steadily in at 1-s intervals. Obtaining the string with the timestamp of each image was a key aspect of the routine developed in Matlab, as this string would later be used for integration with the LiDAR measurement. The relationship between the timestamp and its corresponding encoder value was used to spatially locate each image (*x*-axis, corresponding to the tractor advance).

Image processing techniques applied in the characterization of tomato plants from Kinect images generally followed these steps:

(i) According to Hamuda et al. (2015), the first step in most works regarding image analysis is the pre-processing of the image. In this work, an automatic cropping of the original images was performed (Figure 5.4a), defining a ROI. Because the test was conducted under unstructured light conditions, the white balance and the saturation of the cropped image (Figure 5.4b) were modified;

(ii) Next, the image segmentation step of an object-based image analysis (OBIA) was performed to generate boundaries around pixel groups based on their colour. In this analysis, only the green channel was evaluated to retain most of the pixels that define the plant, generating a mask that isolates them (Figure 5.4c) and classifying the pixels as plant or soil pixels. In addition, morphological image processing (erosion and rebuild actions) was performed to eliminate green pixels that were not part of the plant;

(iii) Each pair of consecutive images was processed by a routine developed in Matlab using the Computer Vision System Toolbox. This routine performs feature detection and extraction based on the Speeded-Up Robust Features "SURF" algorithm (Bay et al., 2008) to generate the key points and obtain the pairings between characteristics of the images.

Once the plant was identified in each image, the location of the stem of each plant was defined according to the following subroutine:

(1) Calculating the distance in pixels between two consecutive images, as well as the encoder distance between these two images, the "forward speed" in mm/pixel was obtained for each image;

(2) For each image, and considering that the value of the encoder corresponds to the centre of the image, the distance in pixels from the stem to the centre of the image was calculated. Considering whether it was to the left or to the right of the centre, this distance was designated positive or negative, respectively;

(3) The stem location was calculated for each image using the relation shown in Equation (5.2) below;

(4) Plant location was obtained for each image in which the plant appeared; the average value of these locations was used to calculate the distance between plants:

$$Stem\ Location = Encoder\ Value \pm Distance\ (from\ stem\ to\ centre) \times motion\ relation\left(\frac{mm}{pixel}\right) \quad (5.2)$$

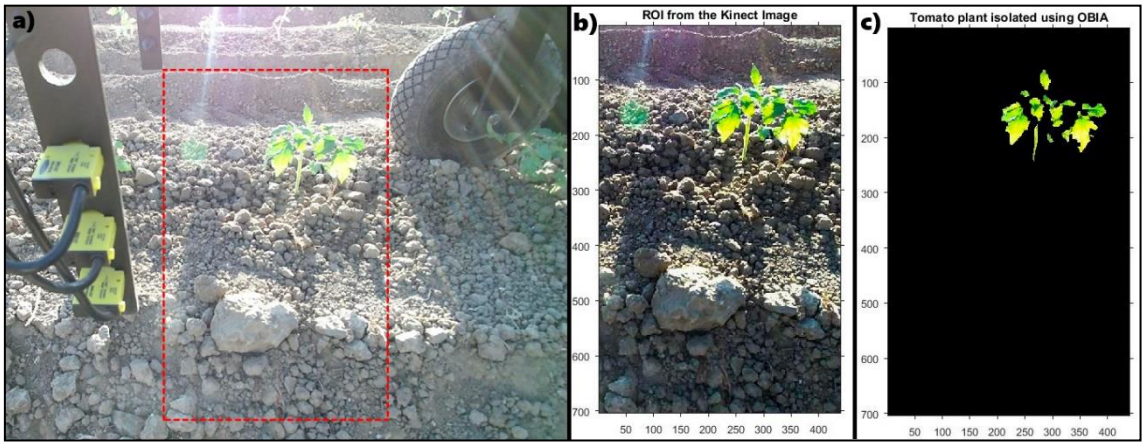

Figure 5.4. (**a**) raw image captured by the Kinect sensor with the ROI indicated; (**b**) ROI with white balance and saturation adjustment; (**c**) OBIA resulting image with isolated plant pixels.

5.3. Results

5.3.1. Laboratory Test Results

Several laboratory tests were conducted to properly adjust and test the sensors. As an example, Figure 5.5 shows various profiles representing detections, comparing the pair of light-beam sensors placed on the bottom (stem detection) with those placed in the middle, detecting the aerial part of the 3D plant. Detections of the third pair of sensors, placed above the plants, were not considered relevant because most of their beam was above the plants. Figure 5 also shows that the detection of the stem using a single pair of light-beam located at a lower height with respect to the soil was more effective and robust than trying distinguish between different plants based on the detection of the aerial part of the plant. From our point of view and in agreement with the results in Garrido et al., (2014), this justifies the use of a single pair of light-beam sensors for the field tests rather than the use of the curtain mode (3 pairs as originally tested in the laboratory). The algorithm to analyze data from a single light-beam is also simpler and faster, being more adequate for real-time usage.

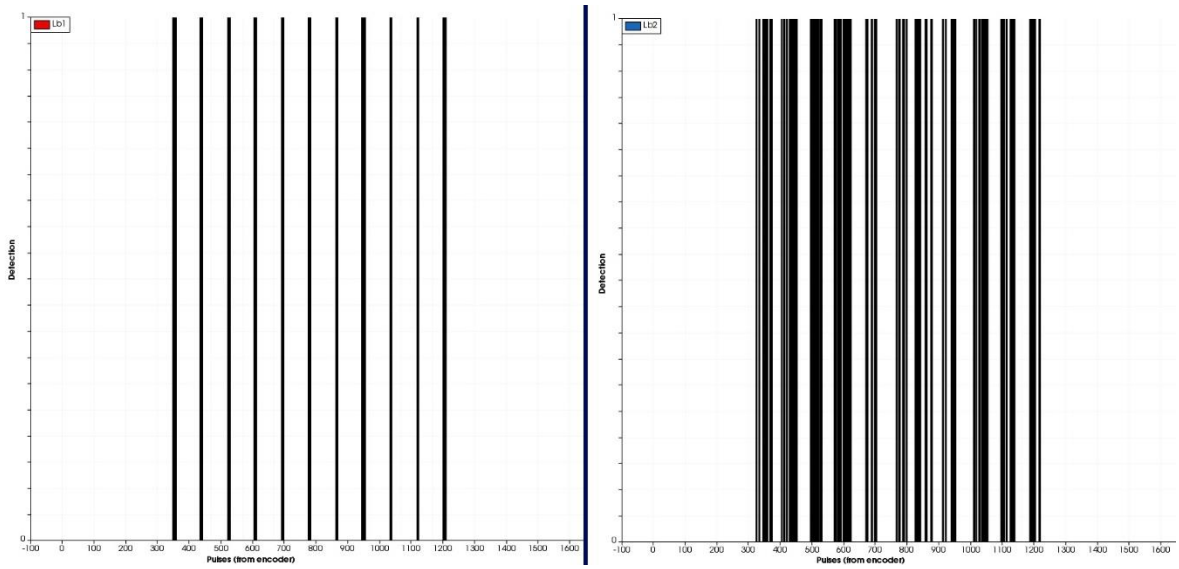

Figure 5.5. (**Left**) Stem detection of the 11 artificial plants through the lower pair of light-beam sensors. (**Right**) Detection of the aerial part (leaves and branches) of the 11 artificial plants through the centre pair of light-beam sensors.

Figure 5.6 shows the positions of the stem detections and the estimated distances between them. In all laboratory tests, 100% of the stems were detected using the light-beam sensor. Notably, under laboratory conditions, there were no obstacles in the simulated crop line, which does not accurately represent field conditions. Figure 5.6 (right) shows the stem diameter measured from a test, with an estimated average diameter of 11.2 mm for an actual value of 10 mm.

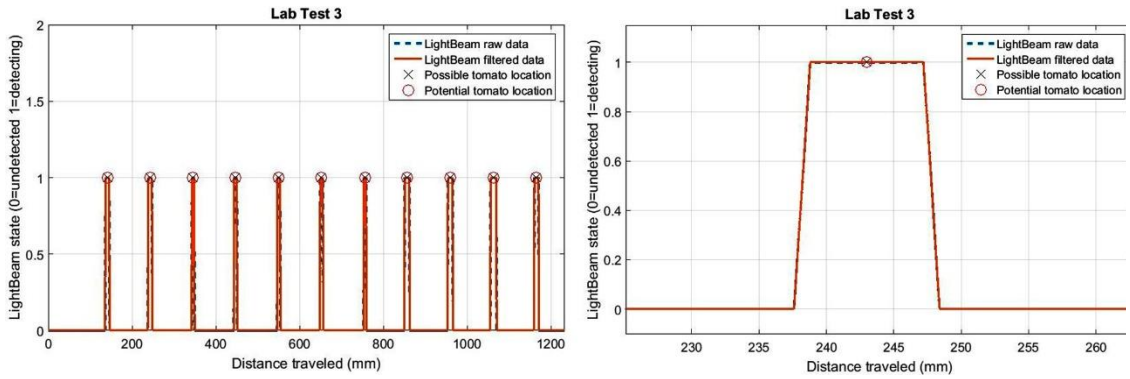

(**a**) (**b**)

Figure 5.6. (**a**) Positions of the stems of the 11 plants in the laboratory test; (**b**) Average plant position for a distance of 11 mm.

Three laboratory tests corresponding to three different stages of the light-beam sensor adjustment process are shown in Figure 5.7.

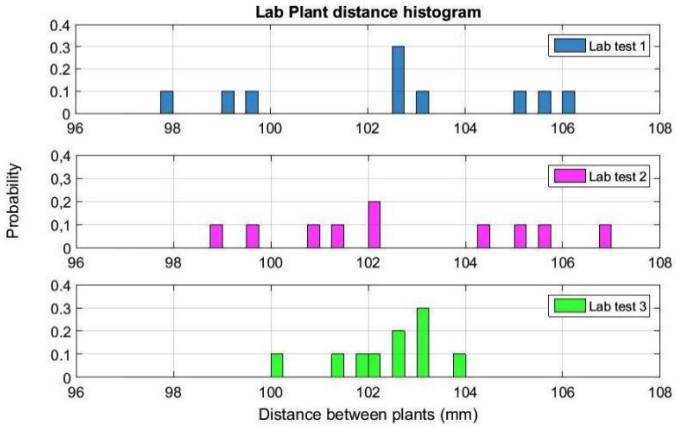

Figure 5.7. Histogram of measured distances between 3d plant stems during the adjusting process of sensors on the detection platform in the laboratory.

The histogram in this figure represents the estimated distances between plant stems, where the average distance is 102.5 mm when the real distance between plants was 100.0 mm. The average standard deviation for the three trials was 2.2 mm. For test 3 (last histogram in Figure 5.7), all distance values between plants were estimated between 100.1 mm and 103.8 mm.

For the results obtained by the LiDAR in the laboratory, as described in Section 5.2.2, multiple scanning configurations and orientations were tested. After a visual comparison of the results of these tests, lateral-scanning orientation gave the best point clouds, and its plant representation and spacing measurements were therefore more accurate. Figure 5.8 shows the point cloud representation of one of the laboratory scans made using the LiDAR sensor with lateral orientation.

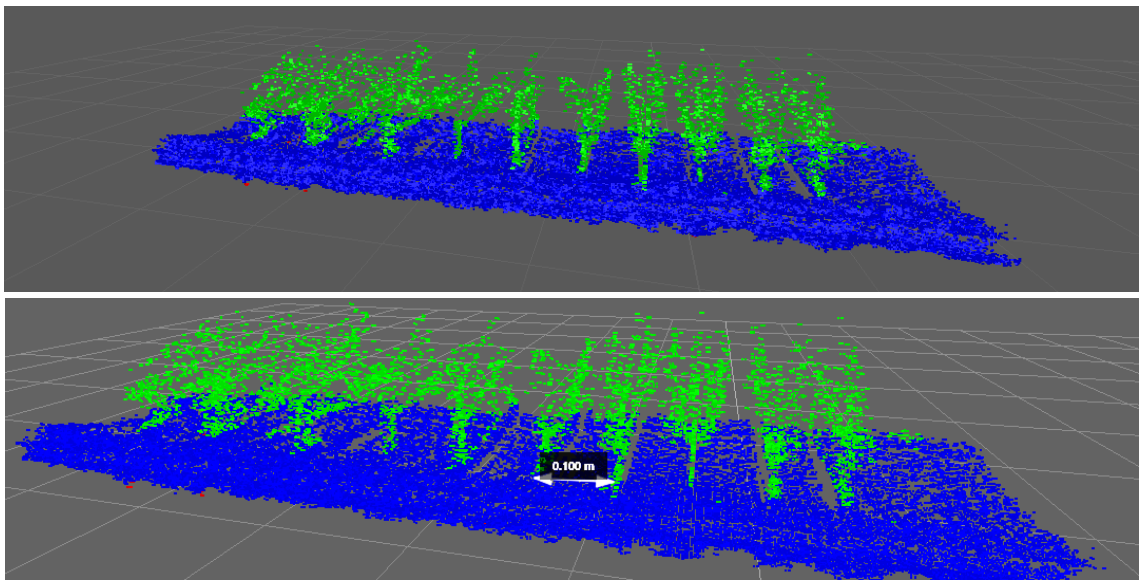

Figure 5.8. Point cloud representation of artificial 3D plants obtained using a lateral-scanning LiDAR sensor during laboratory tests.

5.3.2. Field Tests Results

Preliminary tests results using the light-beam sensors are presented in Figure 5.9a. Unlike laboratory detections, in the field data, the determined distances between stems were more variable. This variability is mainly due to crop plants missing from the line or the presence of a weed very close to the stem of the detected plant. Figure 5.9b reveals that several positions for potential plants (marked with a cross) were established, while only one plant was present (marked with a circle).

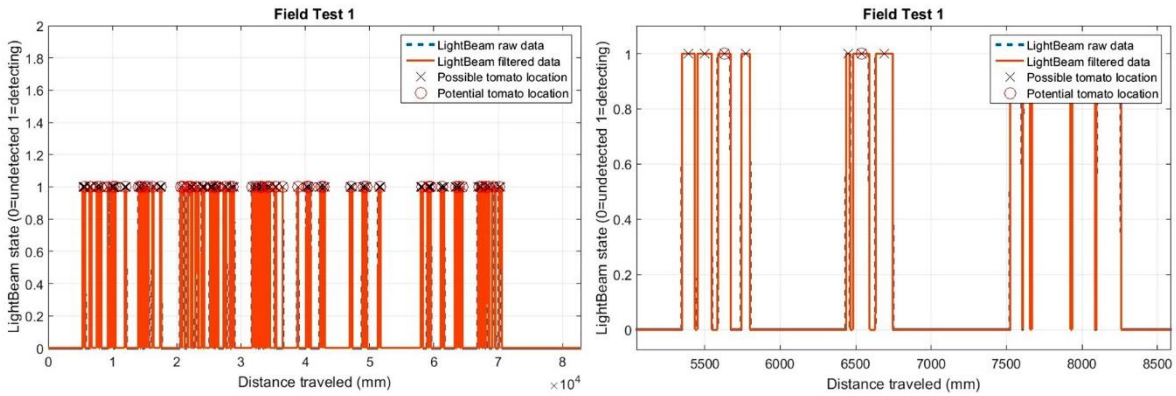

a) **b)**

Figure 5.9. (**a**) Detections and positions of the 41 tomato plants in first field test with IR sensors; and (**b**) detail of the positions of potential plants.

During the first field test, 41 detections occurred when there were 32 real plants growing in the line; thus, for this trial, the error in the number of detections was 22% (Table 5.6). We speculate three possible causes of this error in the initial test: the plants were very close together, soil clods were detected between plants, or the evaluation of the distance between plants for the selection of potential plants was not optimal. However, in trial two, 32 stem detections occurred when 34 real plants were in the line, resulting in a 94% success rate. For test three, the accuracy was 98%.

Table 5.6. Plant detection ratio in field trials.

Test5	Real Plants	Detected Plants	% Accuracy
First test	32	41	78
Second test	34	32	94
Third test	48	49	98

Regarding the experiments conducted to estimate the response of the LiDAR system in real field conditions, the detection system was used on three lines (one with wooden

sticks and two with tomatoes). The system was intended to detect the presence of plant stems correctly and to distinguish between the foliage and the stem. In addition, this system was used to measure the distances between plants accurately, providing valuable information for future herbicide treatments.

Because the use of the laser scanner for detection implies the generation of a very dense cloud of points, in which not all data are relevant, an initial filtering was performed as explained above. Table 5.7 presents the number of original points obtained by eliminating the seedbed, and those considered to be representative of the aerial part of the plant, which comprised only 4.5% of the total.

Table 5.7. Point cloud reduction during plant point cloud extraction.

Test	Seedbed delimit	Gridding	Plant Points
Stick: Test 1	44,708 (100%)	40,903 (91.5%)	1667 (3.7%)
Tomatoes 1: Test 1	374,963 (100%)	328,593 (87.6%)	14,720 (3.9%)
Tomatoes 1: Test 2	237,396 (100%)	220,714 (93%)	13,098 (5.5%)
Tomatoes 2: Test 2	3,807,858 (100%)	340,051 (89.3%)	18,706 (4.9%)

Regarding plant detection, Table 5.8 summarizes the results of some of the tests, implementing the methodology explained previously. Based on these data, it is observed that 100% of the sticks have been correctly detected, without obtaining false positives or negatives. When this analysis was performed on tomato plants, about 3%–21% of false positive or negative detections were found. A plant detected by the LiDAR was defined as a false positive when the estimated plant centre was more than half of the plant spacing from the real plant centre.

Table 5.8. Plant and sticks detection results.

Test	Plant Location Method	Correctly Detected	False Positive	False Negative
Stick with filter Test 1	Centre of the cluster	19	0	0
	Lowest point	19	0	0
	Intersection of stem line and ground line	19	0	0
Tomatoes 1 with filter Test 1	Centre of the cluster	49	2	6
	Lowest point	48	3	7
	Intersection of stem line and ground line	46	5	9

Tomatoes 1 with filter Test 2	Centre of the cluster	53	6	2
	Lowest point	52	7	3
	Intersection of stem line and ground line	47	12	8
Tomatoes 2 with filter Test 2	Centre of the cluster	51	5	0
	Lowest point	48	8	3
	Intersection of stem line and ground line	42	14	9

Related to the data presented in Table 5.8, Figure 5.10 below shows stick and plant LiDAR detection results in three rows. Platform advance information (*x*-axis on the plot) provided by the encoder is given in mm. Each plant/stick detected is marked with different colour (note the overlapping on some plants, explaining false negative and false positive detections).

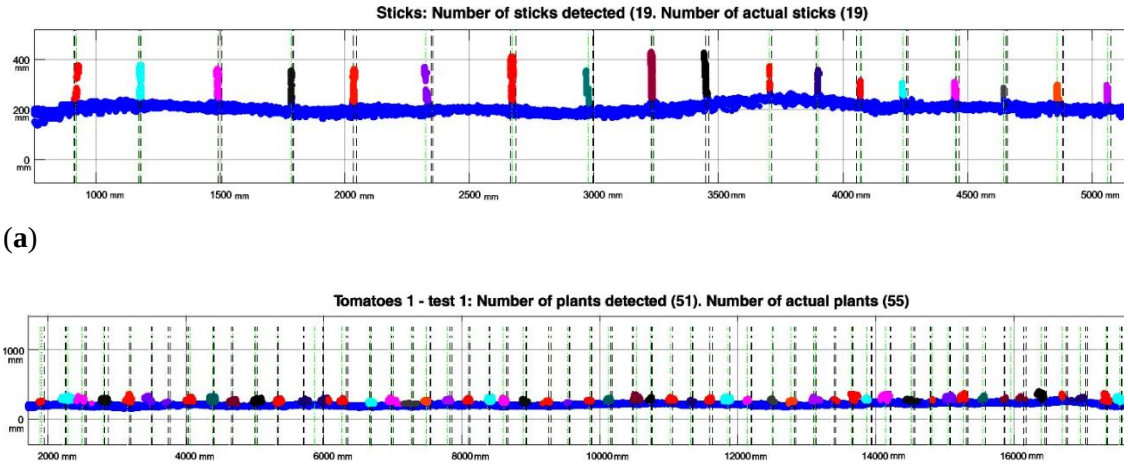

Figure 5.10. Detection results on three tested lines. Green dotted lines represent the cluster centre and black dotted lines the real plant interval obtained by the Kinect image (location ± Std). (**a**) 19 stick detections using LiDAR; (**b**) 51 plants detected during Test 1 in row 1.

As explained in Section 5.2.4.2.2, the plant location method based on the point-to-ground intersection has been evaluated (in addition to the lowest-point and centre-of-cluster methods). Figure 5.11 shows an example of the insertion point obtained from the intersection of the two lines (aerial part and soil line) in tomato plants and sticks.

Plant locations obtained from the LiDAR and Kinect data are shown in Table 5.9. As explained in Section 5.2.4.3, when processing the Kinect images, a value of the encoder was automatically selected for each image. Mean values are obtained from the difference between the actual location and the location obtained with the LiDAR.

The negative mean value obtained for Tomatoes 2 with filter Test 2 for the intersection of the stem and ground line method means that the LiDAR detected the plant at a distance greater than the actual distance (obtained from the

Kinect). High standard deviation values can be explained due to the high variability found in the encoder values assigned to each plant or stick during the image processing.

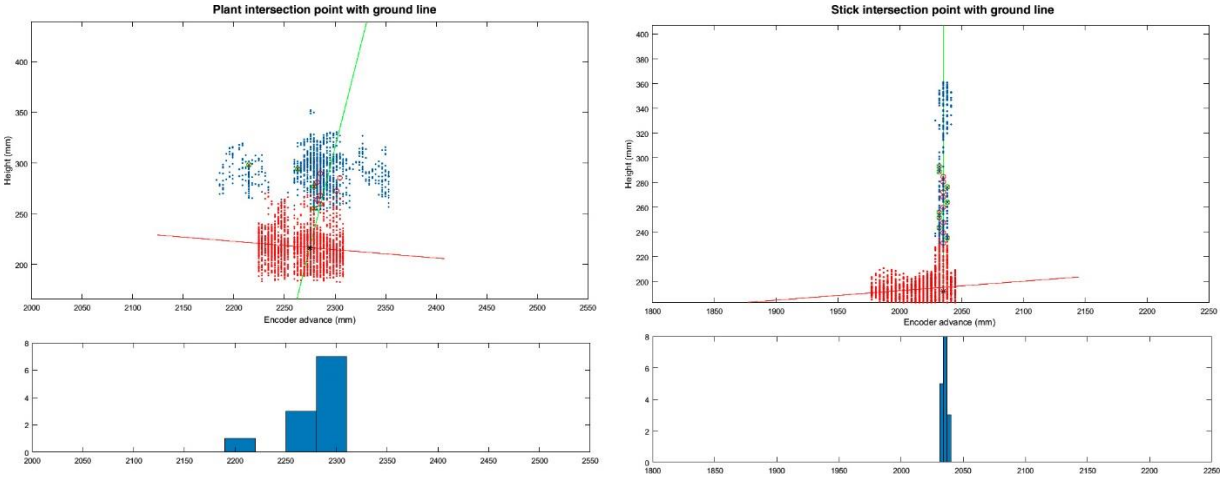

Figure 5.11. Plant location method based on the intersection of stem line and ground line. (**a**) Intersection point between the average aerial part of the plant line (green line) and the average ground line (red line); (**b**) Intersection point between the stick aerial part line (green line) and the ground line (red line). Both histograms of aerial part of the plant points are shown on the bottom.

Table 5.9. Mean and standard deviation (Std.) of the plant and stick locations during the tests.

Test	Plant Location Method	Mean (mm)	Std. (mm)
Stick—Test 1	Centre of the cluster	8.32	10.09
	Lowest point	7.25	8.47
	Intersection of stem line and ground line	6.15	9.45
Tomatoes 1—Test 1	Centre of the cluster	20.74	40.37
	Lowest point	10.06	51.72
	Intersection of stem line and ground line	5.34	62.65
Tomatoes—Test 2	Centre of the cluster	30.42	37.03
	Lowest point	35.48	52.90
	Intersection of stem line and ground line	27.60	50.36
Tomatoes 2—Test 2	Centre of the cluster	1.33	41.49
	Lowest point	10.00	61.86
	Intersection of stem line and ground line	−5.95	53.32

Figure 5.12 shows the plant identifications in each line during the different tests. For each detection previously shown in Figure 5.10, tags for each of the localization methods are shown by colored lines.

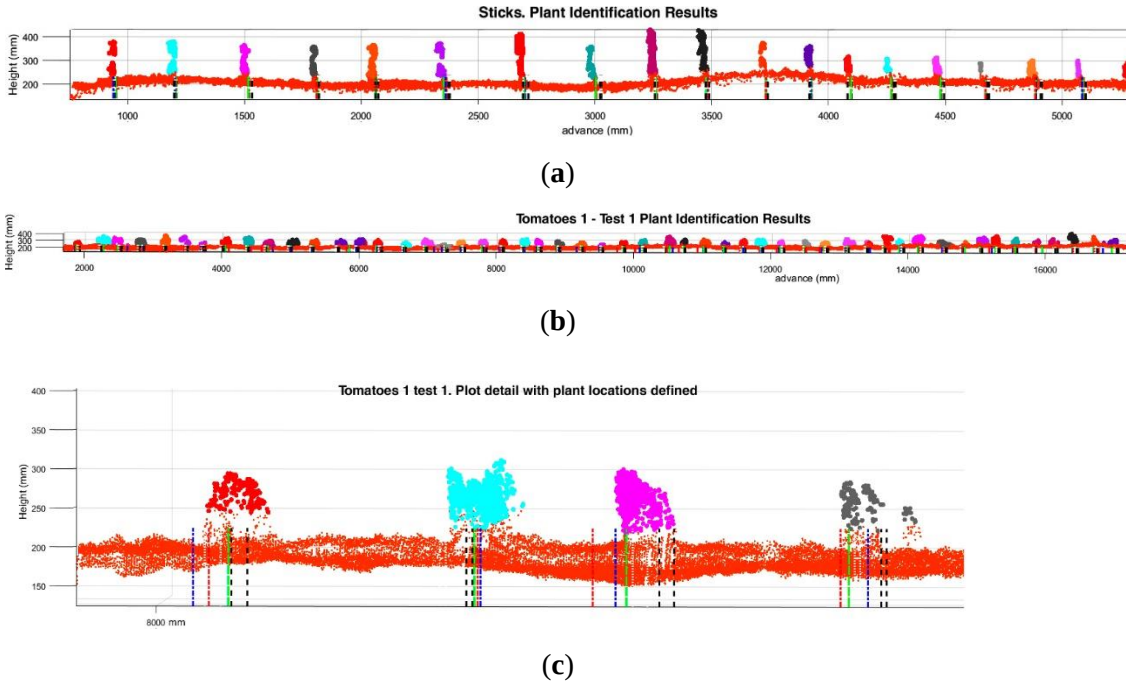

Figure 5.12. Plant and sticks location results obtained by the three different methods: Centre of the cluster; lowest point; and ground-plant intersection. (**a**) Sticks row data using LiDAR; (**b**) Tomato plants detected during Test 1 on row 1; (**c**) Detail of the aerial point cloud of tomato plants generated by the LiDAR during Test 1 on row 1. Each plant location method is marked with different colored dotted line.

The centre of the cluster is marked in green, the lowest point in blue, and the intersection in red. Encoder stick/plant locations by the Kinect image (location ± Std.) are both marked in black lines, and their distances are represented by black doted.

5.4. Conclusions

A combination of optical sensors mounted on a frame on a tractor, which are capable of detecting and locating plants and utilizing ground-wheel odometry to determine a local reference system, was successfully developed and tested. Combining the use of affordable sensors (light-beam and Kinect) with more expensive ones (LiDAR), a laboratory setup platform and two field test platforms have been created. The following conclusions were drawn based upon the results of this research:

- The results obtained from the precise locations of the plants allow us to consider the viability of further methods capable of performing individualized treatments for each of the plants, or accurate agrochemical treatments to remove existing weeds between crop plants in the same row.
- A light-beam detection system was improved by reduction of the number of sensor pairs used. The reduction from three pairs to one pair had no effect on the desired plant detection results. In the field tests, 98% precision of detection was obtained, similar to that obtained by Garrido et al. (2014), showing that this

is a robust technology and can be deployed in the field. Also, light-beam detection data allows faster processing than the LiDAR, so it could be used in real-time applications.

- Based on the methodology presented in the analysis of the data from the LiDAR and the Kinect sensors, different considerations can be established regarding the location of the same plant. According to the structure and morphology of the plant, it is assumed that the aerial part will not always be vertically in line with the stem (in fact, in the tests done this occurred frequently). For this reason, one of three proposed locations can be established as the location of the plant: the aerial part, the cluster centroid of the filtered point cloud or the insertion of the stem. Depending on the type of treatment to be made, one of these locations could be more interesting to evaluate than the others. For example, if a variable foliar herbicide treatment is to be applied (discriminating between weeds and crop plants), the distance between the aerial parts of the plants should be given greater weight in the application system (to avoid applications on the crop plants and maximize efficiency by ensuring the herbicide is applied to weeds). In the case of physical weed-removal systems, as proposed in Perez-Ruiz et al. (2014), priority should be given to the location of stem insertion, and adjustments should be made to detect this element more precisely.
- The high volume of data generated by the more accurate sensors, such as the LiDAR used in this work, can be a hurdle for automatic weed detection machines when working in real time. However, it is important to emphasize the exponential growth of the processing algorithms available for the researcher, which can significantly reduce the time required for point cloud data analysis. Reducing the density of information necessary while continuing to give accurate information is an interesting subject for future work.
- The precise locations of the plants were determined using an encoder. The use of this type of sensor is vital to implementation of low-cost referencing. Correct localization and integration to enable determination of reliable reference of the movement is of great importance.
- Agricultural use of affordable electronic components will lower costs in the near future, but the authors conclude that these systems must be robust and provide a rapid response and processing times.

5.5. References

Arthur, D.; Vassilvitskii, S.; (2007) K-means++: The advantages of careful seeding. *In Proceedings of the Eighteenth Annual ACM-SIAM Symposium on Discrete Algorithms, New Orleans, LA, USA, 7–9 January 2007*; pp. 1027–1035.

Bay, H.; Ess, A.; Tuytelaars, T.; Van Gool, L.; (2008) Speeded-up robust features (SURF). *Computer Vision Image Understanding* 110, 346-359

Blas, A.; Barreireo, P.; Hernández, C.G.; Dias, G.; Griepentrog, H.W. (2013) Even-sowing pattern strategies for a low-input organic system in forage maize. *Agric. Eng. Int*. 15, 992.
Blasco, J.; Aleixos, N.; Roger, J.; Rabatel, G.; Moltó, E.; (2002) Robotic weed control using machine vision. *Biosystems Engineering*. 83, 149-157.

Dedousis, A.P.; Godwin, R.J.; O'Dogherty, M.J.; Tillett, N.D.; Grundy, A.C. (2007) Inter and intra-row mechanical weed control with rotating discs. Precision Agriculture 7, 493-498.

Dworak, V.; Selbeck, J.; Ehlert, D. (2011) Ranging sensor for vehicle-based measurement of crop stand and orchard parameters: A review. *Trans. ASABE 2011*, 54, 1497-1510.

Ehsani, M.R.; Upadhyaya, S.K.; Mattson, M.L.; (2004) Seed location mapping using RTK GPS. *Trans. ASABE 2004*, 47, 909-914.

Fahlgren, N.; Gehan, M.A.; Baxter, I.; (2015) Lights, camera, action: High-throughput plant phenotyping is ready for a close-up. *Current Opinion in Plant Biology*, 24, 93-99.

Frasconi, C.; Fontanelli, M.; Raffaelli, M.; Peruzzi, A.; (2014) Design and full realization of physical weed control (PWC) automated machine within the RHEA project. *In Proceedings International Conference of Agricultural Engineering, Zurich, Switzerland, 6-10 July 2014*.

Garrido-Izard M.; Paraforos, D.; Reiser, D.; Vázquez Arellano, M.; Griepentrog, H.; Valero, C.; (2015) 3D Maize Plant Reconstruction Based on Georeferenced Overlapping LiDAR Point Clouds. Remote Sensing, 7, 17077-17096.

Garrido-Izard, M.; Méndez, V.; Valero, C.; Correa, C.; Torre, A.; Barreiro, P.; (2012) Online dose optimization applied on tree volume through a laser device. *In Proceedings of the First RHEA International Conference on Robotics and Associated High Technologies and Equipment for Agriculture*, Pisa, Italy, 19–21 September 2012

Garrido-Izard, M.; Pérez-Ruiz, M.; Valero, C.; Gliever, C.J.; Hanson, B.D.; Slaughter, D.C.; (2014) Active optical sensors for tree stem detection and classification in nurseries. *Sensors*, 14, 10783-10803.

Hamuda, E.; Glavin, M.; Jones, E. (2016) A survey of image processing techniques for plant extraction and segmentation in the field. *Computer and Electronics in Agriculture*, 125, 184-199.

Klenin, N.I.; Popov, I.F.; Sakun, V.A. (1985) Agricultural Machines: Theory of Operation, Computation of Controlling Parameters, and the Conditions of Operation; *Amerind*: New Delhi, India
Li, L.; Zhang, Q.; Huang, D. (2014) A Review of Imaging Techniques for Plant Phenotyping. *Sensors*, 14, 20078-20111.

López-Granados, F. (2011) Weed detection for site-specific weed management: Mapping and real-time approaches. Weed Research 51, 1-11.

Nakarmi, A.D.; Tang, L. (2012) Automatic inter-plant spacing sensing at early growth stages using a 3D vision sensor. *Computer and Electronics in Agriculture* 2012, 82, 23-31.

Pérez-Ruiz, M.; Slaughter, D.C.; Fathallah, F.A.; Gliever, C.; Miller, B.J; (2014) Co-robotic intra-row weed control system. *Biosystems Engineering*, 126, 45-55.

Pérez-Ruiz, M.; Slaughter, D.C.; Gliever, C.; Upadhyaya, S.K. (2012) Tractor-based Real-time Kinematic-Global Positioning System (RTK-GPS) guidance system for geospatial mapping of row crop transplant. *Biosystems Engineering*, 111, 64-71.

Prasanna Kumar, G.V.; Raheman, H.; (2008) Vegetable Transplanters for Use in Developing Countries—A Review. *Int. J. Veg. Sci*., 14, 232–255.

Rosell, J.R.; Llorens, J.; Sanz, R.; Arnó, J.; Ribes-Dasi, M.; Masip, J.; Escolà, A.; Camp, F.; Solanelles, F.; Gràcia, F.; et al. (2009) Obtaining the three-dimensional structure of tree orchards from remote 2D terrestrial LiDAR scanning. *Agric. For. Meteorol*. 149, 1505-1515.

Shah, R.; Lee, W.S. (2015) An approach to a laser weeding system for elimination of in-row weeds. In *Proceedings of the X European Conference on Precision Agriculture, Tel Aviv, Israel, 12–16 July 2015;* pp. 309–312.

Shi, Y.; Wang, N.; Taylor, R.K.; Raun, W.R.; Hardin, J.A.; (2013) Automatic corn plant location and spacing measurement using laser line-scan technique. *Precision Agriculture* 14, 478-494.

Sun, H.; Slaughter, D.C.; Pérez-Ruiz, M.; Gliever, C.; Upadhyaya, S.K.; Smith R.F.; (2010) RTK GPS mapping of transplanted row crops. *Computer and Electronics in Agriculture*, 71, 32-37.

Torr, P.H.S.; Zisserman, A. (2000) MLESAC: A New Robust Estimator with Application to Estimating Image Geometry. *Comput. Vis. Image Underst*., 78, 138-156.

Waldkirch, S.A. Laser Measurement Systems of the LMS100 Product Family: Operating Instructions. Available online: https://mysick.com/saqqara/im0031331.pdf (Accessed on 2 March 2017).

IV. General Results

At the beginning of this thesis was established as main objective the analysis, implementation and validation of the use of cost-affordable sensors for the study of water stress in row crops such as sugar beet and super high-density olive orchards, and for the detection of tomato plants and measurement of the intra-row distances between plants for automated weed control.

The achievement of this objective has been accomplished through three major milestones, embodied in the three publications that compose the thematic unity of this compendium. The results obtained from these three publications are summarized below, responding to the partial objectives initially proposed.

- An affordable infrared thermometry system was developed and validated, capable of being mounted on a UAV to perform temperature measurements on a sugar beet culture. A high effectiveness and precision in its behaviour was observed, obtaining a narrow margin of difference of only 1ºC with respect to the use of a commercial thermal camera. In addition, the response of the crop to the induced water stress was evaluated, validating the canopy temperature as a reliable indicator of this stress. This will allow better management of irrigation water at the same time as cost savings, both in the input and in the monitoring systems.
- The CWSI index was developed empirically and its NWSBs were obtained based on aerial thermography combined with ground measurements. When determining the NWSB for three RDI periods, the relationship between the difference in air and canopy temperatures and the vapor pressure deficit was directly affected by the incident solar radiation on super high-density olive orchards. The CWSI has been calculated for three different irrigation regimes, obtaining a CWSI in RDI zones around 0.7-0.8, which validates the aerial thermal imaging as a methodology for the study of this index. In addition, a large correlation of the CWSI with other water status indicators such as ψ_L, ψ_{st} and g_s has been obtained, with the g_s showing the highest correlation with an $R^2 = 0.91$.
- A system based on 3 types of optical sensors for the precise determination of the space between plants of the same line and the detection of tomato plants has

been developed. Detection of plant stems using light-beam infrared sensors has reached a 98% success in the field. The LiDAR laser scanner has achieved a 100% detection of test sticks, but has generated a remarkable number of false / negative false positives in the detection of plants in the field. The Kinect RGB sensor has achieved the detection of 100% of elements in the field based on image analysis techniques. The calculation of spacing between plants has been complex due to the heterogeneity of the terrain and the difficulty of progress, but it has been possible to fine tune a low-cost odometric system that acts as a local positioning system. This development constitutes an advance in the intra-row weed localization techniques at a low cost, which will contribute to the adoption of this technology by the producers.

V. General Discussion of Results and Future Work

Irrigation water management and accurate weed control are currently two of the main concerns in the agricultural sector, as they directly affect both crop quality and yield. Social and political demands show that it is necessary to move towards sustainable management levels, which in turn has motivated the growing interest in precision agriculture in the last two decades. This agricultural approach aims to take advantage of the current technological potential to reduce the efforts from producers, managing to increase the productivity and reduce the impact on the environment.

The main contribution of this thesis is the study and validation of the use of affordable sensors, mounted on both aerial and terrestrial platforms, which has been addressed in order to contribute generating management strategies regarding the two major lines of work for this research: irrigation water management and automated weed detection and control, whose overall results based on initial hypotheses are summarized hereunder.

Due to the inherent spatial and temporal variability of crop fields, the adoption of technologies capable of conduct site-specific management is necessary as a first step, in order to be able to deal with this type of issues. A large number of sensors and electronic solutions are available for automated crop sensing, monitoring, and collecting information, but several constraints exist which can limit their application in research work and acceptance by farmers. Features and prices of these commercial sensing devices typically range from low-cost sensors with low resolution, limited inputs or weak manufacturing to very expensive, full-featured devices with high resolution measurement capacity. Usually, this type of expensive sensors needs specialized maintenance, while offers the customer a closed and proprietary environment, dependent on a particular brand both for data collection and analysis, building ecosystems that result incompatible with other manufacturers, which could be one of the causes of the low adoption of these technologies.

In recent years, rapid advances in consumer electronics, coupled with the growth of the *do-it-yourself* (DIY) and *maker* movement, has made fairly inexpensive sensors readily

available. At a very low cost (few euros/dollars), standardized sensors can be acquired for any type of monitoring, automation or data logging tasks, interfacing directly with microcontrollers, which simplifies electronic designs and reach people with limited previous knowledge in electronics. In addition to the sensors, this low-cost sensing approach needs that the microcontroller should also be affordable and easy to programme. Arduino is an open-source electronics prototyping platform based on flexible, easy-to-use hardware and software which could be considered a very good alternative to develop precision agriculture oriented sensors, having a big community of users that employs this platform in multidisciplinary projects (Mesas-Carrascosa et al., 2015; USAID, 2016; Fisher and Gould, 2012).

The characteristics of irrigated crops in arid and semi-arid zones demonstrate the need to develop techniques that allow the efficient use of water resources, providing the right amount of water at the right time and place. One possibility that offers the use of remote sensing is the development of methodologies that allow to delimit uniform management zones, attending to spatial variability of the soil and crops, while also allows irrigation scheduling based on them.

Data obtained through these sensors can be used as an accurate indicator for irrigation management, since through it water status of the plants can be determined; this status is commonly measured in terms of water potential (Jones, 1992), for which the pressure chamber has traditionally been used (Scholander et al., 1965). In this way, the water deficit can be determined from the water potential of the leaves (ψ_L). Although this method is effective for measuring the water status of the plant, it is very slow and laborious and requires continuous analysis that makes it ineffective (Cohen et al., 2005).

For more than 30 years, there are evidences on the usefulness of the measurement of crop temperature to monitor the water status of the crop. When water stress is induced, leaf stomata close, the rate of transpiration is reduced and its cooling effect decreases, which causes leaf temperature to rise. Crop canopy temperature (T_c) is the result of the energy balance between energy gains (air temperature and incident radiation) and losses due to evapotranspiration. ***Chapter 1*** of this thesis addresses the use of a low-cost sensing device for infrared thermometry, in order to determine the temperature of the crop canopy as an alternative method to water potential, for measuring the plant water status. Firstly, laboratory validation of the measurements obtained with the sensor was conducted, comparing them with a conventional thermometer, and an open source hardware/software-based temperature recording system capable of being mounted on board a small multi-rotor UAV was successfully developed.

Under field conditions, the work carried out on sugar beet during a complete growing season had the aim of determine the responsiveness of the crop to induced water stress under different soil and irrigation conditions, dividing the plots according to the texture (sandy or clay texture).

The differences between the canopy and the air temperature ($\Delta T = T_c - T_a$) were measured in both controlled deficit irrigation (CDI) and full irrigated (FI) treatments. The results indicate that the difference in ΔT between DI and FI plants increased as the relative ET values decreased, although a large dispersion was found in the relation between both, possibly due to the influence of other factors such as air vapor pressure deficit, as explained in Maes et al. (2012).

After the validation against a conventional infrared thermometer, the developed system was compared to the canopy temperature measurements performed by a commercial thermal camera several orders of magnitude more expensive. Seven flights at different flight heights were made during the period in which the crop completely covered the soil, mounting the two sensors together on board the UAV.

The similarity in the T_c measurements in both treatment zones using the thermal camera and the low-cost sensors (view Table 3.4) indicates that the developed system can be a promising alternative to expensive thermal cameras. The percentage of good data collected by the sensor averaged the 95%, similar to that obtained by Fisher et al. (2010), with the added challenge of having been gathered aboard an aerial platform. Despite the system demonstrated its robustness in terms of operation and acceptable accuracy, this type of sensor has some drawbacks: In the study of the operational parameters with respect to the measurements, it was revealed that the absence of wind and clouds was a relevant factor in the measurement. This limit the areas in which the T_c can be a reliable indicator, since as stated Jones et al., (1997), infrared thermometry has had several application difficulties in humid regions due to the lower vapour pressure deficit than in semi-arid areas.

Another drawback is the wide FOV (around 90º), doesn't allow knowing which physical element is being targeted by the sensor. This limits its use to measurements that seek to know the temperature of a surface as a whole and not a particular point, especially when mounted on a platform for in-height measurements. In addition, this fact also limits its use in crops that completely cover the soil, to be sure that the measurements correspond to the T_c and not to the soil temperature.

However, this work has demonstrated that the implementation of this type of affordable remote sensors allows the estimation of the water status in large areas using infrared

thermometry and taking advantage of aerial platforms. Therefore, this technology opens up a range of possibilities while at the same time reduces costs, something that will certainly allow its mass adoption even in developing areas.

A relevant aspect to accurately know the crop water status (that was already observed in the first chapter of this thesis) is that unlike other physiological parameters such as leaf water potential (ψ_L) or stomatal conductance (g_s), the canopy temperature is strongly affected by the climatic conditions at the time of measurement. In order to minimize the effect of the environmental variation and to be able to adequately estimate the water status of the crop, it is necessary to develop indexes that have reference temperature values. In the ***Chapter 2*** of this thesis the Crop Water Stress Index (CWSI) has been developed according to the empirical model proposed by Idso et al. (1981), as a reliable estimator of the water status variability in super high-density olive orchards during irrigation season. For this, the non-water-stressed-baseline (NWSB) and its daily and seasonal evolution have been determined. In addition, the CWSI has been calculated based on high resolution aerial thermal images and the suitability of the CWSI to estimate the variation of water status in super high-density olive orchards has been determined.

Three treatments were defined in this olive grove: a full irrigation (FI) treatment that covered the complete demand for water, and two treatments of regulated deficit irrigation (CDI) covering 45% of the demand (one determined by the method of the crop coefficient 45RDI$_{CC}$ and another one based on the leaf turgor 45RDI$_{LT}$). In order to determine the NWSB, the temperature of the canopy was measured continuously for one year using infrared thermometers, permanently placed at a height of one meter above the canopy. From the results obtained regarding the NWSB calculation, a significant correlation between ΔT and VPD was found, with a clear effect of diurnal variation, in which this correlation was greater during the central hours of the day. A seasonal variation was also found, being the period from June - July (in which the angle of solar incidence is higher) in which the relationship between ΔT and VPD was more significant. These variations were previously reported by other authors (Bellvert et, 2014; Testi et al., 2008), and explained by the tight relationship between the solar radiation and NWSB-intercept.

The canopy measurements obtained with the infrared thermometers and the thermal camera mounted on the UAV were used to derive seasonal CWSI in the three irrigation treatments. This CWSI was highly determined by the treatment: while the FI treatment maintained a CWSI near to 0 during all the irrigation season, values for the 45RDI$_{CC}$ and 45RDI$_{LT}$ ranged from 0.8 to 0.2 during the stress seasons. A seasonal trend was also

observed in the data obtained, besides that CWSI showed a linear correlation between stem water potential (ψ_{st}), leaf water potential (ψ_L) and stomatal conductance (g_s).

This work also allowed to corroborate the suitability of aerial thermography to map water stress in discontinuous canopy structures such as the super high-density olive grove, as previously reported in Sepulcre-Cantó et al. (2006). Because the flights were made using a thermal camera with a resolution that can be considered low (324x256 pixels), low altitude flights (20 meters) had to be performed, which, considering the limited autonomy of these equipment, does not allow to cover large areas. As reported in Bellvert et al. (2014), camera resolution plays a determining role in the acquisition of thermal images, and it was recommended not to perform flights whose height generated pixels greater than 30 cm of ground sampling distance (GSD). In our case, the flights were conducted at a height in which the GSD was around 13 cm.

In addition, it was necessary to develop an algorithm of image analysis, which by segmentation techniques was able to extract the pixels that actually corresponded to the vegetation and separate them from those corresponding to the ground or shadows, which have different temperatures.

Chapter 3 of this thesis is devoted to the study of automated weed control, focusing on the plant/weed detection and intra-row plant spacing measurement. This line of work is considered to be of great interest for producers (and also for the author), since sustainable weed management presents a major challenge in the coming years, even more if it is approached from the perspective of automation (Fennimore et al., 2016). The objective defined in this chapter was to design a system capable of detecting the presence of tomato plants of the same crop line, and to determine the distance between them. For this purpose, a system based on three types of optical sensors was developed and tested: i) three pairs of light-beam sensors, in curtain arrangement, that allowed to detect the presence/absence of plants with no ability to discern its morphological structure, only distinguishing between weeds and crops based on its height; (ii) Kinect sensor (camera), a commercial RGB-D sensor capable of obtaining RGB, NIR images and depth images (based on Time-of-Flight); iii) LiDAR sensor, a commercial laser scanner that provide distance measurements along a line scan at a very fast scanning rate, generating 3D point clouds. The first two aforementioned sensors are considered low-cost sensors, since they did not exceed a hundred euros in both cases, while the LiDAR scanner used to perform the validation was much more expensive. The different

sensors mounted on a platform in the front of the tractor were tested under field conditions in California and Seville, assisted by an encoder-based odometry system.

The results obtained with light-beam sensors indicated a very high detection capacity (~ 98% accuracy in California test). The LiDAR sensor was able to detect 100% of sticks that simulated the stem of the tomato plant, whereas when tested on real plants, the developed algorithm obtained between 3-21% of false positives or negatives when detecting the plant. The insertion point of the stem in the ground was demonstrated to be the most difficult to detect. On the other hand, the image analysis from those captured by the Kinect sensor (combined with the odometry system), provided very good results, detecting the 100% of the plants and being able to accurately measure the distance between stems.

These detection results with LiDAR and light-beam sensors are in agreement with the obtained by Garrido-Izard et al., (2014), whereas the precise detection using the Kinect sensor demonstrates the validity of what Fennimore et al. (2016) stated before: computer vision is one of the most promising fields in the challenge of detecting and discriminating weeds mounted on modern implements and farm machinery. The results obtained from the precise locations of the plants demonstrate the viability the low-cost detection system, and contributes to the development of further methods capable of performing individualized treatments to remove existing weeds between crop plants in the same row.

Different considerations can be established regarding the location of the same plant. According to the structure and morphology of the plant, it is assumed that the aerial part will not always be vertically in line with the stem. For this reason, three locations can be established as the location of the plant: the aerial part, the cluster centroid of the filtered point cloud or the insertion of the stem. Depending on the type of treatment to be made, one of these locations could be more interesting to evaluate than the others.

This work showed the importance of the robustness of these systems, despite being low cost, since they are mounted on the tractor and are subject to vibrations and an unstructured environment.

Future work

The contributions of this thesis open new lines of future research that will be interesting to explore.

On the one hand, as already mentioned in the introduction, the integration of affordable sensors is open to help irrigation management systems and complete automation of them. It will be interesting to achieve this integration in these systems for its later

inclusion on the modern FMIS. As has been pointed out, one of the barriers that these FMIS still present, is the lack of adaptation to the local conditions of the crops. Affordable sensors can achieve greater adoption of technology, and generate a cycle of 1) greater data acquisition, 2) algorithm refinement, 3) more accurate decision-making and 4) greater yields in crops.

Based on the response of these sensors and its ability to measure temperature in the field and its relationship with water stress indexes, it will be interesting to see these responses in other crops, as well as to evaluate the suitability of carrying out developments with other affordable and commercial sensors in order to compare the results.

On the other hand, the improvement and price-lowering of detection and localization systems in crops with row-growing patterns will enable the research group to develop agricultural implements that can act accurately on weeds among crop plants. One of the objectives is to develop an intelligent implement capable of eliminating weeds by abrasion using solid waste from other crops.

In addition, the implementation of these detection and measurement methods on robotic platforms opens a very interesting future research route. Author envisions these robotic platforms being commonplace on farms in the next decades, with fully automated operations such as weed control made by smart machinery and implements.

It will also be interesting to continue the development of algorithms for the identification, classification and training of systems based on computer vision. The author finds in this branch a promising way of working in agriculture regarding its use for example for navigation, weed detection, pest identification or yield predictions.

VI. Conclusions

As a summary, the conclusions and final considerations that can be established from the present dissertation are presented below:

- Affordable sensors validated on this thesis have proven their reliability and precision when developing innovative solutions for specific field contexts within data driven agriculture.
- The use of infrared thermometry using low cost sensors to estimate the water status of sugar beet crops can be performed satisfactorily. In addition, it has been shown that the canopy temperature is a reliable indicator of water status, while it is highly conditioned by climatic variables (air temperature, wind speed, presence of clouds, etc.), which limit its use to non-humid regions.
- The variability in water status and sustainability in water management presents a considerable challenge when it comes to evaluating highly technified crops such as super high-density olive groves. Due to the influence of climatic variables in the determination of water status, it is important to use indexes that take into account these environmental conditions, such as CWSI.
- The feasibility of obtaining CWSI maps through the acquisition of thermal imagery using unmanned aerial platforms has been demonstrated. The determination of the NWSBs has allowed to quantify the diurnal and seasonal variability due to the incidence angle of solar radiation.
- Infrared sensors and aerial thermography allows estimating the water status in industrial and woody crops, studying the spatial variability as a function of the temperature of the crop canopy and effectively delimiting areas of homogeneous management for precision irrigation.
- The feasibility of the use of optical sensors for the detection of crop plants and the measurement of the space between tomato stems has been demonstrated. Combining cameras, infrared sensors and LiDAR laser scanner, high detection rates and high localization accuracy have been achieved.
- The use of optical sensors as a detection system can lead to a new era in which precise weed control can be carried out in an affordable manner and be robust in field conditions.
- The most significant technology barriers these affordable sensor presents are: 1) the need of enabling efficient data gathering and transmission, 2) the need of testing and refining analysis to accurately reflect local conditions, and 3) reaching a robustness scale that supports the challenges of field conditions.

References

Adeyemi, O., Grove, I., Peets, S., & Norton, T. (2017). Advanced monitoring and management systems for improving sustainability in precision irrigation. *Sustainability*, 9(3), 353.

Agüera Vega, F.; Carvajal Ramírez, F.; Pérez Saiz, M.; Orgaz Rosúa, F.; (2015) Multi-temporal imaging using an unmanned aerial vehicle for monitoring a sunflower crop, *Biosystems Engineering*, Volume 132, Pages 19-27.

Agüera, J., Carballido, J., Gil, J., Gliever, C.J., Perez-Ruiz, M., (2013) Design of a soil cutting resistance sensor for application in site-specific tillage. *Sensors* 13, 5945–5957.

Ahmed, C. B., Rouina, B. B., Sensoy, S., Boukhris, M., & Abdallah, F. B. (2009). Changes in gas exchange, proline accumulation and antioxidative enzyme activities in three olive cultivars under contrasting water availability regimes. *Environmental and experimental botany*, 67(2), 345-352.

Ajayi, A.E., Olufayo, A.A., (2004) Evaluation of two temperature stress indices to estimate grain sorghum yield and evapotranspiration. *Agronomy Journal* 96, 1282–1287.

Alchanatis, V., Cohen, Y., Cohen, S., Moller, M., Meron, M., Tsipris, J., Orlov, V., Naor, A., Charit, Z., (2006) Fusion of IR and Multispectral Images in the Visible Range for Empirical and Model Based Mapping of Crop Water Status. *2006 ASABE Annual International Meeting* 300.

Alchanatis, V., Cohen, Y., Cohen, S., Moller, M., Sprinstin, M., Meron, M., Tsipris, J., Saranga, Y., Sela, E., (2010). Evaluation of different approaches for estimating and mapping crop water status in cotton with thermal imaging. *Precision Agriculture* 11, 27–41.

Andrade-Sanchez, P., Gore, M.A., Heun, J.T., Thorp, K.R., Carmo-Silva, A.E., French, A.N., Salvucci, M.E., White, J.W., (2014). Development and evaluation of a field-based high-throughput phenotyping platform. *Functional Plant Biology* 41, 68–79.

Andújar, D., Escolá, A., Rosell-Polo, J.R., Fernández-Quintanilla, C., Dorado, J., (2013) Potential of a terrestrial LiDAR-based system to characterise weed vegetation in maize crops. *Computers and Electronics in Agriculture* 92, 11–15.

Andújar, D., Escolà, A., Rosell-Polo, J.R., Sanz, R., Rueda-Ayala, V., Fernández-Quintanilla, C., Ribeiro, A., Dorado, J., (2016). A LiDAR-Based System to Assess Poplar Biomass. *Gesunde Pflanz*. 68, 155–162

Andújar, D., Ribeiro, Á., Fernández-Quintanilla, C., Dorado, J., (2011). Accuracy and feasibility of optoelectronic sensors for weed mapping in wide row crops. *Sensors* 11, 2304–2318.

Aubert, B.A.; Schroeder, A.; Grimaudo, J.; (2012) IT as enabler of sustainable farming: An empirical analysis of farmers' adoption decision of precision agriculture technology. *Decision Support Systems* 54, 510–520.

Bechar, A.; Vigneault, C.; (2016) Agricultural robots for field operations: Concepts and components. *Biosystems Engineering* 149, 94–111.

Bellvert, J., Marsal, J., Girona, J., Gonzalez-Dugo, V., Fereres, E., Ustin, S.L., Zarco-Tejada, P.J., (2016). Airborne thermal imagery to detect the seasonal evolution of crop water status in peach, nectarine and Saturn peach orchards. *Remote Sensing*. 8, 1–17.

Bellvert, J., Marsal, J., Girona, J., Zarco-Tejada, P.J., (2014) Seasonal evolution of crop water stress index in grapevine varieties determined with high-resolution remote sensing thermal imagery. *Irrigation Science* 33, 81–93.

Ben-Gal, A., Agam, N., Alchanatis, V., Cohen, Y., Yermiyahu, U., Zipori, I., Presnov, E., Sprintsin, M., Dag, A., (2009) Evaluating water stress in irrigated olives: Correlation of soil water status, tree water status, and thermal imagery. *Irrigation Science* 27, 367–376.

Berni, J. A., Zarco-Tejada, P. J., Suárez, L., & Fereres, E. (2009). Thermal and narrowband multispectral remote sensing for vegetation monitoring from an unmanned aerial vehicle. *IEEE Transactions on Geoscience and Remote Sensing*, 47(3), 722-738.

Berni, J.A.J., Zarco-Tejada, P.J., Suárez, L., González-Dugo, V., Fereres, E., (2009) Remote sensing of vegetation from UAV platforms using lightweight multispectral and thermal imaging sensors. *International Arch. Photogrammetry Remote Sensing Spatial Information Science* 38, 6 pp.

Blackmore, S. (2014) Farming with robots 2020. *Conference on Greater Lincolnshire Nature Partnership.*http://www.glnp.org.uk/admin/resources/glnp-conference-2014-simon-blackmore.pdf *Last access to online presentation on 05/06/2017*.

Bu, H., Sharma, L.K., Denton, A., Franzen, D.W., (2017) Comparison of satellite imagery and ground-based active optical sensors as yield predictors in sugar beet, spring wheat, corn, and sunflower. *Agronomy Journal* 109, 299–308.

Busemeyer, L.; Mentrup, D.; Möller, K.; Wunder, E.; Alheit, K.; Hahn, V.; Maurer, H.; Reif J.; Würschum T.; Müller J.; Rahe F.; Ruckelshausen A.; (2013) BreedVision—a multi-sensor platform for non-destructive field-based phenotyping in plant breeding. *Sensors*. 13: 2830–47.

Calderón, R., Montes-Borrego, M., Landa, B.B., Navas-Cortés, J.A., Zarco-Tejada, P.J., (2014) Detection of downy mildew of opium poppy using high-resolution multi-spectral and thermal imagery acquired with an unmanned aerial vehicle. *Precision Agriculture* 15, 639–661.

Cassman, K. G. (1999). Ecological intensification of cereal production systems: yield potential, soil quality, and precision agriculture. *Proceedings of the National Academy of Sciences*, 96(11), 5952-5959.

Caturegli, L., Casucci, M., Lulli, F., Grossi, N., Gaetani, M., Magni, S., Bonari, E., Volterrani, M., (2015) GeoEye-1 satellite versus ground-based multispectral data for estimating nitrogen status of turfgrasses. *International Journal of Remote Sensing* 36, 2238–2251.

Cohen, Y., Alchanatis, V., Meron, M., Saranga, Y., & Tsipris, J. (2005). Estimation of leaf water potential by thermal imagery and spatial analysis. *Journal of Experimental Botany*, 56(417), 1843-1852.

Cohen, Y., Alchanatis, V., Prigojin, A., Levi, A., & Soroker, V. (2012). Use of aerial thermal imaging to estimate water status of palm trees. *Precision Agriculture*, 13(1), 123-140.

Colaizzi, P.D., O'Shaughnessy, S.A., Evett, S.R., Mounce, R.B., (2017) Crop evapotranspiration calculation using infrared thermometers aboard center pivots. *Agricultural Water Management* 187, 173–189.

Costa, J.M., Grant, O.M., Chaves, M.M., (2013). Thermography to explore plant-environment interactions. *Journal of Experimental Botany*. 64, 3937–3949.

Davis, S. L., & Dukes, M. D. (2010). Irrigation scheduling performance by evapotranspiration-based controllers. *Agricultural water management*, 98(1), 19-28.

De Rainville, F.-M., Durand, A., Fortin, F.-A., Tanguy, K., Maldague, X., Panneton, B., Simard, M.-J., 2014. Bayesian classification and unsupervised learning for isolating weeds in row crops. *Pattern Analysis and Applications* 17, 401–414

Dedousis, A.P.; Godwin, R.J.; O'Dogherty, M.J.; Tillett, N.D.; Grundy, A.C. (2007), Inter and intra-row mechanical weed control with rotating discs. *Precision Agriculture* 7, 493–498.

Díaz-Varela, R.A.; de la Rosa, R.; León, L.; Zarco-Tejada, P.J. (2015) High-Resolution Airborne UAV Imagery to Assess Olive Tree Crown Parameters Using 3D Photo Reconstruction: Application in Breeding Trials. *Remote Sensing*, 7, 4213-4232.

Doolittle, J.A.; Brevik, E.C. (2014) The use of electromagnetic induction techniques in soils studies, *Geoderma*, Volumes 223–225, pp 33-45.

Doorenbos, J., & Pruitt, W. O. (1977). Crop water requirements. *WO* (1977).

Dugo, V., Zarco-Tejada, P., Nicolás, E., Nortes, P.A., Alarcón, J.J., Intrigliolo, D.S., Fereres, E., (2013) Using high resolution UAV thermal imagery to assess the variability in the water status of five fruit tree species within a commercial orchard. *Precision Agriculture* 14, 660–678

Egea, G., González-Real, M. M., Baille, A., Nortes, P. A., Sánchez-Bel, P., & Domingo, R. (2009). The effects of contrasted deficit irrigation strategies on the fruit growth and kernel quality of mature almond trees. *Agricultural water management*, 96(11), 1605-1614.

Eitel, J.U.H., Long, D.S., Gessler, P.E., Hunt, E.R., Brown, D.J., (2009). Sensitivity of Ground-Based Remote Sensing Estimates of Wheat Chlorophyll Content to Variation in Soil Reflectance. *Soil Science Society of America Journal* 73, 1715.

Ellis K., Baugher T.A., Lewis, K. (2010) Results from Survey Instruments Used to Assess Technology Adoption for Tree Fruit Production *HortTechnology* 20:1043-1048

Erdem Y, Arin L, Erdem T, Polat S, Deveci M, Okursoy H, Gültas HT. (2010). Crop water stress index for assessing irrigation scheduling of drip irrigated broccoli (Brassica oleracea L. var. italica). *Agricultural Water Management* 98, 148–156.

Erdem, Y., Arin, L., Erdem, T., Polat, S., Deveci, M., Okursoy, H., & Gültaş, H. T. (2010). Crop water stress index for assessing irrigation scheduling of drip irrigated broccoli (Brassica oleracea L. var. italica). *Agricultural Water Management*, 98(1), 148-156.

Escolà, A.; Martínez-Casasnovas J.A.; Rufat, J.; Arbonés, A.; Sanz,R.; Sebé, F.; Arnó,J.; Masip, J.;Pascual, M.; Gregorio, E.; Ribes-Dasi, M.; Villar, J.M.; Rosell-Polo, J.R.; (2015) A mobile terrestrial laser scanner for tree crops: point cloud generation, information extraction and validation in an intensive olive orchard. *Precision agriculture '15*

FAO, (2016) The State of Food and Agriculture, Food and Agriculture Organization of the United Nations, Rome 2016 ISBN: 978-92-5-107671-2 I

Fennimore, S.A., Slaughter, D.C., Siemens, M.C., Leon, R.G., Saber, M.N., (2016) Technology for Automation of Weed Control in Specialty Crops. *Weed Technology* 30, 823–837

Fennimore, S.A., Smith, R.F., Tourte, L., LeStrange, M., Rachuy, J.S., (2014) Evaluation and Economics of a Rotating Cultivator in Bok Choy, Celery, Lettuce, and Radicchio. *Weed Technology* 28, 176–188.

Fernández, J.E., (2014) Understanding olive adaptation to abiotic stresses as a tool to increase crop performance. *Environmental and Experimental Botany* 103, 158–179

Ferris, L.; Rahman, Z. (2016) "Responsible Data in Agriculture" *The Engine Room Library. https://library.theengineroom.org/agriculture/* (accessed online 31 of May of 2017)

Fisher, D.K., Gould, P.J., 2012. Open-Source Hardware Is a Low-Cost Alternative for Scientific Instrumentation and Research. *Modern Instrumentation* 1, 8–20.

Forcella, F. (2009) Potential of air-propelled abrasives for selective weed control. *Weed Technology* 23:317–320

Forcella, F. (2012) Air-propelled abrasive grit for post-emergence in-row weed control in field corn. *Weed Technology* 26:161–164

Forcella, F. (2013) Soybean seedlings tolerate abrasion from air- propelled grit. *Weed Technology* 27:631–635

Fountas, S., Sorensen, C.G., Tsiropoulos, Z., Cavalaris, C., Liakos, V., Gemtos, T., (2015) Farm machinery management information system. *Computers and Electrics in Agriculture* 110, 131–138.

Frasconi, C.; Fontanelli, M.; Raffaelli, M.; Peruzzi, A. (2014) Design and full realization of physical weed control (PWC) automated machine within the RHEA project. *Proceedings of the International Conference of Agricultural Engineering*, Zurich, Switzerland, 6–10 July 2014.

Gago, J., Douthe, C., Coopman, R.E., Gallego, P.P., Ribas-carbo, M., Flexas, J., Escalona, J., Medrano, H., (2015). UAVs challenge to assess water stress for sustainable agriculture. *Agricultural Water Management* 153, 9–19.

Gai, J., Tang, L., Steward, B.L., 2015. Plant Recognition through the Fusion of 2D and 3D Images for Robotic Weeding. *2015 ASABE Annual International Meeting*

García-Tejero, I. F., Durán-Zuazo, V. H., Muriel-Fernández, J. L., Jiménez-Bocanegra, J. A. (2011). Linking canopy temperature and trunk diameter fluctuations with other physiological water status tools for water stress management in citrus orchards. *Functional Plant Biology*, 38(2), 106-117.

Giles D., Billing R., (2015) Deployment and performance of a UAV for crop spraying, *Chemical Engineering Transactions*, 44, 307-312

Glenn, D. M., Worthington, J. W., Welker, W. V., & McFarland, M. J. (1989). Estimation of peach tree water use using infrared thermometry. *Journal of the American Society for Horticultural Science* (USA)

González-Dugo, M.P., Moran, M.S., Mateos, L., Bryant, R., (2006) Canopy temperature variability as an indicator of crop water stress severity. *Irrigation Science* 24, 233–240.

Gonzalez-Dugo, V., Goldhamer, D., Zarco-Tejada, P.J., Fereres, E., (2015) Improving the precision of irrigation in a pistachio farm using an unmanned airborne thermal system. *Irrigation Science* 33, 43–52

Gonzalez-Dugo, V., Hernandez, P., Solis, I., Zarco-Tejada, P.J.; (2015). Using high-resolution hyperspectral and thermal airborne imagery to assess physiological condition in the context of wheat phenotyping. *Remote Sensing*. 7, 13586–13605.

Gonzalez-Dugo, V., Zarco-Tejada, P.J., Fereres, E., (2014) Applicability and limitations of using the crop water stress index as an indicator of water deficits in citrus orchards. *Agricultural and Forest Meteorology*. 198–199, 94–104.

Grassini, P., Eskridge, K.M., Cassman, K.G., 2013. Distinguishing between yield advances and yield plateaus in historical crop production trends. *Nature Communications* 4, 1–11.

Gumiere, S.J.; Lafond, J.A.; Hallema, D.W.; Périard, Y.; Caron, J.; Gallichand, J.; (2014) Mapping soil hydraulic conductivity and matric potential for water management of cranberry: Characterisation and spatial interpolation methods. *Biosystems Engineering* 128, 29–40.

Harker, K.N., O'Donovan, J.T., (2013) Recent Weed Control, Weed Management, and Integrated Weed Management. *Weed Technology* 27, 1–11.

Hassan-Esfahani, L., Torres-Rua, A., Ticlavilca, A.M., Jensen, A., McKee, M., (2014) Topsoil moisture estimation for precision agriculture using unmmaned aerial vehicle multispectral imagery. *International Geoscience and Remote Sensing Symposium (IGARSS)* 3263–3266.

Haug, S., Michaels, A., Biber, P., Ostermann, J., 2014. Plant classification system for crop/weed discrimination without segmentation. *2014 IEEE Winter Conference on Applied Computer Vision*, WACV 2014 1142–1149.

Hedley, C. B. and Knox, J. W. and Raine, S. R. and Smith, R. (2014) Water: advanced irrigation technologies. In: *Encyclopedia of agriculture and food systems, 2nd ed. Elsevier* (Academic Press pp. 378-406

Heege, H. J. (2015). Precision in crop farming. Springer.

Hemming J, Nieuwenhuizen AT, Struik LE (2011) Image analysis system to determine crop row and plant positions for an intra-row weeding machine. Tokyo, Japan: *Proceedings of the CIGR International Symposium on Sustainable Bioproduction*. Pp 1–7

Huang Y, Hoffmann W C, Lan Y, Wu W, Fritz B K. (2009) Development of a spray system for an unmanned aerial vehicle platform. *Applied Engineering in Agriculture,* 25(6): 803-809.

Idso, S. B., Jackson, R. D., Pinter, P. J., Reginato, R. J., Hatfield, J. L. (1981). Normalizing the stress-degree-day parameter for environmental variability. *Agricultural Meteorology*, 24, 45-55.

Idso, S. B., Jackson, R. D., Reginato, R. J. (1978). Extending the" degree day" concept of plant phenological development to include water stress effects. *Ecology*, 59(3), 431-433.

Irmak, S., Haman, D. Z., & Bastug, R. (2000). Determination of crop water stress index for irrigation timing and yield estimation of corn. *Agronomy Journal*, 92(6), 1221-1227.

J. Torres-Sánchez, J.M. Peña, A.I. de Castro, F. López-Granados; (2014) Multi-temporal mapping of the vegetation fraction in early-season wheat fields using images from UAV, *Computers and Electronics in Agriculture*, Volume 103, Pages 104-113.

Jackson, R. D. (1982). Canopy temperature and crop water stress. *Advances in irrigation*, 1, 43-85.

Jackson, R. D., Idso, S. B., Reginato, R. J., & Pinter, P. J. (1981). Canopy temperature as a crop water stress indicator. *Water resources research*, 17(4), 1133-1138.

Jackson, R. D., Reginato, R. J., Idso, S. B. (1977). Wheat canopy temperature: a practical tool for evaluating water requirements. *Water resources research*, 13(3), 651-656.

Jones, H. G. (1999). Use of infrared thermometry for estimation of stomatal conductance as a possible aid to irrigation scheduling. Agricultural and forest meteorology, 95(3), 139-149.

Jones, H.G., (1992) Plants and Microclimate: A Quantitative Approach to Environmental Plant Physiology. *Cambridge University Press.*

Jones, H.G., Serraj, R., Loveys, B.R., Xiong, L., Wheaton, A., Price, A.H., (2009) Thermal infrared imaging of crop canopies for the remote diagnosis and quantification of plant responses to water stress in the field. *Functional Plant Biology* 36, 978–989.

Jones, H.G.; Aikman, D.; McBurney, T.A.; (1997) Improvements to infra-red thermometry for irrigation scheduling in humid climates. *Acta Horticulturae* 449, 259–265.

Kaierle S, Marx C, Rath T, Hustedt M (2013) Find and irradiate—lasers used for weed control. *Laser Technology Journal* 10:44–47

Khanal, S., Fulton, J., Shearer, S., (2017) An overview of current and potential applications of thermal remote sensing in precision agriculture. *Computers and Electronics in Agriculture* 139, 22–32.

Kitchen, N.R., (2008) Emerging technologies for real-time and integrated agriculture decisions. *Computers and Electrics in Agriculture* 61, 1–3.

Kitchen, N. R., Sudduth, K. A., Drummond, S. T., Scharf, P. C., Palm, H. l., Roberts, D. F., and Vories, E. D. (2010) Ground-based Canopy reflectance sensing for Variable Rate Corn fertilization. *Agronomy Journal*, 102, 71–82

Kraehmer, H., Laber, B., Rosinger, C., Schulz, A., (2014) Herbicides as Weed Control Agents: State of the Art: I. Weed Control Research and Safener Technology: The Path to Modern Agriculture. *Plant Physiology* 166, 1119–1131

Krishna, K. R. (2016). Push Button Agriculture Robotics, Drones, Satellite-Guided Soil and Crop Management. *CRC Press*.

Lambert, D. M.; Paudel, K. P.; Larson, J. A. (2015). Bundled Adoption of Precision Agriculture Technologies by Cotton Producers. *Journal of Agricultural and Resource Economics*, 40(2), 325-345.

Lati, R.N., Siemens, M.C., Rachuy, J.S., Fennimore, S.A., (2016) Intrarow Weed Removal in Broccoli and Transplanted Lettuce with an Intelligent Cultivator. *Weed Technology* 30, 655–663.

Li, Z.L., Tang, R., Wan, Z., Bi, Y., Zhou, C., Tang, B., Yan, G., Zhang, X., (2009) A review of current methodologies for regional Evapotranspiration estimation from remotely sensed data. *Sensors* 9, 3801–3853.

Llop, J., Gil, E., Llorens, J., Miranda-Fuentes, A., & Gallart, M. (2016). Testing the Suitability of a Terrestrial 2D LiDAR Scanner for Canopy Characterization of Greenhouse Tomato Crops. *Sensors*, 16(9), 1435.

Llorens, J., Gil, E., Llop, J., Escolà, A., (2010). Variable rate dosing in precision viticulture: Use of electronic devices to improve application efficiency. *Crop Protection* 29, 239–248.

López-Granados, F., Torres-Sánchez, J., De Castro, A.I., Serrano-Pérez, A., Mesas-Carrascosa, F.J., Peña, J.M., (2016). Object-based early monitoring of a grass weed in a grass crop using high resolution UAV imagery. *Agronomy for Sustainable Development* 36

Maes, W. H., Steppe, K. (2012). Estimating evapotranspiration and drought stress with ground-based thermal remote sensing in agriculture: a review. *Journal of Experimental Botany*, 63(13), 4671-4712.

Maes, W., Huete, A., Steppe, K., (2017) Optimizing the Processing of UAV-Based Thermal Imagery. *Remote Sensing* 9, 476.

Maes, W.H., Achten, W.M.J., Reubens, B., Muys, B., (2011) Monitoring stomatal conductance of Jatropha curcas seedlings under different levels of water shortage with infrared thermography. *Agricultural and Forest Meteorology* 151, 554–564.

Martínez-Casasnovas, J.A.; Bigorda, D.V.; Ramos, M.C. (2009) Irrigation management zones for precision viticulture according to intra-field variability. *In Proceedings of the EFITA Conference,Wageningen*, The 6–8 July 2009

Martinez-Guanter, J., Garrido-Izard, M., Agüera, J., Valero, C., Pérez-Ruiz, M., 2017. Over-the-row harvester damage evaluation in super-high-density olive orchard by on-board sensing techniques. *Advances in Animal Bioscience* 8, 487–491.

Mesas-Carrascosa, F.J., Verdú Santano, D., Meroño, J.E., Sánchez de la Orden, M., García-Ferrer, A., 2015. Open source hardware to monitor environmental parameters in precision agriculture. *Biosystems Engineering* 137, 73–83.

Miranda-Fuentes, A., Llorens, J., Rodriguez-Lizana, A., Cuenca, A., Gil, E., Blanco-Roldán, G. L.; Gil-Ribes, J. A. (2016). Assessing the optimal liquid volume to be sprayed on isolated olive trees according to their canopy volumes. *Science of The Total Environment*, 568, 296-305.

Möller, M., Alchanatis, V., Cohen, Y., Meron, M., Tsipris, J., Naor, A., ... & Cohen, S. (2007). Use of thermal and visible imagery for estimating crop water status of irrigated grapevine. *Journal of experimental botany*, 58(4), 827-838.

Monteith, J. L. (1981). Evaporation and surface temperature. *Quarterly Journal of the Royal Meteorological Society*, 107(451), 1-27.

Moriana, A., Villalobos, F. J., & Fereres, E. (2002). Stomatal and photosynthetic responses of olive (Olea europaea L.) leaves to water deficits. *Plant, Cell & Environment*, 25(3), 395-405.

Mulla, D.J., (2017) Encyclopedia of GIS. Chapter 1 pp 1-8 DOI:10.1007/978-3-319-23519-6_1652-1.

Nevalainen, O., Honkavaara, E., Tuominen, S., Viljanen, N., Hakala, T., Yu, X., Hyyppä, J., Saari, H., Pölönen, I., Imai, N., Tommaselli, A., (2017). Individual Tree Detection and Classification with UAV-Based Photogrammetric Point Clouds and Hyperspectral Imaging. *Remote Sensing* 9, 185.

Nielsen, D. C. (1990). Scheduling irrigations for soybeans with the crop water stress index (CWSI). *Field Crops Research*, 23(2), 103-116.

Niu, Q.; Fratta, D.; Wang, Y.-H. (2015). The use of electrical conductivity measurements in the prediction of hydraulic conductivity of unsaturated soils. *Journal of Hydrology* 522, 475–487.

Norsworthy, J.K., Ward, S.M., Shaw, D.R., Llewellyn, R.S., Nichols, R.L., Webster, T.M., Bradley, K.W., Frisvold, G., Powles, S.B., Burgos, N.R., Witt, W.W., Barrett, M., (2012) Reducing the Risks of Herbicide Resistance: Best Management Practices and Recommendations. *Weed Science* 60, 31–62

O'Shaughnessy, S. A., Evett, S. R., & Colaizzi, P. D. (2014). Infrared thermometry as a tool for site-specific irrigation scheduling*. In Proceedings of the Central Plains Irrigation Conference*.

O'Shaughnessy, S.A., Hebel, M.A., Evett, S.R., Colaizzi, P.D., (2011) Evaluation of a wireless infrared thermometer with a narrow field of view. *Computers and Electronics in Agriculture* 76, 59–68.

Oerke E-C., Steiner, U. (2010) Potential of digital thermography for disease control. In: Oerke E-C, Gerhards R, Menz G, Sikora RA (eds) *Precision crop protection – the challenge and use of heterogeneity, 1, vol Chapter 11. Springer Science*, pp 167–182

Oerke, E-C., Steiner, U. H-W Dehne, M Lindenthal; (2006) Thermal imaging of cucumber leaves affected by downy mildew and environmental conditions*. Journal Experimental Botany*; 57 (9): 2121-2132

P.J. Zarco-Tejada, V. González-Dugo, J.A.J. Berni, (2012) Fluorescence, temperature and narrow-band indices acquired from a UAV platform for water stress detection using a micro-hyperspectral imager and a thermal camera. *Remote Sensing of Environment*. Volume 117, Pages 322-337.

Pajares, G., (2015) Overview and Current Status of Remote Sensing Applications Based on Unmanned Aerial Vehicles (UAVs). *Photogrammetric Engineering & Remote Sensing*. 81, 281–330.

Paulus, S., Behmann, J., Mahlein, A.K., Plümer, L., Kuhlmann, H., (2014) Low-cost 3D systems: Suitable tools for plant phenotyping. *Sensors* 14, 3001–3018

Peña, J.M., Torres-Sánchez, J., de Castro, A.I., Kelly, M., López-Granados, F.; (2013) Weed Mapping in Early-Season Maize Fields Using Object-Based Analysis of Unmanned Aerial Vehicle (UAV) Images. *PLoS One* 8, 1–11.

Pereira, Luis S., Ian Cordery, and Iacovos Iacovides. (2012) Improved Indicators of Water Use Performance and Productivity for Sustainable Water Conservation and Saving. *Agricultural Water Management* 108: 39–51.

Perez-Ruiz, M., Gonzalez-de-Santos, P., Ribeiro, A., Fernandez-Quintanilla, C., Peruzzi, A., Vieri, M., Tomic, S., Agüera, J.; (2015) Highlights and preliminary results for autonomous crop protection. *Computers and Electronics in Agriculture* 110, 150–161.

Perez-Ruiz, M., Slaughter, D.C., Fathallah, F.A., Gliever, C.J., Miller, B.J., (2014) Co-robotic intra-row weed control system. *Biosystems Engineering* 126, 45–55.

Perez-Ruiz, M., Slaughter, D.C., Gliever, C., Upadhyaya, S.K., (2012). Tractor-based Real-time Kinematic-Global Positioning System (RTK-GPS) guidance system for geospatial mapping of row crop transplant. *Biosystems Engineering* 111, 64–71.

Pérez-Ruiz, M., Slaughter, D.C., Gliever, C.J., Upadhyaya, S.K., (2012) Automatic GPS-based intra-row weed knife control system for transplanted row crops. *Computers and Electronics in Agriculture* 80, 41–49.

Peteinatos, G.G., Weis, M., Andújar, D., Rueda Ayala, V., Gerhards, R., (2014) Potential use of ground-based sensor technologies for weed detection. *Pest Management Science* 70, 190–199.

Piron, A.; Leemans, V.; Lebeau, F.; Destain, M.F. (2009) Improving in-row weed detection in multispectral stereoscopic images, *Computers and Electronics in Agriculture*, Volume 69, Issue 1, Pages 73-79,

Poulton, C.; Dorward, A.; Kydd, J.; (2010). The Future of Small Farms: New Directions for Services, Institutions, and Intermediation. *World Development*. 38, 1413–1428.

Priyadharsini, S., Sathishkumar, B.S., (2015) Developing a Real Time Smart Herbicide Sprayer Robot and Automatic Weed Detection System. *International Journal of Emerging Technology and Advanced Engineering* 5, 323–326.

Quebrajo, L.; Pérez-Ruiz, M.; Rodriguez-Lizana A.; Agüera, J.; (2015) An approach to precise nitrogen management using hand-held crop sensor measurements and winter wheat yield mapping in a Mediterranean environment. *Sensors* 15, 5504–5517.

Rasmussen, J., Griepentrog, H.W., Nielsen, J., Henriksen, C.B., (2012). Automated intelligent rotor tine cultivation and punch planting to improve the selectivity of mechanical intra-row weed control. *Weed Research*. 52, 327–337

Romeo, J., Guerrero, J.M., Montalvo, M., Emmi, L., Guijarro, M., Gonzalez-de-Santos, P., Pajares, G., (2013) Camera sensor arrangement for crop/weed detection accuracy in agronomic images. *Sensors* 13, 4348–4366.

Rud, R., Cohen, Y., Alchanatis, V., Levi, A., Brikman, R., Shenderey, C., Heuer, B., Markovitch, T., Dar, Z., Rosen, C., Mulla, D., Nigon, T., (2014) Crop water stress index derived from multi-

year ground and aerial thermal images as an indicator of potato water status. *Precision Agriculture* 15, 273–289.

Saber, M.N.; Lee, W.S.; Burks, T.F.; MacDonald, G.E.; Salvador, G.A.; (2013) An Automated Mechanical Weed Control System for Organic Row Crop Production. *Transactions of 2013 ASABE Annual International Meeting*

Scholander, P.F., Hammel, H.T., Bradstreet, E.D., Hemmingsen, E.A., (1965). SapPressure in Vascular Plants: negative hydrostatic pressure can be measured inplants. *Science* 148, 339–346.

Sepaskhah, A.R., Kashefipour, S.M., (1994) Relationships between leaf water potential, CWSI, yield and fruit quality of sweet lime under drip irrigation. *Agricultural Water Management* 25, 13–21.

Sepulcre-Cantó, G., Zarco-Tejada, P.J., Jiménez-Muñoz, J.C., Sobrino, J.A., Miguel, E. De, Villalobos, F.J., (2006) Detection of water stress in an olive orchard with thermal remote sensing imagery. *Agricultural and Forest Meteorology* 136, 31–44

Shah, N.G.; Das, I. (2012) Precision Irrigation: Sensor Network Based Irrigation. In Problems, Perspectives and Challenges of Agricultural Water Management; *InTech* pp. 217–232.

Shah, R.; Lee, W.S. (2015) An approach to a laser weeding system for elimination of in-row weeds*. Proceedings of the X European Conference on Precision Agriculture*, Tel Aviv, Israel, 12–16 July 2015; pp. 309–312.

Siegfried, J., Khosla, R., & Longchamps, L. (2017). Infrared thermometry to quantify in-field soil moisture variability. *Journal of Crop Improvement*, 31(1), 72–90.

Slaughter, D. (2014). The Biological Engineer: Sensing the Difference Between Crops and Weeds. In Stephen L.Young & Francis J.Pierce (Eds.) *Automation: The Future of Weed Control in Cropping Systems* (pp 71-95)

Slaughter, D.C., Giles, D.K., Downey, D., (2008) Autonomous robotic weed control systems: A review. *Computers and Electronics in Agriculture*. 61, 63–78.

Smith, B.C.M., Dhuyvetter, K.C., Kastens, T.L., Dietrich, L., Smith, L.M., (2013) Economics of Precision Agricultural Technologies Across the Great Plains. *Journal of the American Society of Farm Managers and Rural Appraisers*. 76, 185–206.

Sun, H., Slaughter, D.C., Ruiz, M.P., Gliever, C., Upadhyaya, S.K., Smith, R.F., (2010) RTK GPS mapping of transplanted row crops. *Computers and Electronics in Agriculture*. 71, 32–37.

Sun, H., Slaughter, D.C., Ruiz, M.P., Gliever, C., Upadhyaya, S.K., Smith, R.F., (2010) RTK GPS mapping of transplanted row crops. *Computers and Electronics in Agriculture* 71, 32–37

Tanner, C. B. (1963). Plant temperatures*. Agronomy Journal*, 55(2), 210-211

Tattaris, M., Reynolds, M.P., Chapman, S.C., (2016) A Direct Comparison of Remote Sensing Approaches for High-Throughput Phenotyping in Plant Breeding. *Frontiers in Plant Science* 7, 1–9

Testi L., Goldhamer D., Iniesta F., Salinas M. (2008) Crop water stress index is a sensitive water stress indicator in pistachio trees. *Irrigation Science* 26:395–405.

Tey, Y. S.; Brindal, M. (2012). Factors influencing the adoption of precision agricultural technologies: a review for policy implications. *Precision Agriculture*, 13(6), 713-730.

Torres-Sánchez, J., López-Granados, F., De Castro, A.I., Peña-Barragán, J.M., 2013. Configuration and Specifications of an Unmanned Aerial Vehicle (UAV) for Early Site-Specific Weed Management. *PLoS One* 8.

Turner, N. C., Schulze, E. D., & Gollan, T. (1984). The responses of stomata and leaf gas exchange to vapour pressure deficits and soil water content. *Oecologia*, 63(3), 338-342.

Underwood, J.P.; Jagbrant, G.; Nieto, J.I.; Sukkarieh, S.; (2015) Lidar-Based Tree Recognition and Platform Localization in Orchards. *Journal of Field Robotics* 32(8), 1056–1074.

Urbahs, A., Jonaite, I., (2013) Features of the use of unmanned aerial vehicles for agriculture applications. *Aviation* 17, 170–175.

USAID (2016) Low-Cost Sensors for Agriculture. *Key Findings Report. June 2-3, 2016* Available Online:https://static.globalinnovationexchange.org/s3fs-ublic/asset/document/USAID%20Sensors4Ag%20Key%20Findings%20FINAL_FOR%20DISTRIBUTION.pdf Accesed on 13th June 2017.

VAROS (Variable Rate Operations in Orchards) project. (2016) ICT-Agri and robotics for sustainable agriculture Program http://ict-agri.eu/node/36325 Accessed on 10 June 2017

Wang, D.; Gartung, J. (2010) Infrared canopy temperature of early-ripening peach trees under postharvest deficit irrigation. Agricultural Water Management, 97, 1787–1794.

Wang, L., Qiu, G. Y., Zhang, X., & Chen, S. (2005). Application of a new method to evaluate crop water stress index. *Irrigation Science*, 24(1), 49-54.

Wang, X., Yang, W., Wheaton, A., Cooley, N., & Moran, B. (2010). Automated canopy temperature estimation via infrared thermography: A first step towards automated plant water stress monitoring. *Computers and Electronics in Agriculture*, 73(1), 74-83.

Wendel, A., Underwood, J., 2016. Self-supervised weed detection in vegetable crops using ground based hyperspectral imaging. *2016 IEEE International Conference on Robotics and Automation (ICRA)* 5128–5135.

West, J.S., Canning, G.G.M., Perryman, S.A., King, K., 2017. Novel Technologies for the detection of Fusarium head blight disease and airborne inoculum. *Tropical Plant Pathology* doi:10.1007/s40858-017-0138-4

Whipker, L.D., and J.T. Akridge. (2009) Precision Agricultural Services: Dealership Survey Results. *West Lafayette, IN: Center for Food and Agricultural Business*, Purdue University.

Wired Magazine "Re-Planting a Forest, One Drone at a Time.". (2015) Accessed via Web on June 2017. https://www.wired.com/brandlab/2015/07/re-planting-forest-one-drone-time/

Wortman, S. (2014). Integrating weed and vegetable crop management with multifunctional air-propelled abrasive grits. *Weed Technology* 28:243–252

Yang, H., Yang, X., Heskel, M., Sun, S., Tang, J., (2017) Seasonal variations of leaf and canopy properties tracked by ground-based NDVI imagery in a temperate forest. Scientific Reports 7, 1267.

Yao, Y., Liu, Q., Liu, Q., (2009) Canopy modeling and validation for row planted crops of key growth stages. *International Geoscience Remote Sensing Symposium*. 2, 686–689.

Young, S.L. and Giles, D.K. (2014) Targeted and Microdose Chemical Applications. In Stephen L.Young & Francis J.Pierce (Eds.) *Automation: The Future of Weed Control in Cropping Systems* (pp 139-148)

Yu, X., Wu, P., Han, W., & Zhang, Z. (2013). A survey on wireless sensor network infrastructure for agriculture. *Computer Standards & Interfaces*, 35(1), 59-64.

Zaman-Allah, M., Vergara, O., Araus, J.L., Tarekegne, A., Magorokosho, C., Zarco-Tejada, P.J., Hornero, A., Albà, A.H., Das, B., Craufurd, P., Olsen, M., Prasanna, B.M., Cairns, J., (2015) Unmanned aerial platform-based multi-spectral imaging for field phenotyping of maize. *Plant Methods* 11, 35.

Zhang P, Deng L, Lyu Q, He S L, Yi S L, Liu Y D. (2016) Effects of citrus tree-shape and spraying height of small unmanned aerial vehicle on droplet distribution. *International Journal of Agricultural and Biological Engineering*; 9(4): 45－52

Zhang, C., Kovacs, J.M., (2012). The application of small unmanned aerial systems for precision agriculture: A review. *Precision Agriculture* 13, 693–712.

Zhang, H., Wang, D., Gartung, J., (2017) Influence of Irrigation Scheduling Using Thermometry on Peach Tree Water Status and Yield under Different Irrigation Systems. *Agronomy* 7, 12.

Zhang, Y.; Slaughter, D.C.; (2011) Hyperspectral species mapping for automatic weed control in tomato under thermal environmental stress, *Computers and Electronics in Agriculture*, Volume 77, Issue 1, Pages 95-104

Zhang, Y.; Staab, E.S.; Slaughter,D.C.; Giles, D.K.; Downey,D. (2012) Automated weed control in organic row crops using hyperspectral species identification and thermal micro-dosing, *Crop Protection*, Volume 41, Pages 96-105, ISSN 0261-2194

Zhenyang, G.; Wangwang, W., Yingjie, Y., Ruiqing, Z. (2013). Design of Mechanical Arm for Laser Weeding Robot. *Proceedings of the 2nd International Conference on Computer Science and Electronic Engineering* (ICCSEE 2013) 2340–2343.

Zude-Sasse, M.; Fountas, S.; Gemtos, T. A.; Abu-Khalaf, N.; (2016). Applications of precision agriculture in horticultural crops. *European Journal of Horticultural Science*. 81(2), 78–90.